

Seismicity analysis

Contents

1. Introduction	3
2. Research part (back analysis)	10
3. Methodology	14
3.1 Aftershock sequence identification	14
3.2 Background seismicity	16
3.3 Stochastic modelling	17
4. Statistical analysis of the aftershock sequences in the Kiruna mine	23
4.1 MOF parameters and b-value of the subsequent aftershock sequences	23
4.2 Examples of the distribution analysis of distances between aftershocks hypocenters	68
4.3 RETAS model example	70
4.4 Statistical relations between aftershock sequence parameters	72
5. Forecasting the aftershock rate and occurrence probability evolution	76
6. Software	79
6.1 mXrap	79
6.2 ForA1.0	79
7. Comments and outlook	81
8. Appendix A (ForA1.0 user's guide)	84
9. Appendix B (Correlation trigger magnitude – T_a, R_a)	99

1 Introduction [\(bck\)](#)

Labor safety in deep mines is becoming an increasingly important issue, because due to the reduction of raw materials, the mining depth is constantly increasing, which leads to new challenges in the organization and control of the work process in mines. It is no coincidence that where efforts are made to create a safer workplace, fewer accidents occur and there are shorter interruptions to the work process. As underground hard rock mines get deeper, they experience more challenges in terms of seismicity and control of mine operations.

Seismicity in underground mines is directly related to the mining process, as mining causes local stress changes. Under typical conditions, the underground rock is very stable in a pre-mining state – where there is no mining, there are no seismic events.

Rock stresses increase with depth and as the mine progresses there are more excavations and active walls that experience changes in stress. High stresses trigger seismic events, and the energy released by high-magnitude events often causes damage to existing openings.

This raises new challenges and topics to be analyzed including some catastrophic events often encountered in deep mining engineering: rock bursts, gas bursts, high in situ and redistributed stresses, large deformation, squeeze and rock creep, high temperature, and last but not least, seismicity caused by mining activity.

Although mine seismic events are small compared to natural seismicity, they can pose a hazard to mine infrastructure, operations, and worker safety. To reduce the risk of injury, some mine areas may be temporarily closed in the event of increased seismicity or a greater likelihood of larger seismic events. The duration of mine aftershock sequences, along with the short-term prediction of the probability of strong aftershocks, are among the seismicity characteristics considered for temporary mine closures. In such cases, the question of re-entry rules arises.

The present analysis is focused on the analysis of mining seismicity in Kiruna mine, Sweden, with the purpose to verify whether and how mining seismicity rate changes can be applied to re-entry protocol cons The Kiruna mine is the largest and most modern underground iron ore mine in the world. The mine is located in Kiruna in Norrbotten County, Lapland, Sweden. The mine is owned by Luossavaara-Kiirunavaara AB (LKAB), a large Swedish mining company. The Kiruna mine reaches a depth of up to 2 km (see "Kiruna Iron Ore Mine, Sweden"). As of 2020 the main

haulage level is 1365 m below the ore outcrop at Kiirunavaara that existed prior to mining.

Mining started in 1898 as an open pit mine. In mid-1950, the mine started a transition to underground mining and passed to only underground mining in 1962. Mining seismicity in Kiruna mine started to be a major topic of interest in 2007-2008 when the deepest mining level was 907 m (ca. 670 m below surface). The mine now has one of the largest seismic networks in the world the number of the sensors (geophones with natural frequencies of 4.5, 14, and a few of 30 Hz) reaching over 250. This broad monitoring system allows the compilation of detailed catalog data of seismic events and hence the deep study of different aspects of the seismic processes in Kiruna mine.

The investigation of mining seismicity has been the purpose of many research studies concerning mines in Sweden and in other countries. Duplancic and Brady (1999) suggested a conceptual model for the caving zone, in which various regions of the zone were categorized with respect to their seismic and discontinuity responses. Umar (2014) studied the rock mass behavior and cap rock stability at the Malmberget mine. The intrinsic characteristics of the rock mass governing deformation and caving activities were investigated by Umar et al. (2013). A paper by Perman et al. (2013) explored the performance of numerical models of mining-induced seismicity, with some examples from mines in Sweden. Larsson (2004) performs a quite thorough investigation on induced seismicity in Sweden. Mining activity poses hazard not only on personnel in the mine but also to towns nearby on the ground. Wettainen and Martinsson (2014) performed analysis on the future ground vibration levels in Malmberget town due to mining-induced seismic activity. Woodward (2015) had worked on the identification and delineation of mining induced seismic responses.

Certain research has been devoted to seismicity in the Kiruna mine itself. The mXrap team has developed a software package, which provides a lot of tools to compile, keep and analyze catalogs of mining seismicity (Harris & Wesseloo, 2015; Wesseloo & Harris, 2015). Malovichko et al. (2015) analyzed two strong events in Kiruna mine which occurred in 2013 and 2014 and Swedberg et al. (2015) examined rockfalls on some mine levels.

Seismic hazard has always been one of the main topics of study of mining seismicity. Kijko & Funk (1994) worked on the assessment of seismic hazards in mines. While most strong events in Kiruna mine concern hazard in the mine, some earthquakes are strong enough to provoke a more thorough study. On May 18, 2020

an earthquake of approximate 4.9 Mw was triggered in the footwall of the mine. The earthquake was not natural but induced by the mining activity. A multi-approach investigation of this event was performed (Dineva et al., 2022). Dahnér & Dineva (2020) and Kozłowska et al. (2020) studied stress changes in Kiruna mine while Gospodinov et al. (2022) verified the applicability of stochastic modelling to analyze aftershock temporal distribution of a seismic sequence in the mine.

Another major research topic for mining processes is the development of rules concerning closure and re-entry in the mine in case of increased hazard. Different approaches to develop guidelines and subsequently re-entry protocols for mines have been in development in recent years, some of which are based on correlation between mining production and seismicity (Vallejos and McKinnon 2011). Other studies (Malek and Leslie 2006) investigate the relation between seismic risk and some seismicity parameters like seismic work, spatial clustering, and strain rate (see definitions in Vallejos 2010). Considering the essential influence of strong event magnitude on seismic risk in mines, Vallejos and Estay (2018) investigated the correlations between mining seismic parameters and the magnitude of the main event. Mendecki et al. (2019) tested the concept that induced seismicity prior to relatively large mining tremor can be inferred from the cumulative Benioff strain release as power law time-to-failure before the strong event. Nordstrom et al. (2020) examined the behavior of several short-term hazard indicators for Kiirunavaara Mine such as Seismic Activity Rate, Cumulative Seismic Moment, Energy Index, etc. prior to an impending strong seismic event.

The single most important parameter that is monitored for re-entry purposes is the seismicity rate (number of events per unit time). Studying changes in seismic activity in the mines and relating these changes to increased seismic risk are the main focus of many scientific studies. Some investigations explore the change-point of linear trends of seismicity rate (Kubacki et al. 2014). Other authors try to approach the seismic risk problem by examining blast-related mining sequences and the correlation between production and mining seismicity (Woodward and Wesseloo 2015; Woodward et al. 2017; Dineva and Boskovic 2017).

Similar to the natural earthquakes, some of the stronger mining-induced seismic events are followed by a temporary rise of seismicity rate (aftershocks). In mines, the aftershock rate gradually decays to background levels within hours to days. Although the magnitudes of the aftershocks are not large and the extent of aftershock area in

the mine is relatively small, the rock mass in the vicinity of the main shock, which was already damaged or with decreased competence, can be damaged further by the aftershocks. Observations showed that single events or aftershocks with magnitude as low as 0.5 can cause rock damage in Kiruna mine.

The decision for re-entry after closure is commonly based on the requirement for some monitored parameters to return to a previously defined background/normal level for a given time window. If the monitored parameter exceeds a pre-set threshold during that time window, the re-entry clock is reset and the restriction continues. Re-entry rules for temporary closure and re-opening after large seismic events in mines were discussed in Vallejos and Estay (2018), Vallejos and McKinnon (2008), and Tierney and Morkel (2017). The probabilistic forecasting of natural seismicity is based on stochastic modeling of the aftershock sequence (Marzocchi and Lombardi 2009; Jordan et al. 2011; Marzocchi et al. 2012; Gospodinov et al. 2015) and the same can apply to mining seismicity. These models are statistical fits of empirical functions to common patterns of aftershock sequences and regardless of whether they explain the underlying physics of the problem the patterns, which they fit, are valuable for re-entry protocol applications.

When considering stochastic modeling of aftershock rate decay, the simplest and most widely applied model is the modified Omori formula (MOF; Utsu 1961) which is applicable both, for natural and mining-induced earthquakes. In this model, the main event controls the entire aftershock sequence. First, McGarr and Green (1978) applied it successfully to describe the duration and number of aftershocks after two mine tremors. Later Spottiswoode (2000) established that post-blast seismicity (blast aftershocks) were in agreement with the MOF for eleven sequences in four different mines. Vallejos and McKinnon (2009) and Vallejos (2010) statistically demonstrated that the MOF model could be adequately used to describe the event decay rate of mining-induced aftershock sequences. The authors examined the application of several criteria, based on MOF, for preliminary estimate of the time, which may be considered appropriate to re-enter the mine area, among them (1) when a preset level in the MOF cumulative density function is reached; (2) when MOF rate decays to a previously defined rate level; and (3) when MOF curve reaches its maximum curvature.

MOF, however, is not applicable for aftershock sequences, which include secondary excitations after strong aftershocks. For such more complex cases, Vallejos (2010) applied the Epidemic-Type Aftershock Sequence (ETAS) model, developed by Ogata

(1988) and Ogata and Zhuang (2006), to model aftershock temporal evolution in mines. This model is based on a point process in which every event can produce its offspring of events and the model can be considered as an extension of a single modified Omori's formula. In his study, Vallejos (2010) set all ETAS model parameters as a-priori calculated site specific averages.

Reasenbergs and Jones (1994) combined the MOF and Gutenberg and Richter (1944) scaling relations in a stochastic parametric model, which provides the possibility to assess the occurrence probability of either significant aftershocks or an event stronger than the main shock during time intervals following the main event. Vallejos (2010) used the Reasenbergs and Jones model for mining seismicity to estimate occurrence probabilities of aftershocks of one magnitude unit weaker than the main shock for subsequent time intervals.

The ETAS model was used by Marzocchi and Lombardi (2009) and Marzocchi et al. (2012) to perform true real-time prospective forecasts of natural seismicity rate for L'Aquila and Emilia earthquake sequences, respectively, with their model being calibrated on data before the main shock occurrence.

MOF and ETAS are based on two end assumptions, the first considering one trigger event (the main), and the second, assuming all aftershocks to be capable of inducing secondary events. In that way, these two models do not consider cases in which not all but only some stronger aftershocks control the rate decay process. This gap was covered by a model, offered by Gospodinov and Rotondi (2006) which presumes that only aftershocks above a certain magnitude level can trigger new events. The authors applied the model for natural seismicity to model aftershock activity after two sequences in Italy and Bulgaria. The model was named Restricted Epidemic-Type Aftershock Sequence (RETAS) model due to its similarity to ETAS. Gospodinov et al. (2015) applied it also to examine the temporal evolution of the occurrence probability of strong aftershocks in the 2014 Kefalonia aftershock sequence in Greece. The model was successfully used to model mining seismicity on an aftershock sequence in Kiruna mine, Sweden (Gospodinov et al., 2022)

The main purpose of the present analysis is to make a comprehensive study of the aftershock activity at Kiruna Mine by examining all the aftershock series that occurred over a selected time period and then using the obtained results for re-open protocol considerations. The emphasis of the work is on the development of algorithms and corresponding software for studying not individual aftershock series one by one, which

is already provided by the mXrap software (Harris & Wesseloo, 2015), but automatic simultaneous study of all series in a certain time period and spatial volume. In this way, the spatio-temporal characteristics of all aftershock series and their average values for the entire studied volume or for individual sub-volumes can be obtained relatively quickly. These spatio-temporal averaged parameters of aftershock activity can then be used to model and forecast the evolution of aftershock activity immediately after a new strong earthquake (above a certain magnitude threshold). Further, decision makers can use the results of the aftershock evolution forecasting after a strong mining earthquake to judge their choices of closure and re-open periods for mine operations.

Defining the main purpose of the analysis also outlines the main tasks and stages of the work and their sequence. Below are shown the main directions in which the research was carried out:

- Research part (back analysis) – this direction starts with the initial data analysis, including common catalog compiling, data unification, magnitude of completeness estimation etc. After that the research focuses on the aftershock sequence identification and the background seismicity estimation. Generally, an aftershock sequence includes all seismic events in the mine within the spatio-temporal window after a strong earthquake, the window parameters being provided interactively by the operator. What is left out of all sequences then could be regarded as the background seismicity. At first the plan was to analyze background seismicity for the entire volume and time period, covered by the initial catalog. Considering, however, the fact that the background seismicity is specifically needed to estimate the completion of an aftershock sequence, the approach has changed to analyzing the background for each specific sequence in time and space. As already mentioned, a lot of effort had to be put on the automatic sequential modelling of the aftershock sequences and obtaining of the averaged parameter estimation.
- Methodological part for automatic processing – this is another direction that applies to all areas of this work analysis. While various programs have been developed for the analysis of an individual aftershock series, among them the mXrap software (Harris & Wesseloo, 2015), the automatic processing of a large group of aftershock sequences is a significantly more complex task and requires careful algorithmization and programming. Considering the main goal of the

project, a lot of effort has been put on the modelling and visualization of the aftershock sequence evolution in space and time.

- Technical part – it is a direction related to elements of the final programming of the developed algorithms in the Python environment. The work turned out to be associated with quite a few "pitfalls" with the presentation of the evolution of the aftershock series in real time.

2. Research part (back analysis) [\(bck\)](#)

Initial catalog – Kiruna mine possesses an extensive seismic monitoring system, provided mainly by the Institute of Mine Seismology (IMS). The number of sensors has been increased stepwise and is now over 250. The equipment consists of a few 1 Hz geophones but mainly 4.5 Hz ($\frac{1}{3}$) and 14 Hz ($\frac{2}{3}$) geophones. For energy classification of the mining earthquakes LKAB uses the same local magnitude scale (M_L), which is based on seismic energy (E) and moment (M), as many South African mines (Wettainen & Martinsson, 2014).

As expected, the initial catalog for my work was extracted from the mXrap catalog. For this we had to make choices about the time duration and the mine volume, which the catalog should cover. I performed some analysis on the total catalog of all existing events. Through discussions with Savka Dineva and Christina Dahner, it was decided to investigate the seismicity in the following volume blocks of Kiruna mine, taking into account the relevance of the seismicity in them:

GMZ BI 04-12, GMZ BI 12-15, GMZ BI 15-26, GMZ BI 26-30, GMZ BI 34-v2, GMZ BI 38, GMZ BI 41

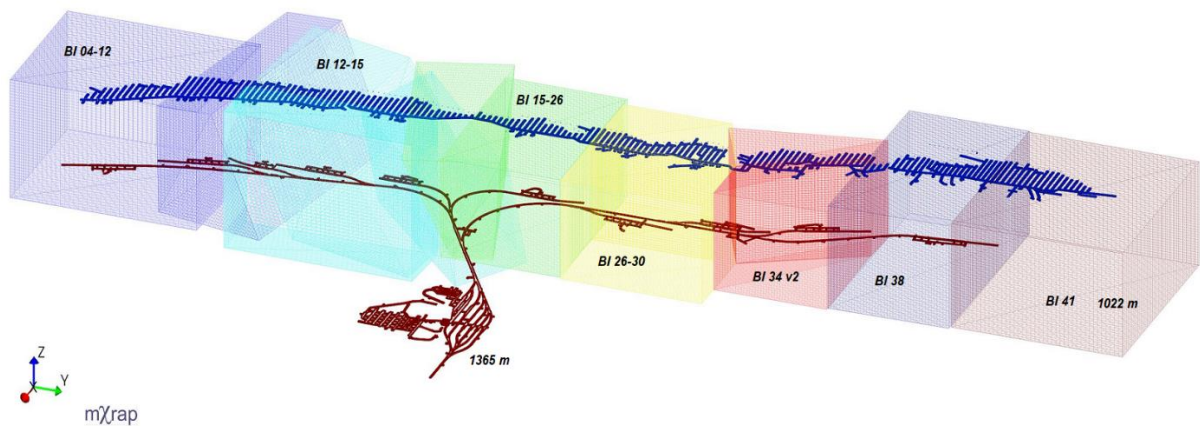


Fig.2.1 Positioning of GMZ volumes and levels 1022 m and 1365 m in Kiruna mine (mXrap)

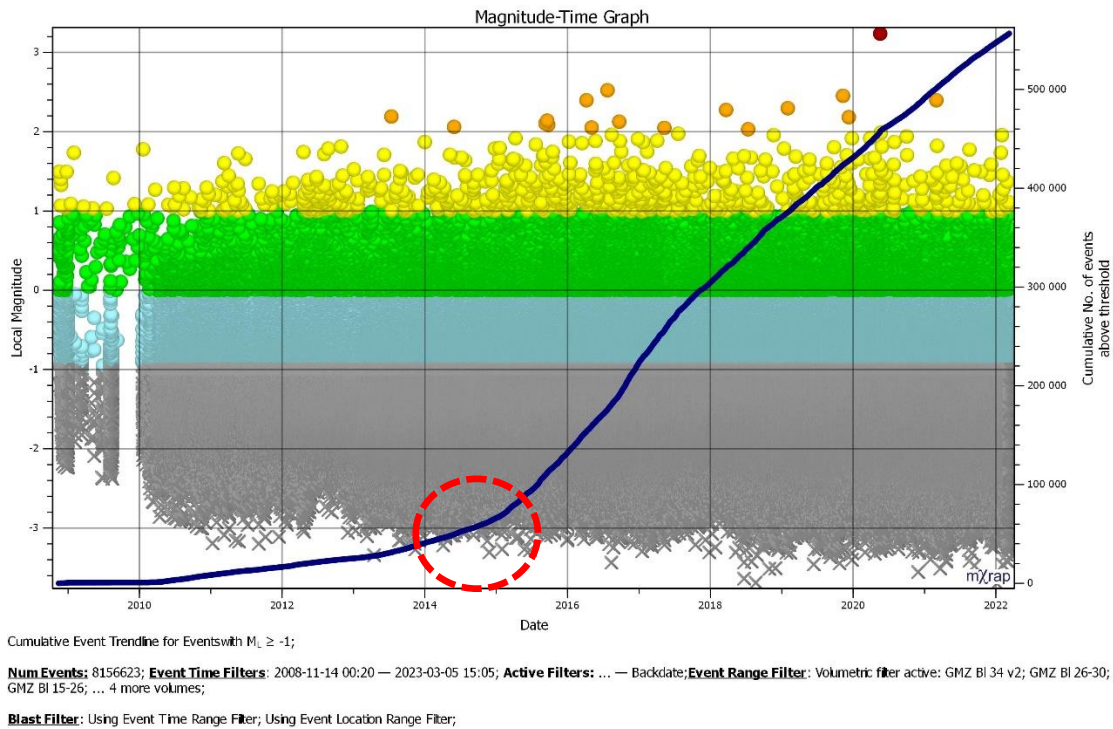


Fig.2.2 Magnitude with time and cumulative number of seismic events of the GMZ volumes in Kiruna mine (mXrap). Red circle denotes the case after which the cumulative curve follows a linear behavior

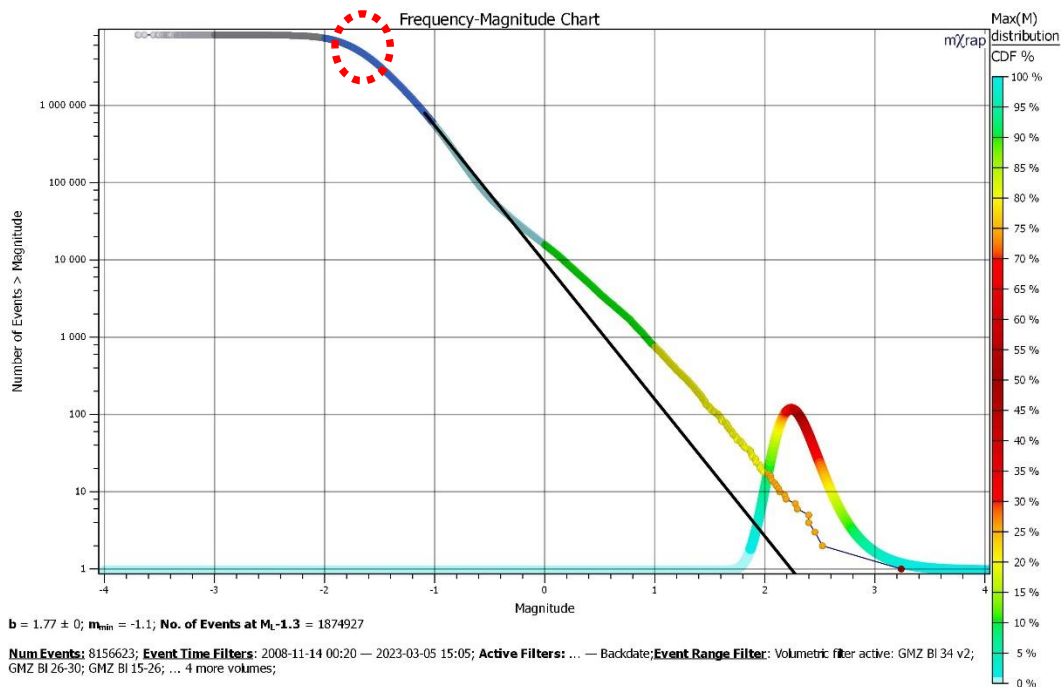


Fig.2.3 Gutenberg-Richter law for all events of the GMZ volumes in Kiruna mine (mXrap). Red circle denotes the case after which the catalog is complete (magnitude of completeness $M_0 = -1.1$)

The relative positions of the investigated volumes in Kiruna mine is shown on Fig.2.1 together with the locations of working levels 1022 m and 1365 m. One of the first tasks to be completed was the selection of the time period to be covered by the initial catalog. We stopped our choice on 2015 (Fig.2.2) to be the beginning of this period as the cumulative curve after that follows a linear behavior which means that most probably there weren't any external factors, causing considerable rate changes.

The catalog data unification is an important issue which is specifically relevant for the events magnitudes. After some discussions we decided to use the magnitudes used by LKAB for the mining events. There the seismic events energy classification is performed after a local magnitude scale (M_L). This scale is based on seismic energy (E) and moment (M) (see eq.1), as is the case for many South African mines (Wettainen & Martinsson, 2014).

$$M_L = 0.272 \log E + 0.392 \log M - 4.63 \quad 2.1$$

In some specific cases of strong seismic events in mines (Dineva et al. , 2022) the matter about the used magnitude scale could be raised again because such events are also classified by the Swedish National Seismic Network ([SNSN](#)). Another matter of importance are the possible errors in the initial catalog. I checked the catalog importing it in Excel but later a module was developed in the ForA1.0 software to check for some errors (empty fields or empty fields)

The Gutenberg-Richter distribution law (Gutenberg & Richter, 1944) for the GMZ volumes in Kiruna mine (number of events $N=8156623$) was plotted on Fig.2.3 and it points to a value of the magnitude of completeness $M_0 = - 1.1$. This analysis allowed to compile the initial catalog of $N=733574$ events with magnitudes $M_L \geq M_0$.

Two issues are worth considering for the future implementation of the developed algorithms and software:

- The format of the future initial catalogs to be analyzed should be the same as the one foreseen in the software at present (it will be specifically presented in the report later)
- On my request the mXrap team presented an option to export data with an additional column carrying information about the volume each event comes from. This is important for the averaged parameter estimation if separate GMZ volumes are to be considered.

The information about the seven GMZ volumes in which each event has occurred was not included as a separate column in the catalog exported from mXrap. As this data is needed for the further analysis, the problem was first solved by exporting the data volume by volume, adding a column for the volume name and then compiling a common generalized catalog. Later this problem was completely resolved by the mXrap team by providing the possibility to export the entire catalog with a column for the volume block name.

The initial catalog contains the following information in the different columns (Fig.2.4). It was exported from the mXrap program (general analysis), and in this case we limited ourselves to 12 columns.

Date [D.M.Y.]	Time [HH:MM:SS.SSS]	X [m]	Y [m]	Z [m]	ML	Vol	Seism Moment [Nm]	Total Radiated Energy [J]	Apparent Stress [Mpa]	Residual [m]	Potency [m ³]
1.1.2015	00:22:03.107	-6540.5	3352.9	-1337.9	-0.34	GMZ_BI_34_v2	9.52E+08	6.90E+02	2.17E-02	12	3.17E-02
1.1.2015	00:28:15.243	-6410.8	3044.2	-1259.7	-1.1	GMZ_BI_26-30	2.37E+08	8.40E+00	1.06E-03	10	7.90E-03
1.1.2015	01:51:30.082	-6307.5	3479.1	-1029.8	-0.55	GMZ_BI_34_v2	5.89E+08	2.28E+02	1.16E-02	6	1.96E-02
1.1.2015	02:08:17.505	-6253.6	1410.6	-910.7	-0.06	GMZ_BI_12-15	6.77E+09	4.22E+02	1.87E-03	44	2.26E-01
1.1.2015	02:23:27.643	-6136.8	1457	-1185	-0.84	GMZ_BI_12-15	1.01E+08	2.41E+02	7.16E-02	4	3.37E-03
1.1.2015	02:25:04.288	-6397.2	3678.2	-980.1	-0.74	GMZ_BI_38	6.29E+08	4.14E+01	1.98E-03	48	2.10E-02

Fig.2.4 Format of the initial catalog file. The header row is shown only for demonstration here. In the initial catalog itself this row was removed for reasons of simplicity in the processing.

The more important data for our analysis is contained in the first seven columns, while the information in the remaining five columns is not used for now. The major columns (header row - left to right) are Date, Time, hypocenter coordinates X, Y, Z according to Kiruna mine coordinate system, local magnitude ML and mine volume (seven GMZ volumes) in which the event has occurred. As mentioned in the table on Fig.2.4, the header row is not included in the initial catalog which simplifies the subsequent processing of the file.

3. Methodology [\(bck\)](#)

The methodological approach to fulfil the tasks of the current analysis includes several different groups of algorithms and methods corresponding to the different goals. Some of the methods have been chosen on information taken from scientific publications (stochastic modelling) and previous experience and some of the algorithms were specially developed for the implementation of the present investigation (aftershock sequence identification and defining of back ground seismicity).

3.1 Aftershock sequence identification [\(bck\)](#)

Aftershock sequence analysis is a primary task in the current project hence the recognition of the aftershock events after a trigger was one of the first issues I've focused my attention on. Usually aftershock series are identified by user defined values of the duration (in time) and the radius around the main event hypocenter (in space). These values depend on the user's experience and the specific mining seismicity features. This is the way it is done in mXrap and such method is very much like the so called Knopoff window (Gardner & Knopoff, 1974). Seismic hazard estimation is based on initial seismicity declustering and many studies have been pointed to its realization (Christoskov & Lazarov, 1981; Peresan & Gentili, 2020; Reasenber, 1985; Zhuang et al., 2002; etc.). A lot of them, however, aim at general catalog declustering, needed for the seismic hazard estimation. What is necessary in our project is to identify aftershocks following each trigger and compile a catalog for each sequence which further to be analyzed.

Under these circumstances, I decided to apply the following methodology to identify a separate aftershock series. Initially a sequence is recognized using user defined spatio-temporal window. Some variations of the values in space and time were tested for Malberget mine using mXrap (by default duration value there is around 23 hours and radius value is 150 m). Finally, basing on the mXrap results, it was decided to use bigger values for the spatio-temporal window (300 m x 60 h). Following this window, the algorithm investigates the initial catalog, exported from mXrap and defines the primary aftershock sequence after each trigger. The window has been chosen to be large enough so that later to decrease the space-time value to the optimal ones. This step of the algorithm is compulsory for the implementation of the next step which is final aftershock sequence identification. This is so because it is based on the analysis

of each initially identified aftershock sequence. The algorithm of final aftershock identification is developed after these main assumptions:

- The aftershock zone is modeled in space as a sphere whose center coincides with the trigger hypocenter
- Aftershock density decreases with the increase of the distance between aftershock hypocenters and the trigger
- Aftershock rate decreases with the increase of the time period between aftershock occurrence and the trigger occurrence

The above suppositions seem quite reasonable as this has been the case with many aftershock sequences, both crustal and in mines. Following these hypotheses one could consider the final radius of the aftershock zone to be the one for which aftershock hypocenter density decays to background density, calculated for the same sphere on events before the sequence has started.

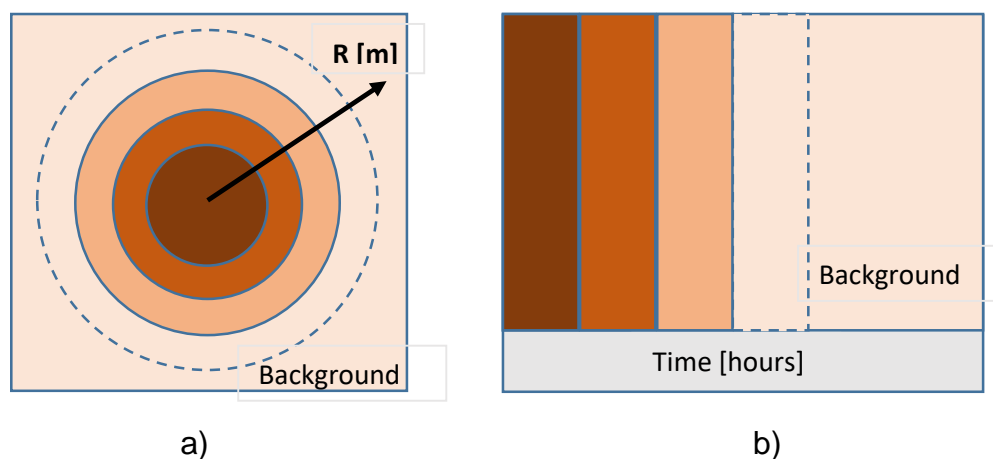


Fig.3.1 Demonstration of the algorithm on which final aftershock identification is based: a) in space; b) in time (see details in text)

One can see a graphical demonstration of this idea on Fig.3.1a, where the darker color denotes higher density and the sequence radius is the one for which densities (colors), both for aftershocks and for background events coincide (dashed line). A similar approach is applied for the final estimation of the aftershock sequence duration Fig.3.1b. It is considered that the time when the aftershock rate (number per unit interval) decays to the background rate (for the same space volume) marks the duration of the sequence (coinciding colors on Fig.3.1b).

Then the purpose of this step is to open the initial aftershock sequence for a specific trigger, to analyze it following the above algorithm and to provide a final aftershock sequence. All this is done for every sequence and the corresponding final sequences are saved. In fact, what practically is being performed: in space – dividing the space into subsequent spherical layers around the trigger hypocenter, counting the number of aftershocks in the subsequent layers until this number systematically tends to the background, which marks the final aftershock zone radius; in time - dividing the time into subsequent periods after the trigger time, counting the number of aftershocks in the subsequent periods until this number systematically tends to the background and this marks the final aftershock sequence duration.

It is significant to make the right choice of the number of distance intervals by which to divide the user defined radius and the number of time intervals by which to divide the user defined duration for the final identification. Some tests have revealed that 25 m space interval and a 3 hour time interval is a proper choice and this could be taken into consideration when selecting the number of intervals.

3.2 Background seismicity [\(bck\)](#)

As pointed out in 3.1, background seismicity is necessary to perform the final aftershock sequence identification. That means that an algorithm had to be developed for background seismicity definition, recognition and estimation. At first it was originally intended to consider background seismicity for the entire Klrana mine. The estimated background is needed, however, for the aftershock sequence zones. So, I put my focus on the compiled catalog of background events and the background level estimation for these zones. Firstly, a definition had to be elaborated for the background seismicity. It seems quite natural to suppose that background seismicity is what is left in the catalog after all aftershock sequences are removed out of it. This is the idea on which I based my algorithm. A separate catalog was compiled which contained only mining seismic events which were not aftershocks of any of the triggers. For the aftershock zone of each sequence this catalog has been analyzed to capture events before the trigger for certain period (60 days in our case). The number of events in each spherical layer (time period respectively – see chapter 3.1) has been counted to estimate the background seismic activity. On my knowledge, the mXrap software provides a tool (re-entry group options of mXrap) to perform retrospective analysis (after the sequence

is over) on the ratio of aftershock rate to background activity, the latter being calculated not only on the aftershock sequence zone.

The difference in my approach is that the background level is calculated on the aftershock spatial volume only and the aim is to forecast the sequence temporal evolution prospectively immediately after the occurrence of the trigger event.

3.3 Stochastic modelling [\(bck\)](#)

Stochastic modelling is an approach to the analysis of many objects and phenomena where the processes are random, such as the process of earthquake occurrence (both for crustal or mining events). This fully applies to the aftershock process, where the object of statistical modeling is the spatial, energy and temporal distribution of the aftershocks. Such probabilistic models are important in the study of mine seismicity because they offer an analytical form of the distributions and hence provide a possibility for simulation and probabilistic forecasting of the seismic process.

Stochastic modeling of aftershock activity provides the analytical basis to simulate the process and probabilistically evolve it

Temporal distribution of aftershocks – in the current project activity we shall mention several stochastic models of aftershock activity but for our goals we have chosen the Modified Omori Formula (MOF; Utsu, 1961) model as it is widely used for aftershock rate decay modelling and most importantly it can be applied to estimate the aftershock sequence duration. The model can also be used to provide a picture of the sequence evolution.

Each stochastic model is developed on the basis of some basic physical assumptions. For MOF it is supposed that the total relaxation process is controlled by the stress field changes caused by a main shock. The aftershocks are conditionally independent and follow a nonstationary Poisson process. By the MOF model the decaying frequency of aftershocks per unit time is described to follow a negative power law (Utsu, 1961)

$$n(t) = \frac{K}{(t+c)^p} \tag{3.1}$$

where t is the time elapsed from the occurrence of the main shock, K is a parameter related to the magnitude of the main shock and to the magnitude cut-off, p is a coefficient of attenuation and c is a constant.

The frequency $n(t)$ in Eq. (3.1) corresponds to the intensity function of a point process, i.e.

$$n(t) \approx \lambda(t) \quad (3.2)$$

where $\lambda(t)$ is the conditional intensity function. Such consideration allows the construction of the likelihood function of the process and estimation of the maximum likelihood estimates of the MOF parameters.

More compound cases with one or more secondary aftershock sequences led Ogata (1988) to consider aftershock clustering as a self-similar process, where all aftershocks can induce further aftershocks, with the triggering capacity depending on their magnitude. The model was named Epidemic Type Aftershock Sequence (ETAS) model and its rate is decomposable into separate terms representing the time and magnitude distribution. Hence, the expected resultant rate of aftershocks is given by Ogata (1988):

$$\lambda(t | H_t) = \mu + \sum_{t_i < t} \frac{K_0 e^{\alpha(M_i - M_0)}}{(t - t_i + c)^p} \quad (3.3)$$

where μ (shocks/day) is the rate of background activity, the history H_t consists of the times t_j (days) and magnitudes m_j of all the events which occurred before t and the summation is taken over every j -th aftershock with a magnitude stronger than the cut-off $m_j \geq M_0$ i.e. over all events in the sample.

The MOF and the ETAS model are two limit cases, the former with only one parent event and the latter with all events sharing in the generation of the subsequent ones. Gospodinov and Rotondi (2006) offer the Restricted Epidemic Type Aftershock Sequence (RETAS) model, which is based on the assumption that not all events in a sample but only aftershocks with magnitudes larger than or equal to a threshold M_{th} can induce secondary seismicity. Then the conditional intensity function for the model is formulated by eq.(3.4)

$$\lambda(t | H_t) = \mu + \sum_{\substack{t_i < t \\ M_i \geq M_{th}}} \frac{K_0 e^{\alpha(M_i - M_0)}}{(t - t_i + c)^p} \quad (3.4)$$

In eq.(3.4) the summation is only over events with magnitudes $M \geq M_{th}$. For this reason, the model was named Restricted Epidemic Type Aftershock Sequence (RETAS) model. I have provided short information about the ETAS and the RETAS models but for our purposes we have chosen the MOF model (eq.(3.1)) to perform the temporal modeling of the aftershock process.

Energy distribution of aftershocks – the energy distribution of earthquakes including aftershocks is most often modelled by the so called Gutenberg-Richter law (Gutenberg & Richter, 1944) presented by eq.(3.5)

$$\lg N(M) = a - bM \quad (3.5)$$

where N is the number of events with magnitudes exceeding M and a and b are constants. This final form of the law can be developed starting from eq.(3.6) (see Estay et al., 2020; Vallejos & Estay, 2018).

$$f(M, \beta) = \beta e^{-\beta(M - M_{min})} \quad (3.6)$$

Here f is the probability density function, M is the magnitude, considered as a continuous random variable, M_{min} is the minimum magnitude allowed and β is a constant. Such consideration allows the development of a formula for the b-value estimation from eq.(3.5) presented by eq.3.7 (Vallejos & Estay, 2018).

$$b = \frac{\log(e)}{\bar{M}_w - M_{w,c} + \Delta M_{bin}/2} \quad (3.7)$$

In eq.(3.7) \bar{M}_w is the mean magnitude of events that $M_w \geq M_{w,c}$ (magnitude of completeness). ΔM_{bin} is the binning width of the catalogue and each bin usually has a width of 0.1. I stopped my selection at eq.(3.7) based on the Gutenberg-Richter law for the estimation of the b-value and it was implied in the algorithm and the corresponding software.

There are other approaches to consider earthquake (aftershock) energy distribution. One of them is based again on eq.(3.6) and it studies the probability distribution of the difference between events magnitudes (Gospodinov, 2004). Another approach provides a stochastic model of the cumulative strain release (Gospodinov, 2016; 2017) and it could be used to analyze aftershock energy release. These last two models are beyond the scope of the present project but could be considered for future investigations.

Spatial distribution of aftershocks – the spatial distribution of aftershocks is characterized by strong clustering and therefore cluster recognition is among the main goals of events spatial analysis (Peresan & Gentili, 2020; Reasenber & Jones, 1994). The mXrap software provides good options for aftershock identification on user defined space and time filters. In the ForA1.0 software I had elaborated possibilities for the implementation not only of user defined identification as in mXrap but also for automatic optimization of the filters and final identification of each aftershock sequence in the initial catalog.

An important direction in studying the spatial distribution of earthquakes is the analysis of the distances between the hypocenters of the events - between the trigger and aftershocks, between successive aftershocks, etc. Analytical solutions have been offered for the distance distribution considering distance as a random quantity (Reasenber, 1985; Gospodinov & Christoskov; Gospodinov, 2004). The latter approach provides the opportunity to examine non-random features of earthquake spatial distribution including aftershocks.

In the event that it is not possible to find an analytical solution for the distribution of the distances, a suggestion is proposed in which the null hypothesis of randomness of the distances is represented by the distribution of all possible distances between events hypocenters (Gospodinov, 2004). If, for example, the distribution of distances between trigger and aftershocks or between consecutive aftershocks deviates significantly from that of the null hypothesis, this is an indication of the presence of regularity. It can be seen on Fig.3.2 (an example), that there is a deviation of the subsequent events distribution from the one of all possible aftershocks. For shorter distances the former distribution exceeds the latter one (red dashed circle on Fig.3.2 which could point to a process of secondary sub-clustering in this sequence.

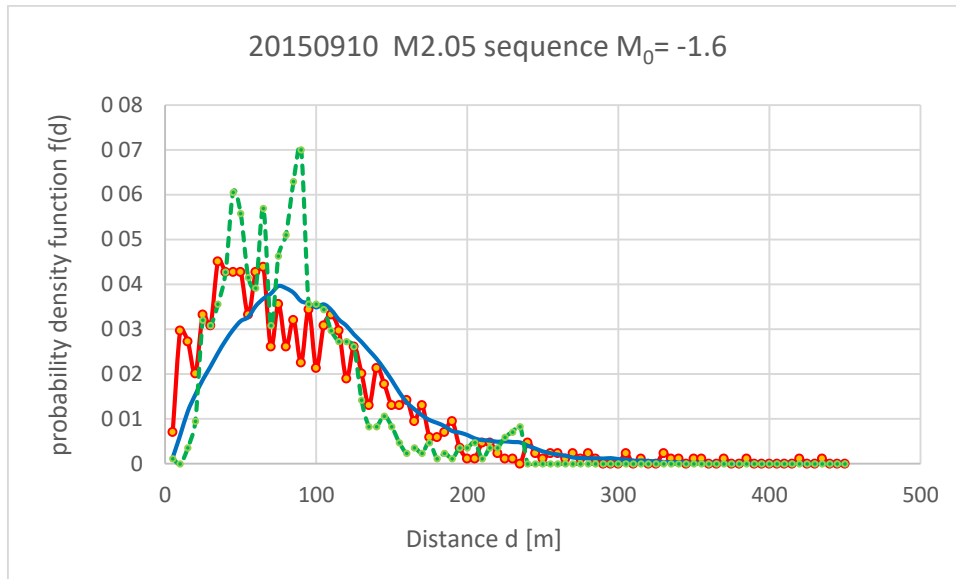


Fig.3.2 Distribution of distances between hypocenters of aftershocks: thick blue line – distribution of all possible distances between different events; red line with points – distribution of distances between subsequent events; green dashed line – distribution of distances between the trigger and the aftershocks

The example plot on Fig.3.2 is for a sequence from Kiruna mine. The described approach is not part of the current project objectives but I have analyzed several more vigorous aftershock sequences in Kiruna mine and the results are provided in chapter 4.2. The results on Fig.3.2 show a significant deviation of distances between subsequent events distribution and that of all possible shocks. The former exceeds the latter for small distances (up to 60 m), which means that subsequent events cluster more than if completely random. This could be caused by some processes of aftershock diffusion or secondary clustering in the sequence.

Occurrence probability of strong aftershocks – Reasenberg and Jones (1989, 1994) developed a hazard model based on a formula from the probability theory for a nonstationary Poisson process (eq.(3.8))

$$P(M_1, M_2; T_1, T_2) = 1 - \exp \left[- \int_{M_1}^{M_2} \int_{T_1}^{T_2} \lambda(t, M) dM dt \right] \quad (3.8)$$

According to eq.(3.8) the probability P for at least one aftershock of magnitude between M_1 and M_2 , to occur in the period (T_1, T_2) after the main shock can be calculated after the assumption that the magnitude and the temporal distributions are independent.

$$\lambda(t, M) = \lambda(t) \cdot \lambda(M) \tag{3.9}$$

The magnitude distribution in eq.(3.8) and (3.9) is provided by eq.(3.6) and the temporal distribution can be presented by eq.(3.1) or eq.(3.4) (for RETAS; see Gospodinov et al., 2015). In the current project I applied eq.(3.1) to calculate and present the occurrence probability of strong aftershocks in the 'Aftershock evolution' module of the ForA1.0 software.

4. Statistical analysis of the aftershock sequences in Kiruna mine [\(bck\)](#)

The ForA1.0 software, developed within the framework of the current project, provides the possibility to quickly analyze the energy and the temporal distributions of a number of aftershock sequences which have been previously identified. One can see below the results of the energy and temporal analysis of all identified sequences in Kiruna mine for the period after January, 1st, 2015. The user defined values for the initial aftershock identification were chosen to be $R = 300$ m (meters) and $\Delta T = 60$ h (hours). We chose these expanded values to be sure that the initial sequences contain all aftershocks for the following final identification procedure. The number of identified sequences is $N = 103$ which is by two bigger than the sequences identified by mXrap for the same filters. For some reasons mXrap misses two sequences with trigger magnitudes exactly $M = 1.5$.

4.1 MOF parameters and b-values of the subsequent aftershock sequences

[\(bck\)](#)

In this chapter I have provided the MOF parameters and the b-values of the final aftershock sequences, recognized in the initial catalog. It is important to note the p-value range, set in the FORTRAN module, called by the ForA1.0 software which is $[0.6, 2.0]$. Only sequences with number of aftershocks $N \geq 5$ have been considered for the analysis described in chapter 4.1. The subsequent plots display the cumulative curves of the aftershocks in time: thick line – model cumulative numbers after the identified best fit MOF model; dashed lines – error bounds; red circles – real cumulative numbers; green circles - magnitudes.

The first considered sequence (Fig.4.1) is one of $N = 35$ aftershocks. The estimated sequence duration and zone radius are correspondingly $T_a = 60$ hours and $R_a = 300$ meters. The strongest aftershock is of magnitude $M_2 = 0.42$, at a distance $dt_2 = 104.31$ m and time 18.40 hours from the trigger. It is evident from the plotted figure that the MOF model is not adequate for these data because the aftershock rate is rather constant but not decaying with time hence the p-value is quite low (the lowest possible). The sequence has few events with magnitudes $M \geq 0.0$ (high b-value).

I will not comment all cumulative curve plots one by one (the reader can examine them by himself) but will generalize some of the obtained results. The temporal distribution of a certain number of the sequences ($\sim 35\%$) are not well fitted by the

MOF model. For some of them this is due to small or no decay of the aftershock rate (Fig.4.1, 4.11, 4.13, 4.27, 4.45, 4.58, 4.62, etc.) and for another part of the sequences the reason could be the existence of sub-clusters with time which couldn't be captured by the MOF model (Fig.4.5, 4.6, 4.7, 4.8, 4.15, 4.29, 4.34, 4.35, 4.37, 4.43, 4.51, 4.68 etc.)

Considering the magnitude distribution of the aftershocks in the different sequences, for some sequences a considerable number of events with magnitude $M \geq 0.0$ is found (Fig.4.7, 4.14, 4.16, 4.23, 4.24, 4.25, 4.28, 4.30 etc.)

The general number of triggers (sequences) in the initial catalog file is $N=103$ but for 21 of them the number of aftershocks in the sequence are less than five and these sequences were not analyzed.

In fact, more details on the trigger events and the analyzed aftershock sequences are provided in Table 4.1 where except the b-value and the MOF parameter values, the user can also find additional information about sequence duration, radius etc.

Sq.No	Date	Time	X	Y	Z	M main	Vol	b	K	p	c	Ta [h]	Ra [m]	M2	N	dl2 [m]	dt2 [h]
1	'11.1.2015'	'01:33:10.526'	-6544.9	4023	-989.8	1.6	GMZ_BI_38	0.94	19.86	0.60	0.77	60	300	0.42	35	104.31	18.40

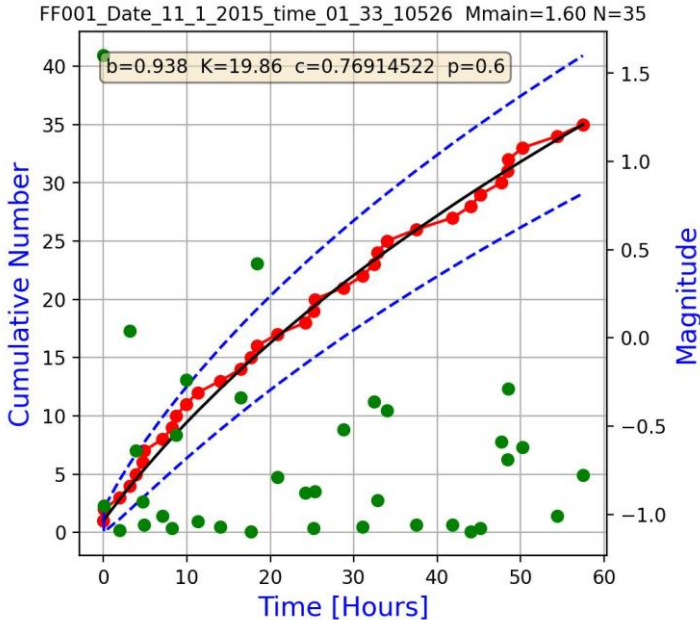


Fig.4.1 Cumulative curves of the aftershocks in time: thick line – model cumulative numbers after the identified best fit MOF model; dashed lines – error bounds; red circles – real cumulative numbers

Sq.No	Date	Time	X	Y	Z	M main	Vol	b	K	p	c	Ta [h]	Ra [m]	M2	N	dl2 [m]	dt2 [h]
2	'17.1.2015'	'01:49:21.085'	-6541.6	3984.5	-1019.8	1.66	GMZ_BI_38	0.60	2.90	1.10	0.00	9	225	0.14	29	75.88	0.25

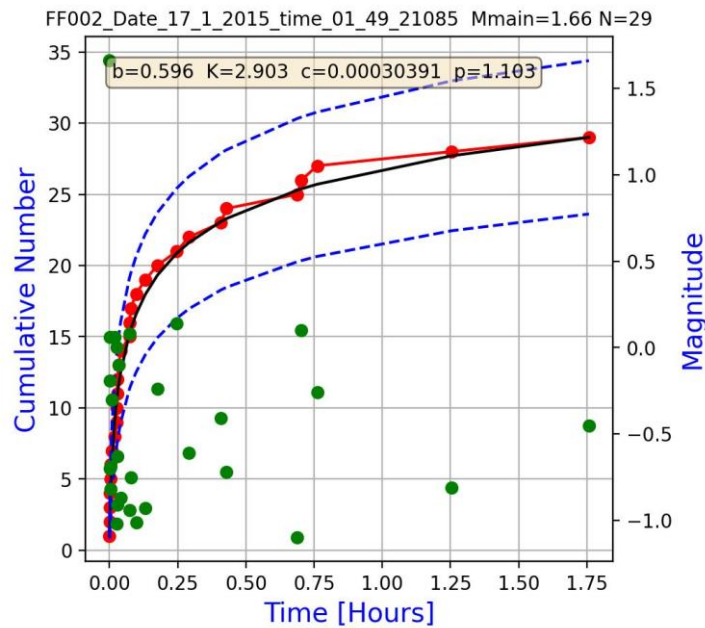


Fig.4.2 Cumulative curves of the aftershocks in time: thick line – model cumulative numbers after the identified best fit MOF model; dashed lines – error bounds; red circles – real cumulative numbers

Sq.No	Date	Time	X	Y	Z	M main	Vol	b	K	p	c	Ta [h]	Ra [m]	M2	N	dl2 [m]	dt2 [h]
3	'17.1.2015'	'03:35:14.579'	-6380.5	3980.4	-1012.5	1.8	GMZ_BI_38	0.63	6.32	0.91	0.00	27	250	0.64	41	208.76	1.44

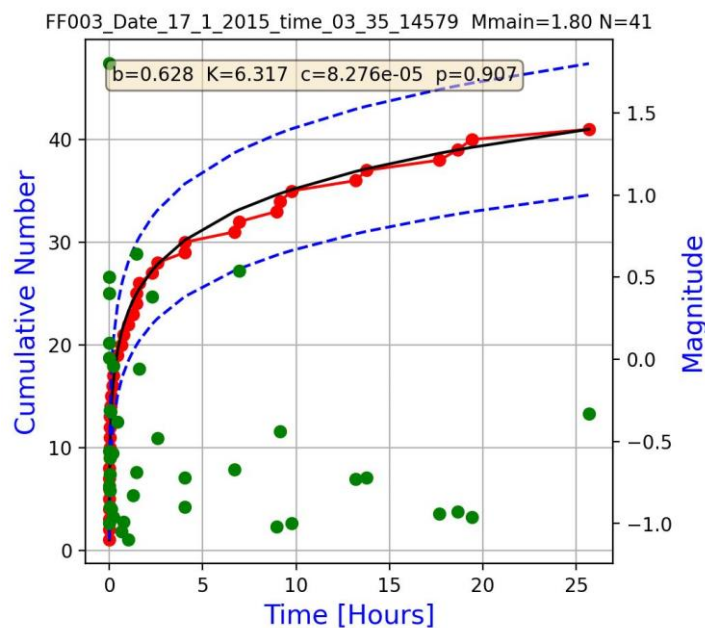


Fig.4.3 Cumulative curves of the aftershocks in time: thick line – model cumulative numbers after the identified best fit MOF model; dashed lines – error bounds; red circles – real cumulative numbers

Sq.No	Date	Time	X	Y	Z	M main	Vol	b	K	p	c	Ta [h]	Ra [m]	M2	N	dl2 [m]	dt2 [h]
4	'4.3.2015'	'16:44:53.156'	-6217.6	2624.9	-1000.8	1.6	GMZ_BI_26-30	0.63	10.67	0.71	0.00	9	225	1.24	23	108.79	1.69

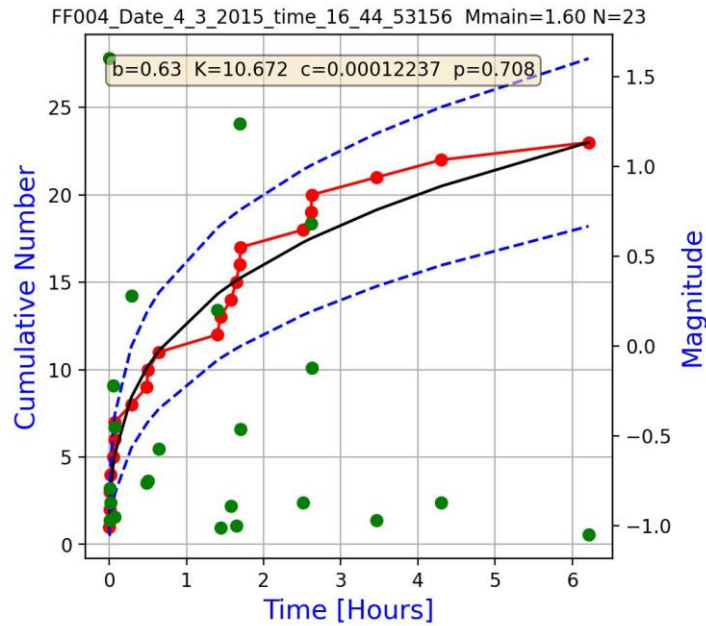


Fig.4.4 Notation as in Fig.4.3

Sq.No	Date	Time	X	Y	Z	M main	Vol	b	K	p	c	Ta [h]	Ra [m]	M2	N	dl2 [m]	dt2 [h]
5	'18.3.2015'	'01:46:47.964'	-6488.5	4515.3	-996.2	1.58	GMZ_BI_41	0.77	11.52	0.60	0.000359	48	300	0.26	35	194.50	24.50

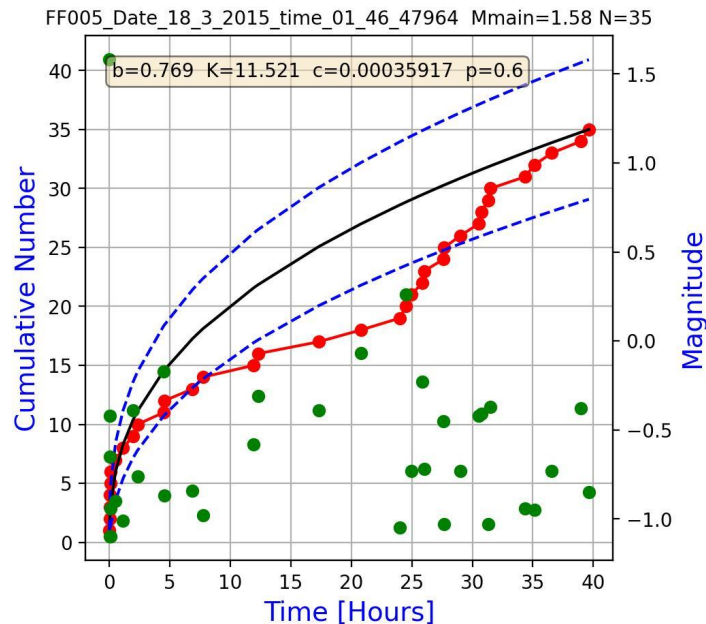


Fig.4.5 Cumulative curves of the aftershocks in time: thick line – model cumulative numbers after the identified best fit MOF model; dashed lines – error bounds; red circles – real cumulative numbers

Sq.No	Date	Time	X	Y	Z	M main	Vol	b	K	p	c	Ta [h]	Ra [m]	M2	N	dl2 [m]	dt2 [h]
6	'25.3.2015'	'13:29:34.315'	-6290.3	2581.2	-1144.4	1.59	GMZ_BI_26-30	0.74	0.84	1.16	0.000341	6	125	-0.43	10	75.78	0.00

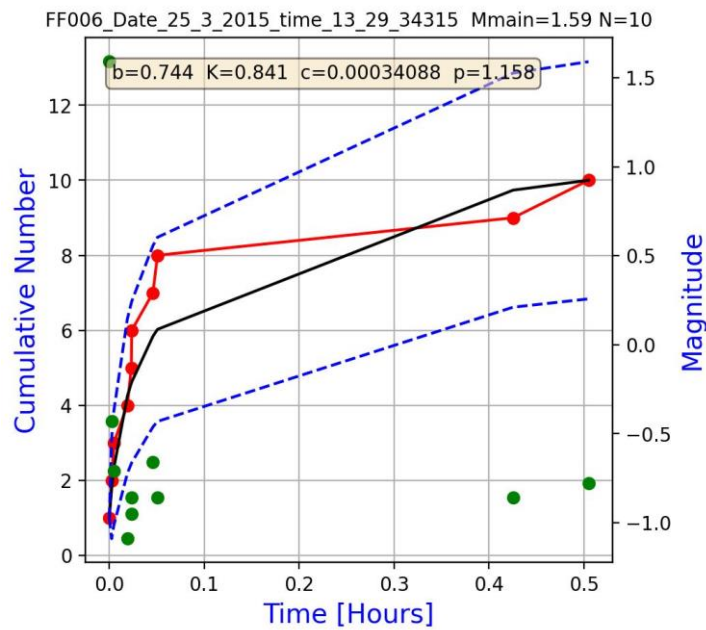


Fig.4.6 Notation as in Fig.4.5

Sq.No	Date	Time	X	Y	Z	M main	Vol	b	K	p	c	Ta [h]	Ra [m]	M2	N	dl2 [m]	dt2 [h]
7	'25.3.2015'	'14:02:00.734'	-6298	2566.8	-1118.2	1.65	GMZ_BI_26-30	0.83	19.99	0.69	0.000040	18	175	0.84	56	53.74	0.10

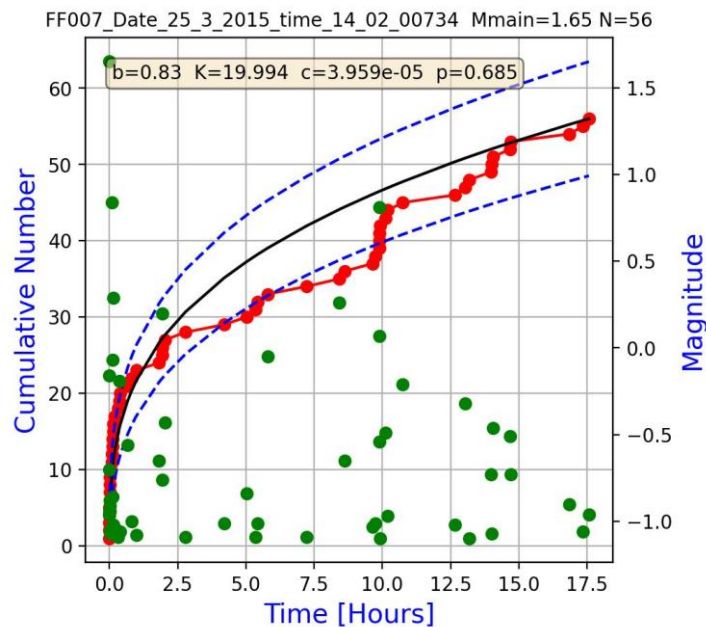


Fig.4.7 Cumulative curves of the aftershocks in time: thick line – model cumulative numbers after the identified best fit MOF model; dashed lines – error bounds; red circles – real cumulative numbers

Sq.No	Date	Time	X	Y	Z	M main	Vol	b	K	p	c	Ta [h]	Ra [m]	M2	N	dl2 [m]	dt2 [h]
8	'28.3.2015'	'20:48:46.008'	-6359.9	2178.2	-1201.2	1.66	GMZ_BI_15-26	0.64	5.63	0.72	0.000047	9	125	0.5	14	33.22	0.14

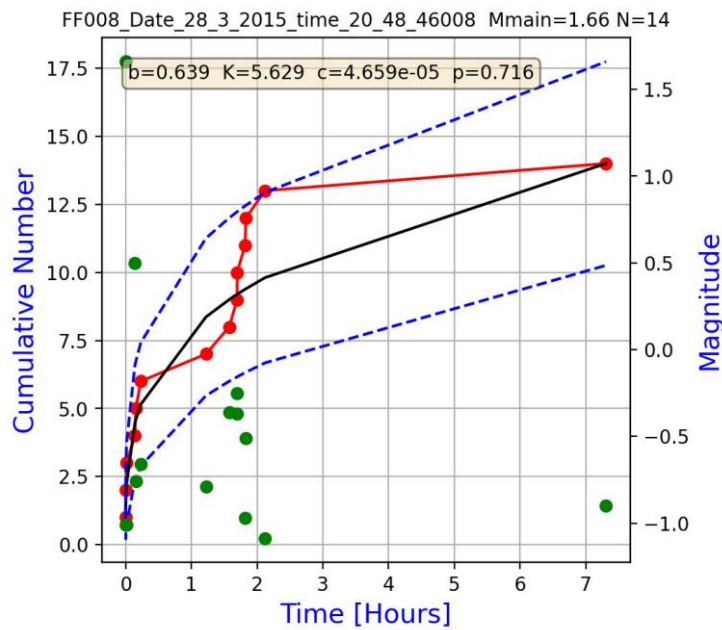


Fig.4.8 Notation as in Fig.4.7

Sq.No	Date	Time	X	Y	Z	M main	Vol	b	K	p	c	Ta [h]	Ra [m]	M2	N	dl2 [m]	dt2 [h]
9	'9.4.2015'	'01:33:56.941'	-6191	2501.7	-1122.4	1.92	GMZ_BI_26-30	0.63	0.45	1.17	0.000188	9	125	-0.14	9	42.93	0.32

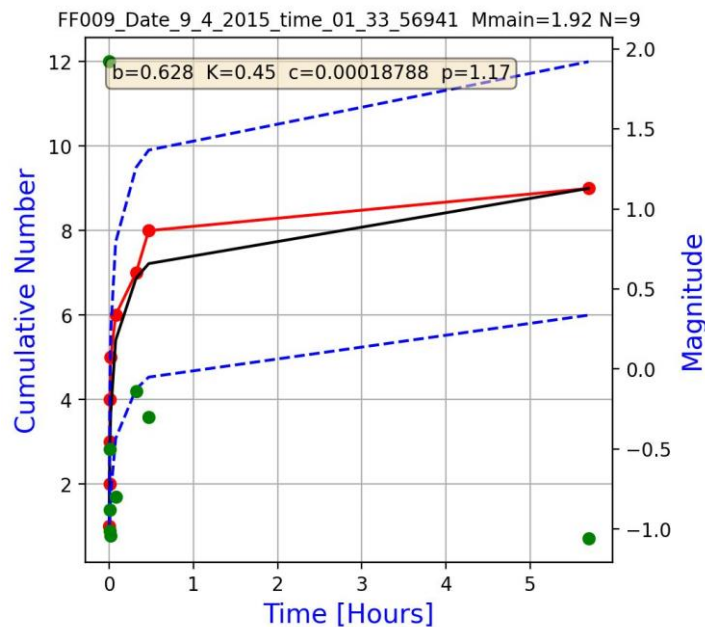


Fig.4.9 Cumulative curves of the aftershocks in time: thick line – model cumulative numbers after the identified best fit MOF model; dashed lines – error bounds; red circles – real cumulative numbers

Sq.No	Date	Time	X	Y	Z	M main	Vol	b	K	p	c	Ta [h]	Ra [m]	M2	N	dl2 [m]	dt2 [h]
10	'15.4.2015'	'01:58:39.523'	-6185.6	2704.5	-996.4	1.64	GMZ_BI_26-30	0.61	4.33	0.65	0.000096	6	150	0.02	7	52.99	3.23

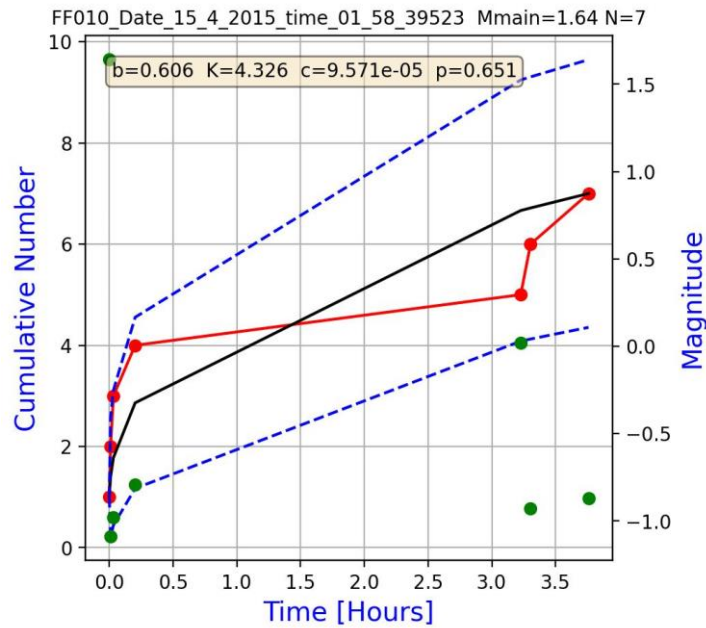


Fig.4.10 Notation as in Fig.4.9

Sq.No	Date	Time	X	Y	Z	M main	Vol	b	K	p	c	Ta [h]	Ra [m]	M2	N	dl2 [m]	dt2 [h]
11	'31.5.2015'	'03:03:08.345'	-6346.1	2197.2	-1216.1	1.57	GMZ_BI_15-26	0.69	46.93	0.60	2.000000	6	125	-0.46	8	22.18	3.81

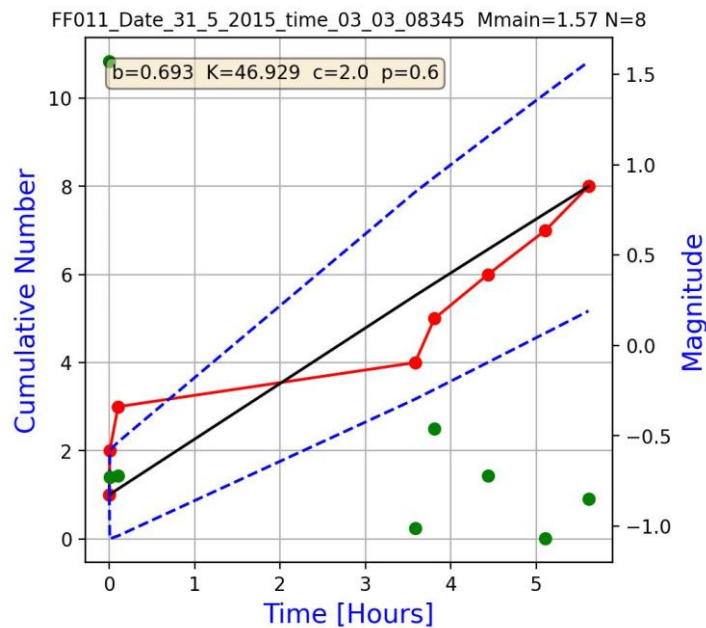


Fig.4.11 Cumulative curves of the aftershocks in time: thick line – model cumulative numbers after the identified best fit MOF model; dashed lines – error bounds; red circles – real cumulative numbers

Sq.No	Date	Time	X	Y	Z	M main	Vol	b	K	p	c	Ta [h]	Ra [m]	M2	N	dl2 [m]	dt2 [h]
12	'22.7.2015'	'04:15:07.227'	-6250.8	2546.7	-1026	1.84	GMZ_BI_26-30	0.82	5.32	0.81	0.000077	12	225	0.38	20	64.92	5.45

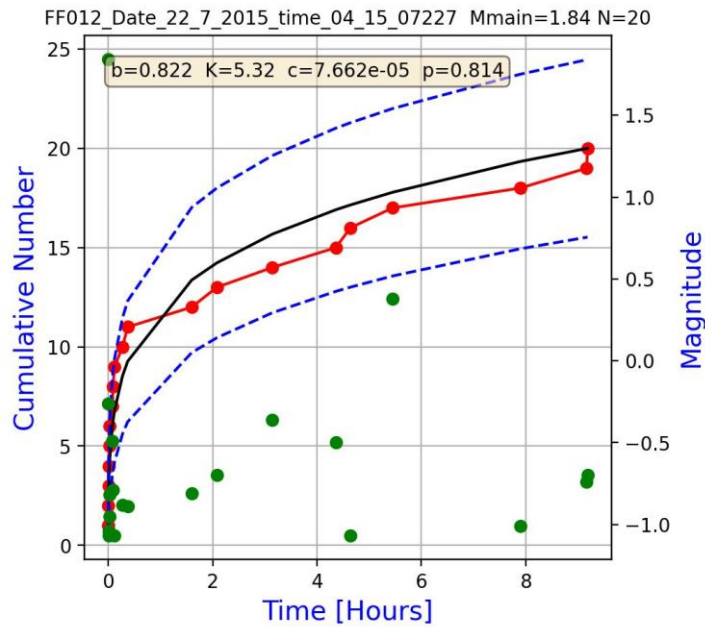


Fig.4.12 Notation as in Fig.4.11

Sq.No	Date	Time	X	Y	Z	M main	Vol	b	K	p	c	Ta [h]	Ra [m]	M2	N	dl2 [m]	dt2 [h]
13	'16.8.2015'	'19:59:09.589'	-6440.5	3358.1	-1143.3	1.58	GMZ_BI_34_v2	1.05	35.90	0.63	2.000000	24	175	0.16	21	105.17	14.70

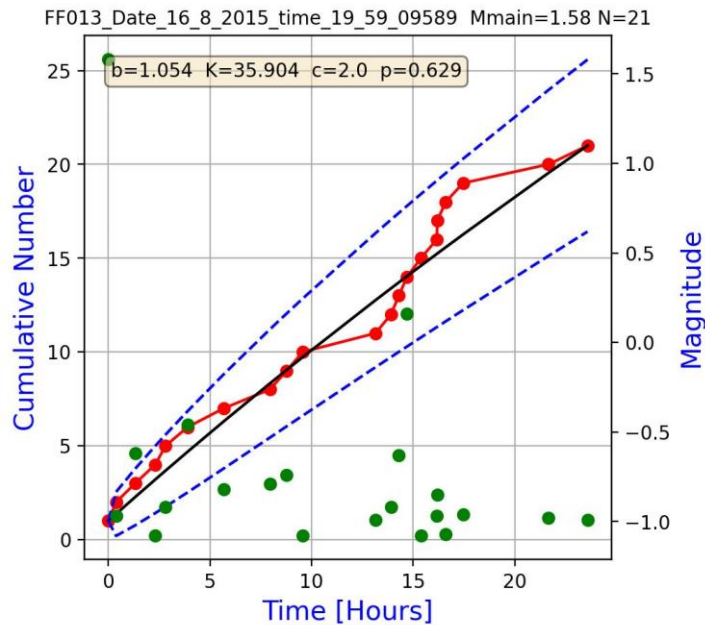


Fig.4.13 Cumulative curves of the aftershocks in time: thick line – model cumulative numbers after the identified best fit MOF model; dashed lines – error bounds; red circles – real cumulative numbers

Sq.No	Date	Time	X	Y	Z	M main	Vol	b	K	p	c	Ta [h]	Ra [m]	M2	N	dl2 [m]	dt2 [h]
16	'10.9.2015'	'08:51:45.498'	-6303.2	2635.3	-1127.1	2.1	GMZ_BI_26-30	0.69	11.72	0.92	0.000536	15	150	0.66	54	91.35	6.22

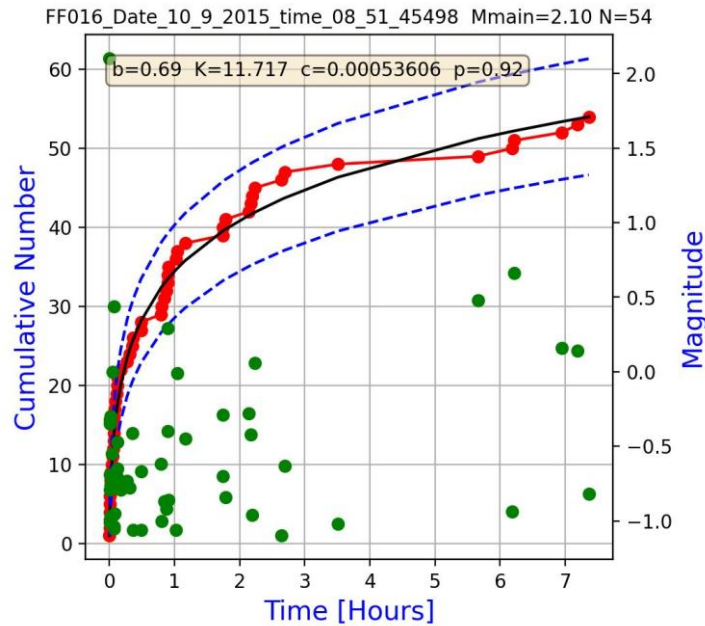


Fig.4.14 Cumulative curves of the aftershocks in time: thick line – model cumulative numbers after the identified best fit MOF model; dashed lines – error bounds; red circles – real cumulative numbers

Sq.No	Date	Time	X	Y	Z	M main	Vol	b	K	p	c	Ta [h]	Ra [m]	M2	N	dl2 [m]	dt2 [h]
17	'10.9.2015'	'16:17:26.345'	-6286.4	2627.6	-1120.9	1.62	GMZ_BI_26-30	0.81	8.18	0.91	0.000469	12	175	0.14	39	121.50	0.06

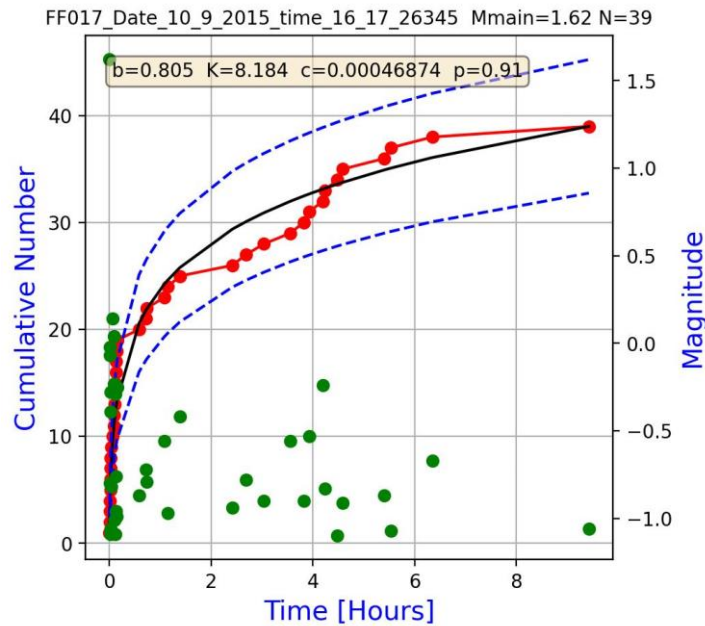


Fig.4.15 Cumulative curves of the aftershocks in time: thick line – model cumulative numbers after the identified best fit MOF model; dashed lines – error bounds; red circles – real cumulative numbers

Sq.No	Date	Time	X	Y	Z	M main	Vol	b	K	p	c	Ta [h]	Ra [m]	M2	N	dl2 [m]	dt2 [h]
18	'17.9.2015'	'13:30:33.860'	-6319.3	2595.2	-1198.6	2.14	GMZ_BI_26-30	0.84	24.10	0.98	0.000748	45	275	0.79	176	222.72	19.36

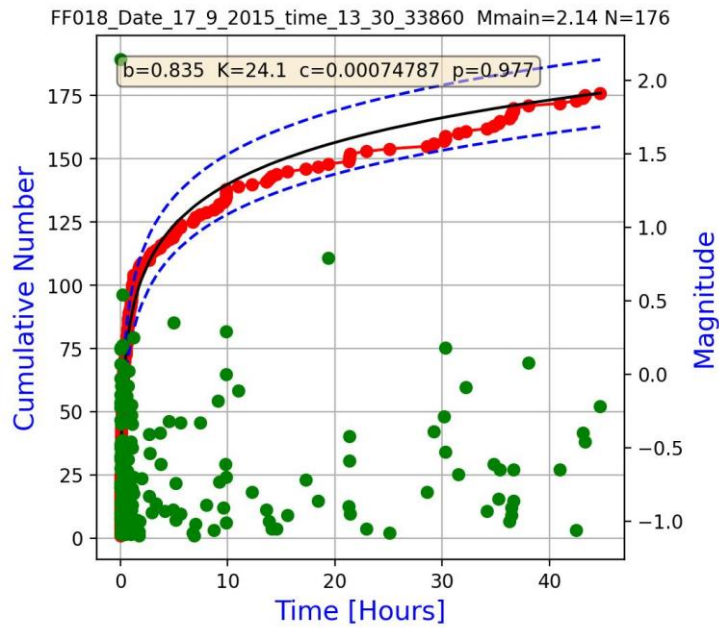


Fig.4.16 Cumulative curves of the aftershocks in time: thick line – model cumulative numbers after the identified best fit MOF model; dashed lines – error bounds; red circles – real cumulative numbers

Sq.No	Date	Time	X	Y	Z	M main	Vol	b	K	p	c	Ta [h]	Ra [m]	M2	N	dl2 [m]	dt2 [h]
19	'24.9.2015'	'00:04:52.980'	-6301	2916	-1116	2.09	GMZ_BI_26-30	0.77	15.70	0.79	0.000082	18	200	0.45	61	67.06	0.00

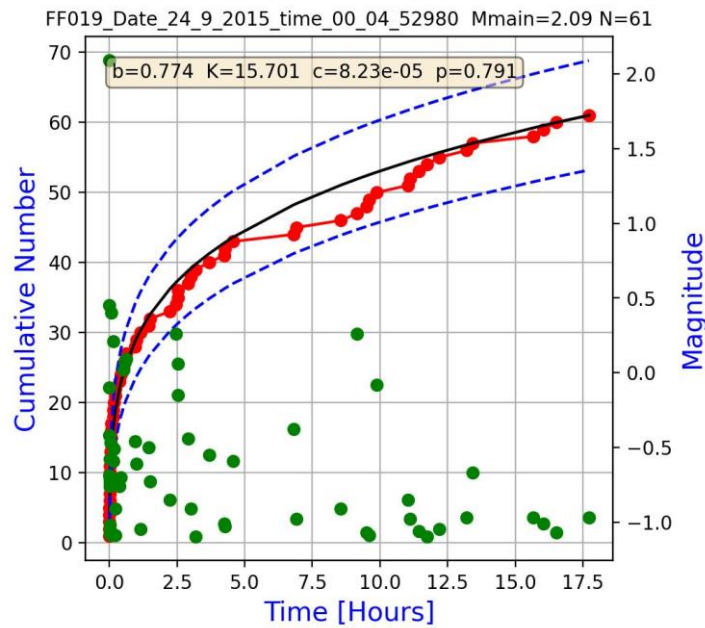


Fig.4.17 Cumulative curves of the aftershocks in time: thick line – model cumulative numbers after the identified best fit MOF model; dashed lines – error bounds; red circles – real cumulative numbers

Sq.No	Date	Time	X	Y	Z	M main	Vol	b	K	p	c	Ta [h]	Ra [m]	M2	N	dl2 [m]	dt2 [h]
20	'13.10.2015'	'22:19:44.791'	-6322.1	2381.1	-1027.1	1.68	GMZ_BI_15-26	0.48	5.93	0.60	0.000354	9	175	0.93	10	66.47	1.58

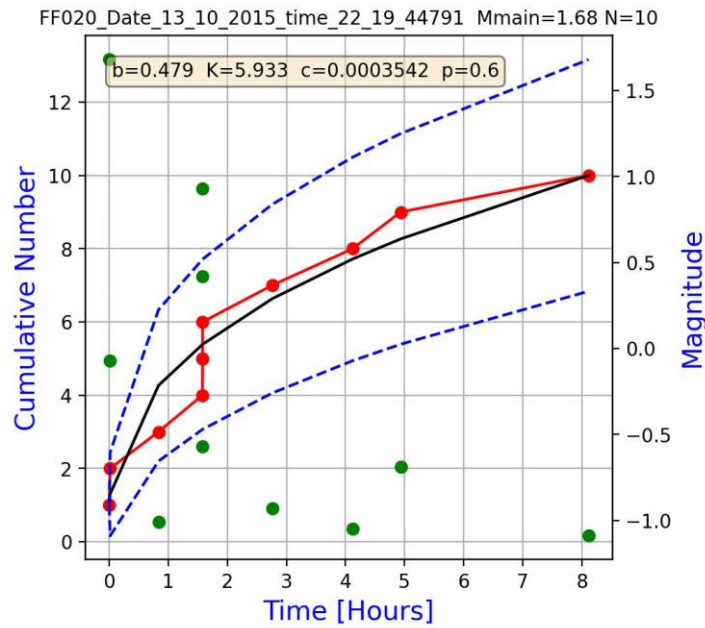


Fig.4.18 Cumulative curves of the aftershocks in time: thick line – model cumulative numbers after the identified best fit MOF model; dashed lines – error bounds; red circles – real cumulative numbers

Sq.No	Date	Time	X	Y	Z	M main	Vol	b	K	p	c	Ta [h]	Ra [m]	M2	N	dl2 [m]	dt2 [h]
25	'15.3.2016'	'03:50:28.289'	-6565.8	4150.6	-1077.8	1.86	GMZ_BI_38	0.70	0.92	1.13	0.001001	9	175	-0.27	10	77.78	0.13

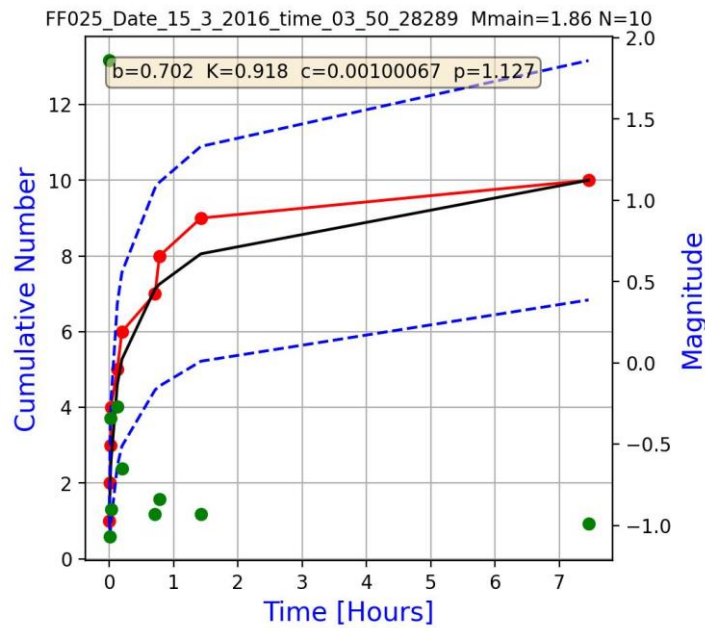


Fig.4.19 Cumulative curves of the aftershocks in time: thick line – model cumulative numbers after the identified best fit MOF model; dashed lines – error bounds; red circles – real cumulative numbers

Sq.No	Date	Time	X	Y	Z	M main	Vol	b	K	p	c	Ta [h]	Ra [m]	M2	N	dl2 [m]	dt2 [h]
26	'7.4.2016'	'01:36:57.699'	-6551.8	4508.8	-1123.2	2.4	GMZ_BI_41	0.72	6.53	0.82	0.001759	21	225	0.01	23	116.20	0.06

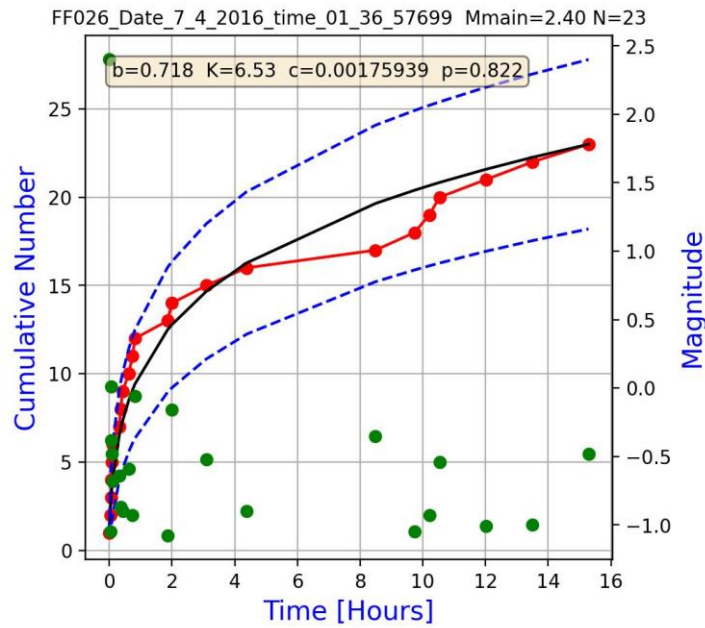


Fig.4.20 Cumulative curves of the aftershocks in time: thick line – model cumulative numbers after the identified best fit MOF model; dashed lines – error bounds; red circles – real cumulative numbers

Sq.No	Date	Time	X	Y	Z	M main	Vol	b	K	p	c	Ta [h]	Ra [m]	M2	N	dl2 [m]	dt2 [h]
27	'3.5.2016'	'07:29:06.907'	-6555	4047.5	-1088.6	2.05	GMZ_BI_38	0.82	12.89	0.74	0.000084	15	275	0.2	37	134.27	1.40

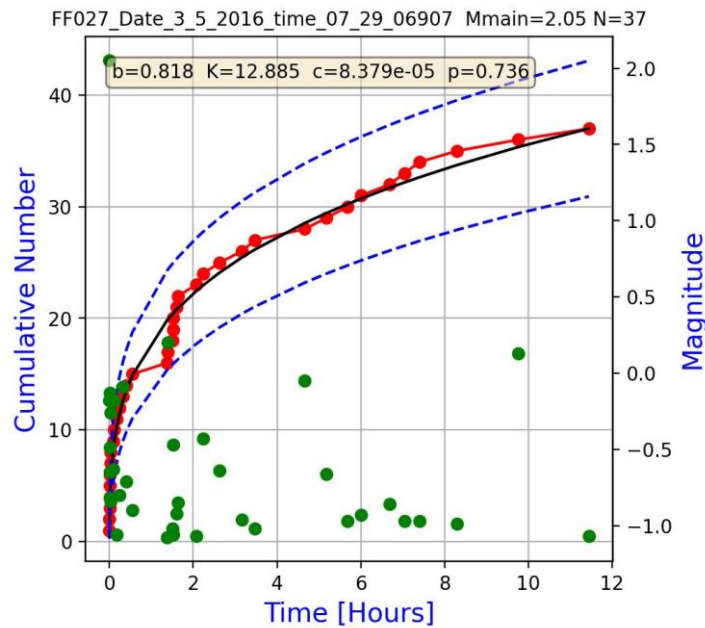


Fig.4.21 Cumulative curves of the aftershocks in time: thick line – model cumulative numbers after the identified best fit MOF model; dashed lines – error bounds; red circles – real cumulative numbers

Sq.No	Date	Time	X	Y	Z	M main	Vol	b	K	p	c	Ta [h]	Ra [m]	M2	N	dl2 [m]	dt2 [h]
28	'19.5.2016'	'19:03:59.971'	-6299.4	2670.8	-1007.4	1.51	GMZ_BI_26-30	0.47	2.91	1.00	0.053993	9	150	-0.19	5	85.82	3.89

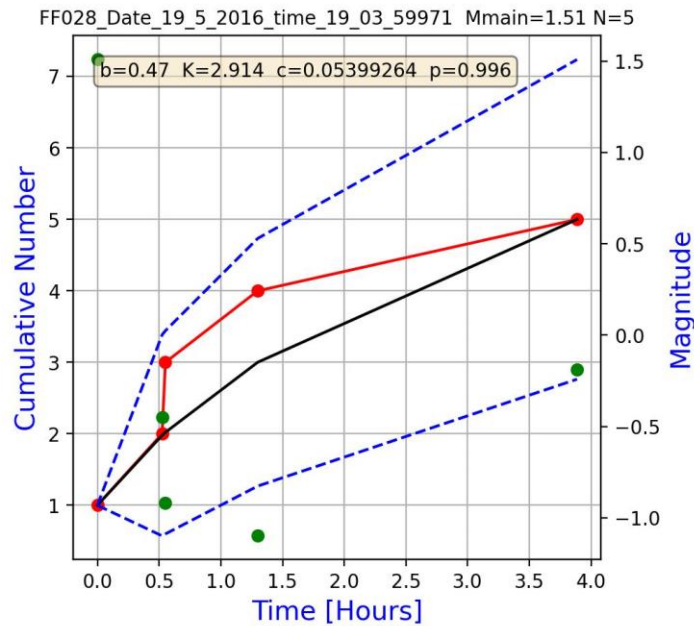


Fig.4.22 Cumulative curves of the aftershocks in time: thick line – model cumulative numbers after the identified best fit MOF model; dashed lines – error bounds; red circles – real cumulative numbers

Sq.No	Date	Time	X	Y	Z	M main	Vol	b	K	p	c	Ta [h]	Ra [m]	M2	N	dl2 [m]	dt2 [h]
29	'22.5.2016'	'02:31:16.146'	-6406.1	3355.1	-1127.3	1.88	GMZ_BI_34_v2	0.75	23.22	0.78	0.000065	24	225	1.12	92	88.98	0.02

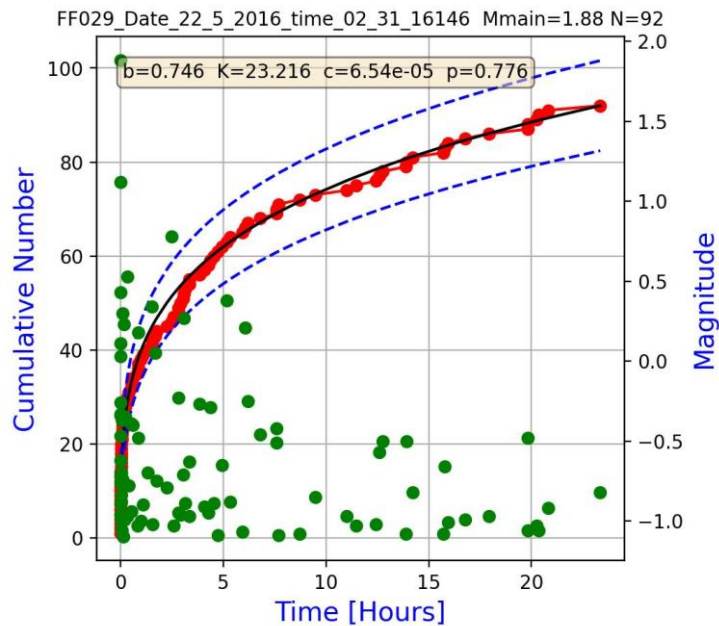


Fig.4.23 Cumulative curves of the aftershocks in time: thick line – model cumulative numbers after the identified best fit MOF model; dashed lines – error bounds; red circles – real cumulative numbers

Sq.No	Date	Time	X	Y	Z	M main	Vol	b	K	p	c	Ta [h]	Ra [m]	M2	N	dl2 [m]	dt2 [h]
31	'26.5.2016'	'21:59:36.899'	-6426.1	3475	-1081.1	1.55	GMZ_Bl_34_v2	0.72	34.63	0.82	0.000105	36	250	1.18	167	30.52	0.01

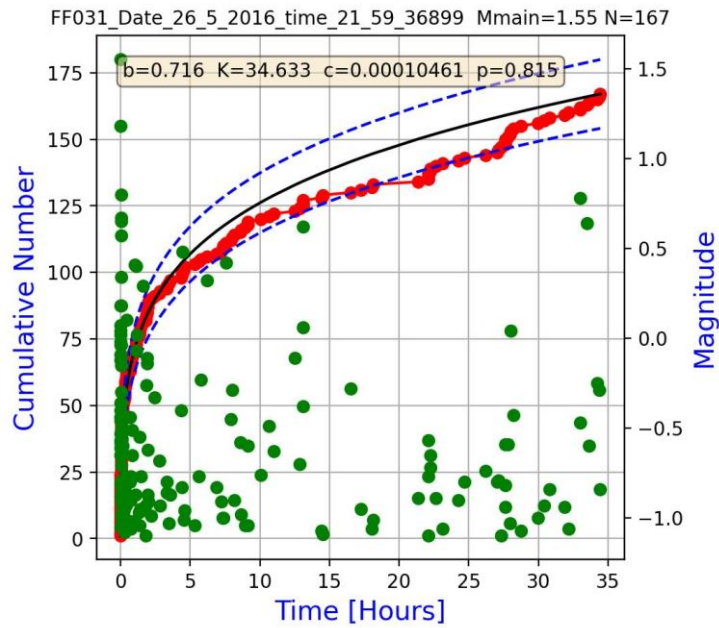


Fig.4.24 Cumulative curves of the aftershocks in time: thick line – model cumulative numbers after the identified best fit MOF model; dashed lines – error bounds; red circles – real cumulative numbers

Sq.No	Date	Time	X	Y	Z	M main	Vol	b	K	p	c	Ta [h]	Ra [m]	M2	N	dl2 [m]	dt2 [h]
33	'22.7.2016'	'10:59:35.670'	-6300	2569.5	-1070.8	2.52	GMZ_Bl_26-30	0.86	25.64	0.88	0.000377	60	300	0.59	158	119.87	18.97

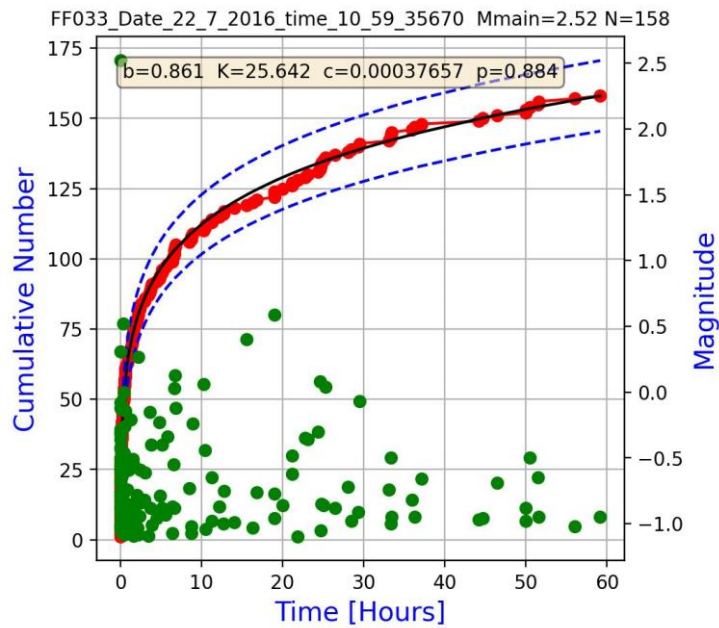


Fig.4.25 Cumulative curves of the aftershocks in time: thick line – model cumulative numbers after the identified best fit MOF model; dashed lines – error bounds; red circles – real cumulative numbers

Sq.No	Date	Time	X	Y	Z	M main	Vol	b	K	p	c	Ta [h]	Ra [m]	M2	N	dl2 [m]	dt2 [h]
34	'13.8.2016'	'11:52:45.992'	-6462.5	3472.3	-1072.4	1.96	GMZ_BI_34_v2	0.67	6.97	0.77	0.000163	9	200	0.38	21	141.39	0.11

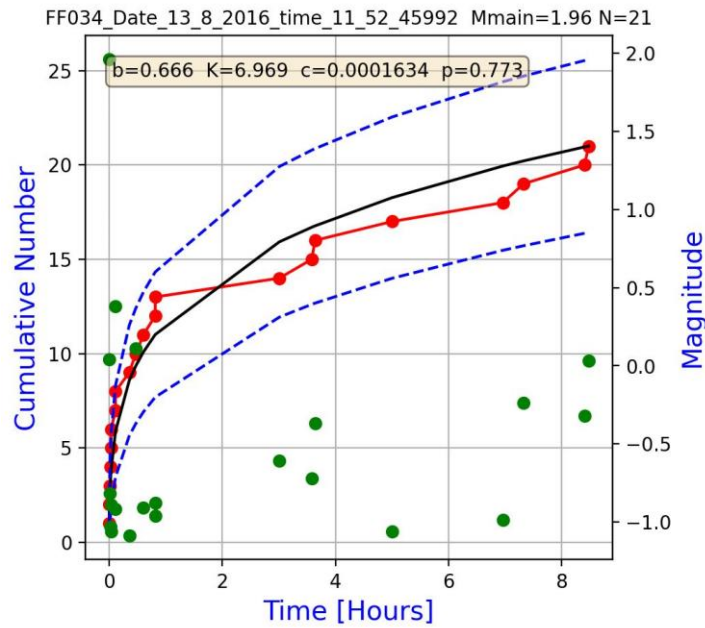


Fig.4.26 Cumulative curves of the aftershocks in time: thick line – model cumulative numbers after the identified best fit MOF model; dashed lines – error bounds; red circles – real cumulative numbers

Sq.No	Date	Time	X	Y	Z	M main	Vol	b	K	p	c	Ta [h]	Ra [m]	M2	N	dl2 [m]	dt2 [h]
35	'25.8.2016'	'09:59:31.061'	-6264.4	1263.1	-1128.4	1.61	GMZ_BI_12-15	1.25	230.60	0.60	1.050746	6	200	-0.4	53	81.13	0.75

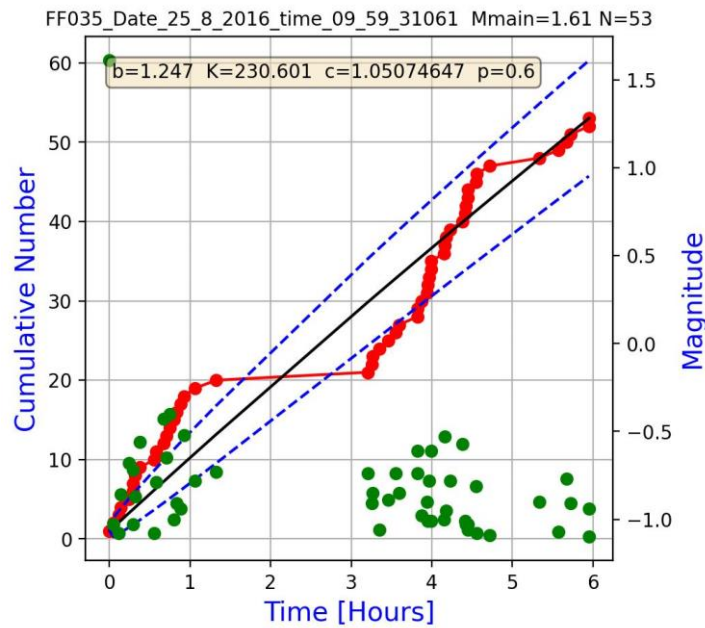


Fig.4.27 Cumulative curves of the aftershocks in time: thick line – model cumulative numbers after the identified best fit MOF model; dashed lines – error bounds; red circles – real cumulative numbers

Sq.No	Date	Time	X	Y	Z	M main	Vol	b	K	p	c	Ta [h]	Ra [m]	M2	N	dl2 [m]	dt2 [h]
36	'20.9.2016'	'05:47:51.609'	-6367.6	2918.1	-1168.4	2.13	GMZ_BI_26-30	0.81	26.85	0.82	0.000328	24	250	0.9	114	191.56	0.26

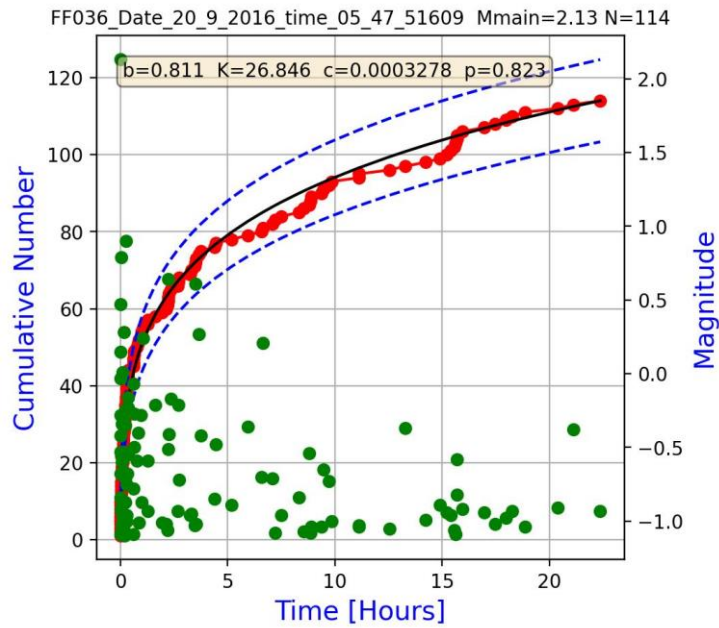


Fig.4.28 Cumulative curves of the aftershocks in time: thick line – model cumulative numbers after the identified best fit MOF model; dashed lines – error bounds; red circles – real cumulative numbers

Sq.No	Date	Time	X	Y	Z	M main	Vol	b	K	p	c	Ta [h]	Ra [m]	M2	N	dl2 [m]	dt2 [h]
37	'24.9.2016'	'08:11:27.279'	-6278.5	2168.8	-1020.8	1.88	GMZ_BI_15-26	0.93	4.34	0.89	0.000076	24	175	-0.31	25	102.25	17.37

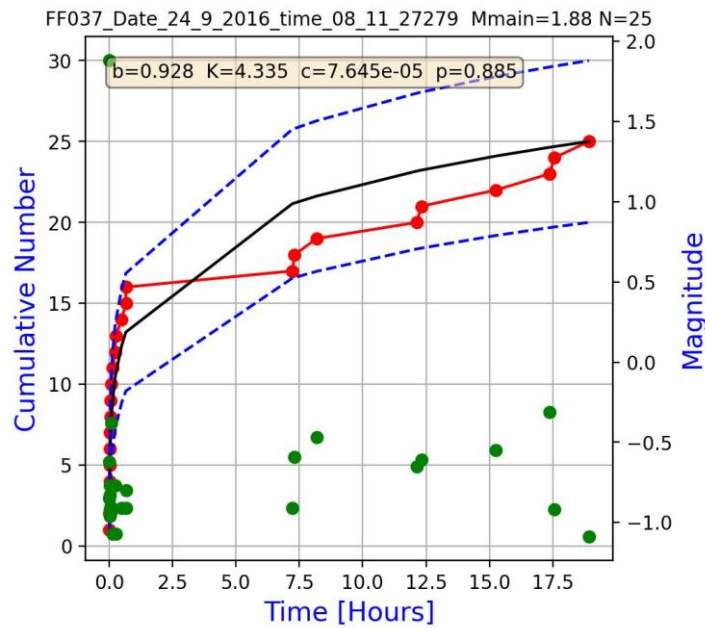


Fig.4.29 Cumulative curves of the aftershocks in time: thick line – model cumulative numbers after the identified best fit MOF model; dashed lines – error bounds; red circles – real cumulative numbers

Sq.No	Date	Time	X	Y	Z	M main	Vol	b	K	p	c	Ta [h]	Ra [m]	M2	N	dl2 [m]	dt2 [h]
38	'1.10.2016'	'05:58:22.947'	-6661.9	4111.5	-1106.5	1.75	GMZ_BI_38	0.63	21.91	0.66	0.000107	12	275	1.34	49	219.73	7.09

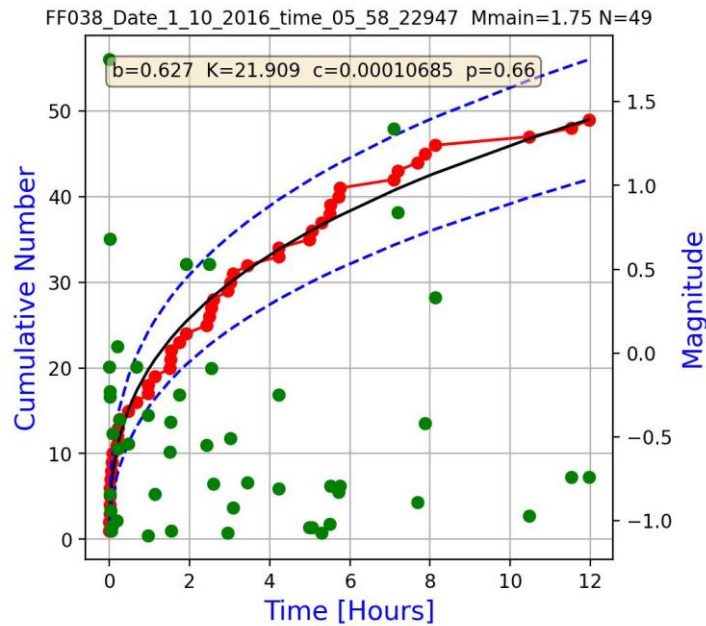


Fig.4.30 Cumulative curves of the aftershocks in time: thick line – model cumulative numbers after the identified best fit MOF model; dashed lines – error bounds; red circles – real cumulative numbers

Sq.No	Date	Time	X	Y	Z	M main	Vol	b	K	p	c	Ta [h]	Ra [m]	M2	N	dl2 [m]	dt2 [h]
39	'6.11.2016'	'06:52:15.830'	-6388.4	3386.5	-1114.5	1.58	GMZ_BI_34_v2	0.93	33.69	0.60	0.000078	21	200	1	78	89.01	2.27

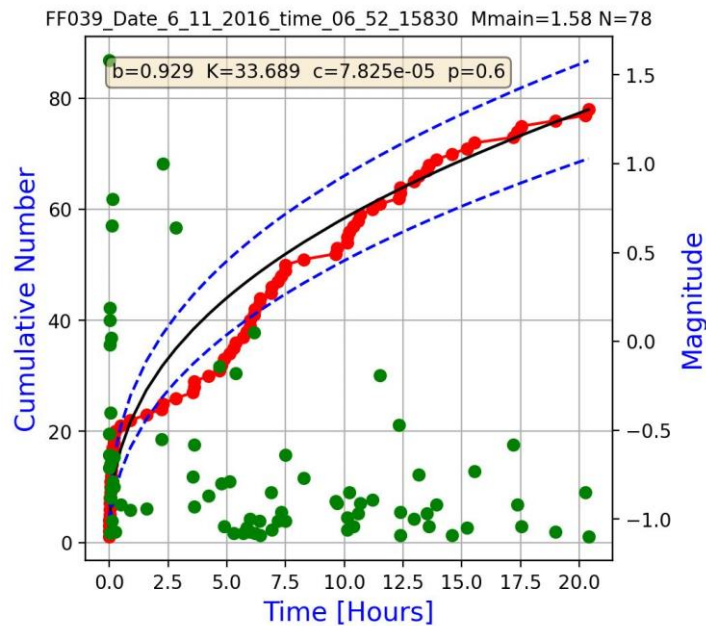


Fig.4.31 Cumulative curves of the aftershocks in time: thick line – model cumulative numbers after the identified best fit MOF model; dashed lines – error bounds; red circles – real cumulative numbers

Sq.No	Date	Time	X	Y	Z	M main	Vol	b	K	p	c	Ta [h]	Ra [m]	M2	N	dl2 [m]	dt2 [h]
41	'26.12.2016'	'03:31:24.239'	-6424.9	3440.3	-1077.2	1.91	GMZ_BI_34_v2	0.70	5.62	1.15	0.000851	9	175	0.46	66	164.00	0.34

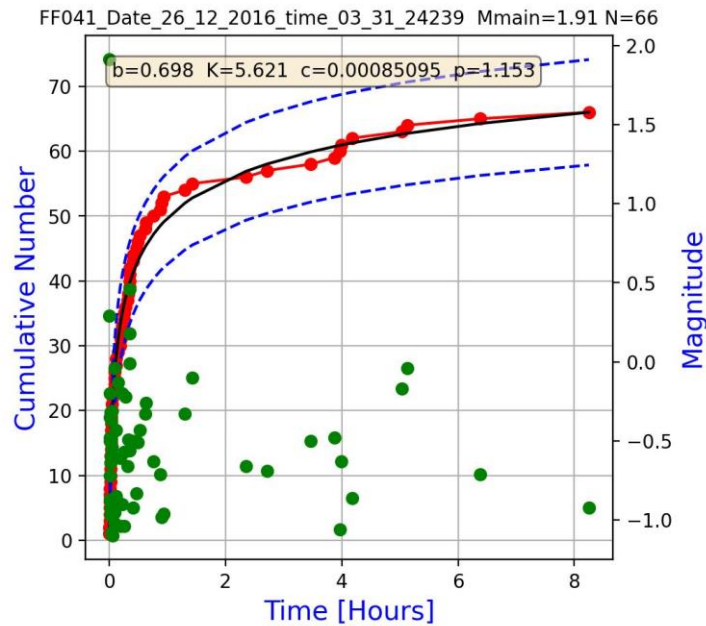


Fig.4.32 Cumulative curves of the aftershocks in time: thick line – model cumulative numbers after the identified best fit MOF model; dashed lines – error bounds; red circles – real cumulative numbers

Sq.No	Date	Time	X	Y	Z	M main	Vol	b	K	p	c	Ta [h]	Ra [m]	M2	N	dl2 [m]	dt2 [h]
42	'17.1.2017'	'07:16:03.212'	-6339.2	3011.6	-1153.9	1.51	GMZ_BI_26-30	0.98	12.75	0.75	0.000096	12	150	-0.08	39	37.92	0.23

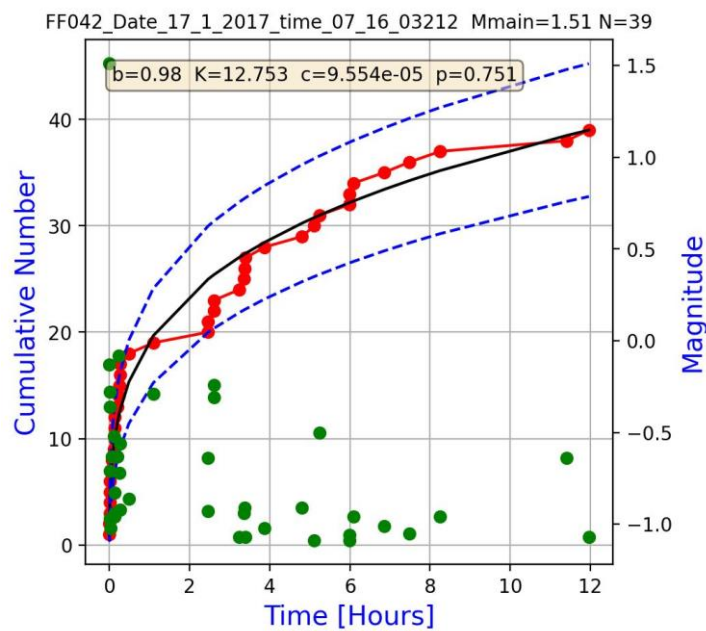


Fig.4.33 Cumulative curves of the aftershocks in time: thick line – model cumulative numbers after the identified best fit MOF model; dashed lines – error bounds; red circles – real cumulative numbers

Sq.No	Date	Time	X	Y	Z	M main	Vol	b	K	p	c	Ta [h]	Ra [m]	M2	N	dl2 [m]	dt2 [h]
43	'20.1.2017'	'03:52:06.529'	-6181.5	1997.1	-1020.2	1.87	GMZ_BI_15-26	0.69	9.67	0.66	0.000080	33	225	0.92	29	80.42	4.95

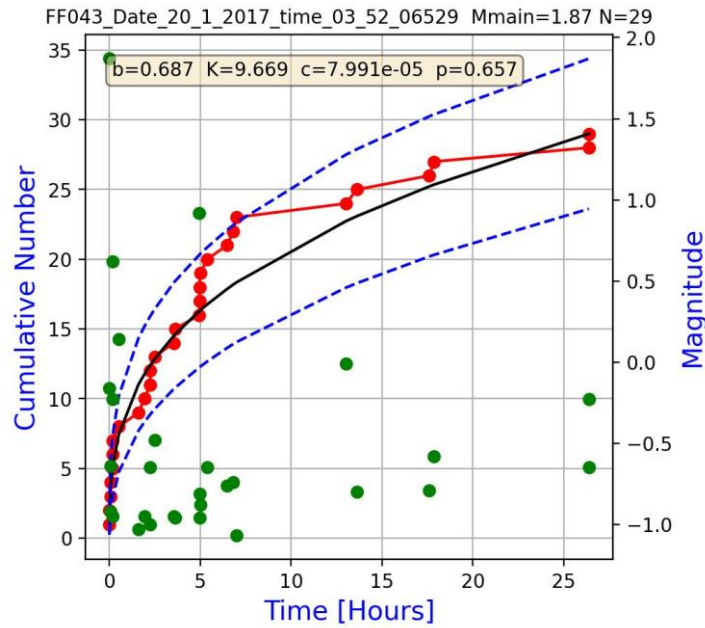


Fig.4.34 Cumulative curves of the aftershocks in time: thick line – model cumulative numbers after the identified best fit MOF model; dashed lines – error bounds; red circles – real cumulative numbers

Sq.No	Date	Time	X	Y	Z	M main	Vol	b	K	p	c	Ta [h]	Ra [m]	M2	N	dl2 [m]	dt2 [h]
45	'11.2.2017'	'05:40:12.759'	-6423.4	3316.8	-1123.5	1.75	GMZ_BI_34_v2	0.66	7.43	0.92	0.000205	9	225	0.84	39	42.45	0.00

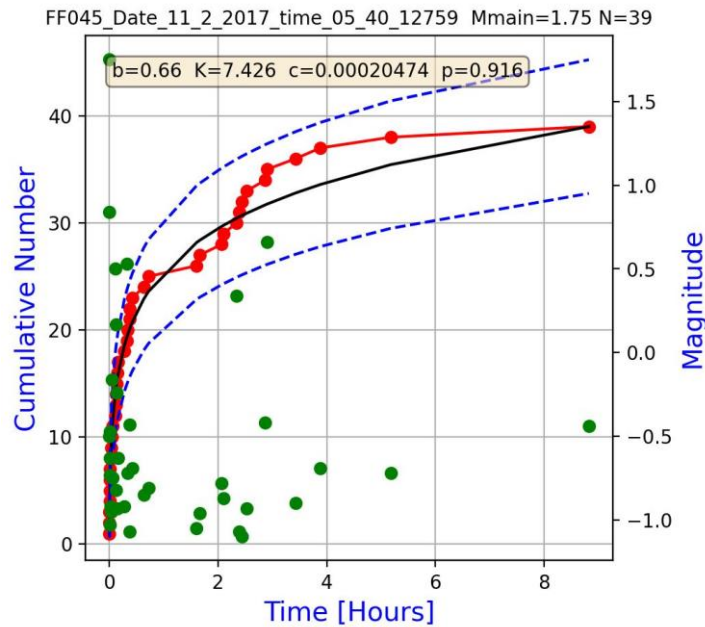


Fig.4.35 Cumulative curves of the aftershocks in time: thick line – model cumulative numbers after the identified best fit MOF model; dashed lines – error bounds; red circles – real cumulative numbers

Sq.No	Date	Time	X	Y	Z	M main	Vol	b	K	p	c	Ta [h]	Ra [m]	M2	N	dl2 [m]	dt2 [h]
46	'2.4.2017'	'19:42:37.152'	-6333.1	2923.1	-1129.4	1.89	GMZ_BI_26-30	0.84	10.91	0.60	0.000233	9	125	-0.03	18	72.23	6.31

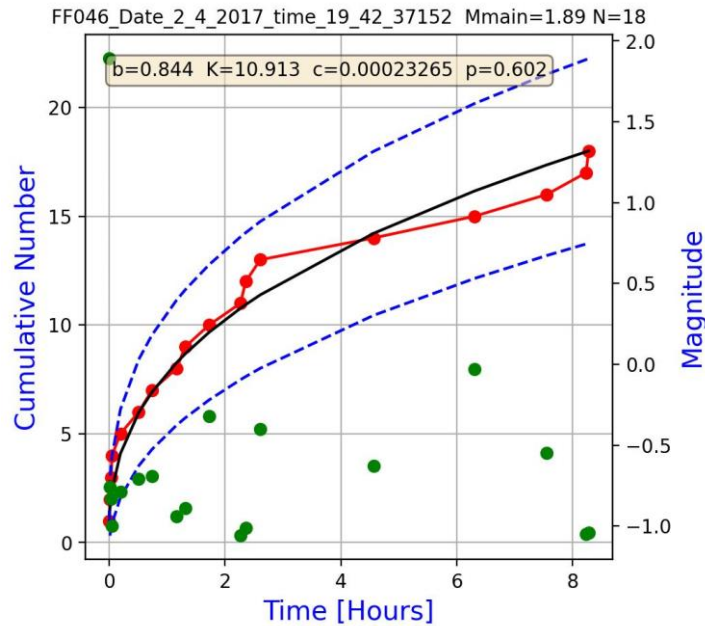


Fig.4.36 Cumulative curves of the aftershocks in time: thick line – model cumulative numbers after the identified best fit MOF model; dashed lines – error bounds; red circles – real cumulative numbers

Sq.No	Date	Time	X	Y	Z	M main	Vol	b	K	p	c	Ta [h]	Ra [m]	M2	N	dl2 [m]	dt2 [h]
47	'10.5.2017'	'04:54:33.435'	-6460.3	3447.1	-1147.1	2.05	GMZ_BI_34_v2	1.12	72.29	0.62	0.000077	48	275	0.58	238	91.33	0.00

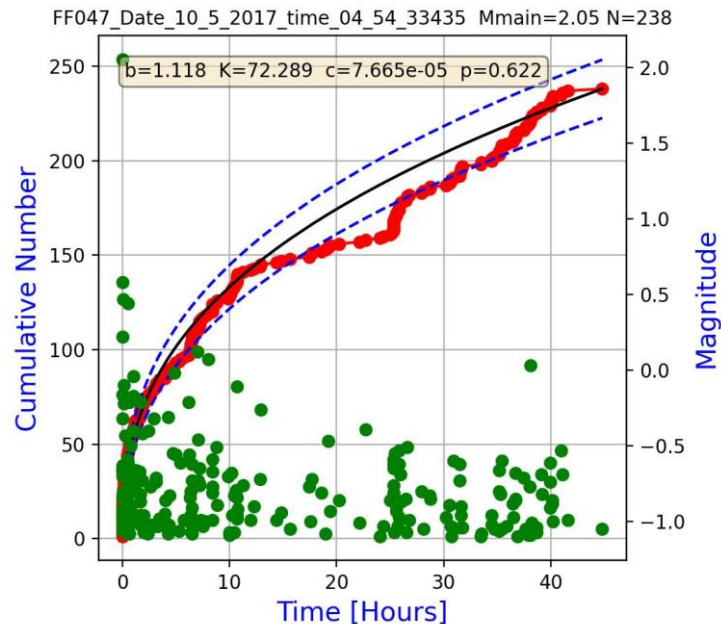


Fig.4.37 Cumulative curves of the aftershocks in time: thick line – model cumulative numbers after the identified best fit MOF model; dashed lines – error bounds; red circles – real cumulative numbers

Sq.No	Date	Time	X	Y	Z	M main	Vol	b	K	p	c	Ta [h]	Ra [m]	M2	N	dl2 [m]	dt2 [h]
50	'24.9.2017'	'05:48:57.552'	-6539.6	4017.7	-1099	1.56	GMZ_BI_38	0.53	5.45	0.69	0.000011	9	125	0.29	8	71.09	0.30

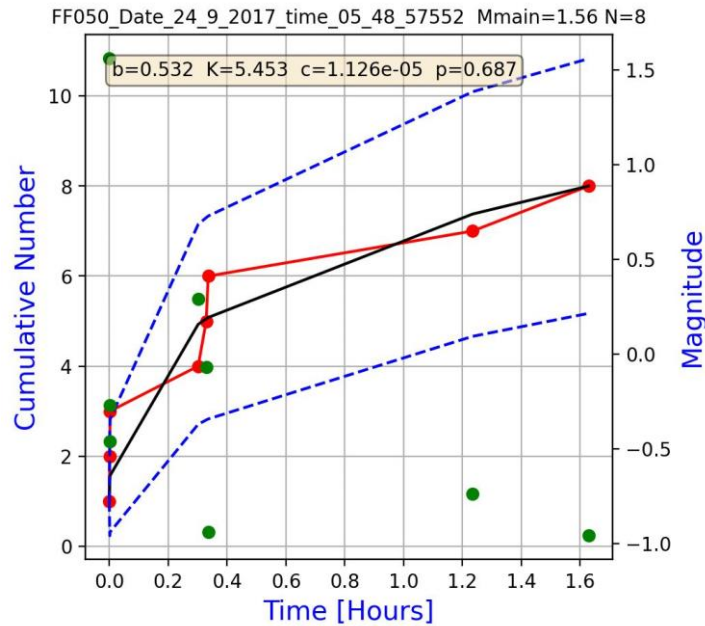


Fig.4.38 Cumulative curves of the aftershocks in time: thick line – model cumulative numbers after the identified best fit MOF model; dashed lines – error bounds; red circles – real cumulative numbers

Sq.No	Date	Time	X	Y	Z	M main	Vol	b	K	p	c	Ta [h]	Ra [m]	M2	N	dl2 [m]	dt2 [h]
51	'27.10.2017'	'22:51:15.302'	-6564.8	4580	-1163.1	1.64	GMZ_BI_41	0.66	2.09	0.97	0.001423	9	175	-0.1	11	19.27	0.01

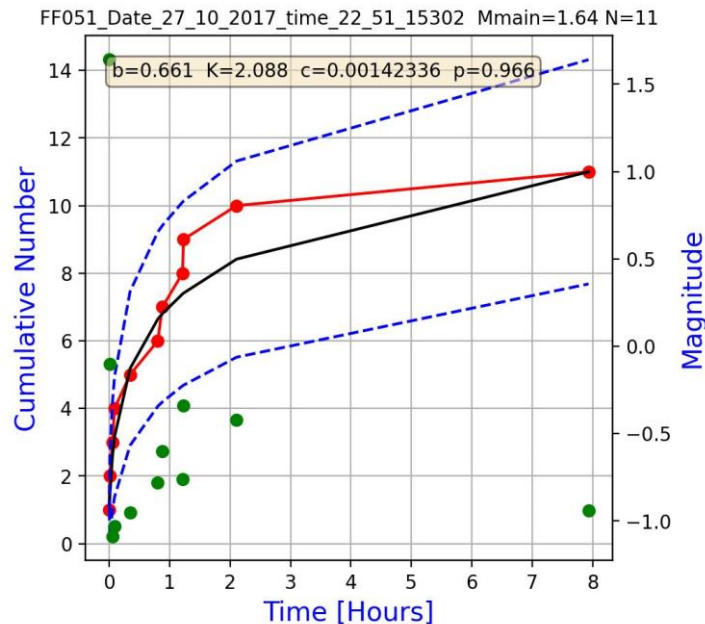


Fig.4.39 Cumulative curves of the aftershocks in time: thick line – model cumulative numbers after the identified best fit MOF model; dashed lines – error bounds; red circles – real cumulative numbers

Sq.No	Date	Time	X	Y	Z	M main	Vol	b	K	p	c	Ta [h]	Ra [m]	M2	N	dl2 [m]	dt2 [h]
52	'4.11.2017'	'13:14:44.823'	-6319.1	2543.3	-1210.9	1.69	GMZ_BI_26-30	0.63	1.66	1.06	0.000140	9	150	0.26	17	56.84	0.26

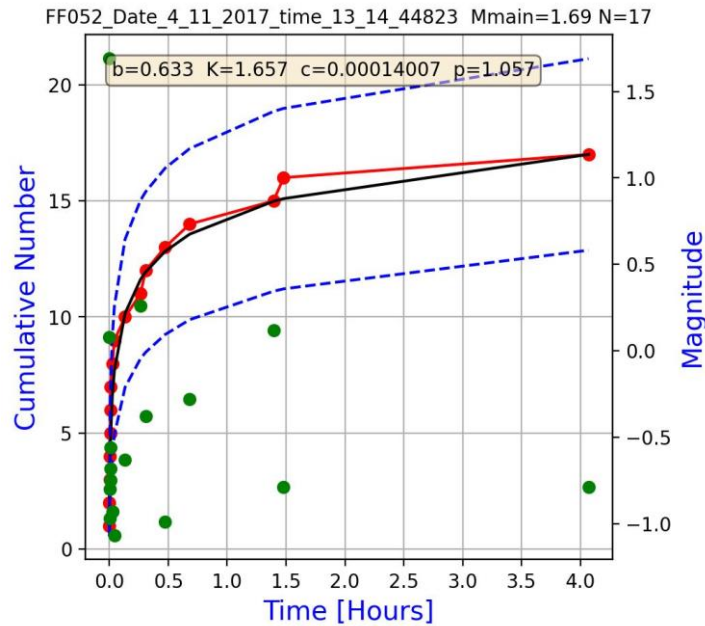


Fig.4.40 Cumulative curves of the aftershocks in time: thick line – model cumulative numbers after the identified best fit MOF model; dashed lines – error bounds; red circles – real cumulative numbers

Sq.No	Date	Time	X	Y	Z	M main	Vol	b	K	p	c	Ta [h]	Ra [m]	M2	N	dl2 [m]	dt2 [h]
53	'28.12.2017'	'09:15:37.747'	-6556.5	4567.5	-1149.2	1.54	GMZ_BI_41	0.57	4.93	0.61	0.000257	36	150	0.33	14	41.48	0.54

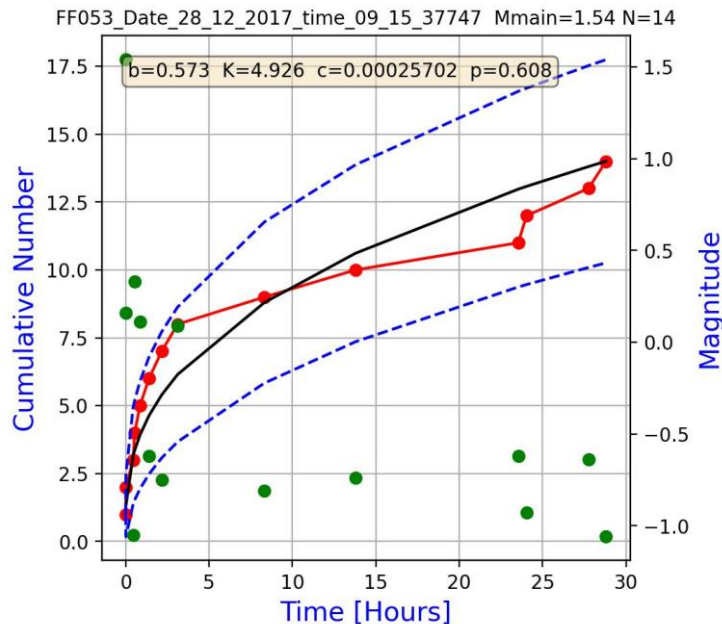


Fig.4.41 Cumulative curves of the aftershocks in time: thick line – model cumulative numbers after the identified best fit MOF model; dashed lines – error bounds; red circles – real cumulative numbers

Sq.No	Date	Time	X	Y	Z	M main	Vol	b	K	p	c	Ta [h]	Ra [m]	M2	N	dl2 [m]	dt2 [h]
54	'19.3.2018'	'11:05:04.002'	-6480.7	4662.7	-1161.3	1.5	GMZ_Bl_41	0.62	1.68	0.95	0.000378	9	175	0.41	10	136.03	0.32

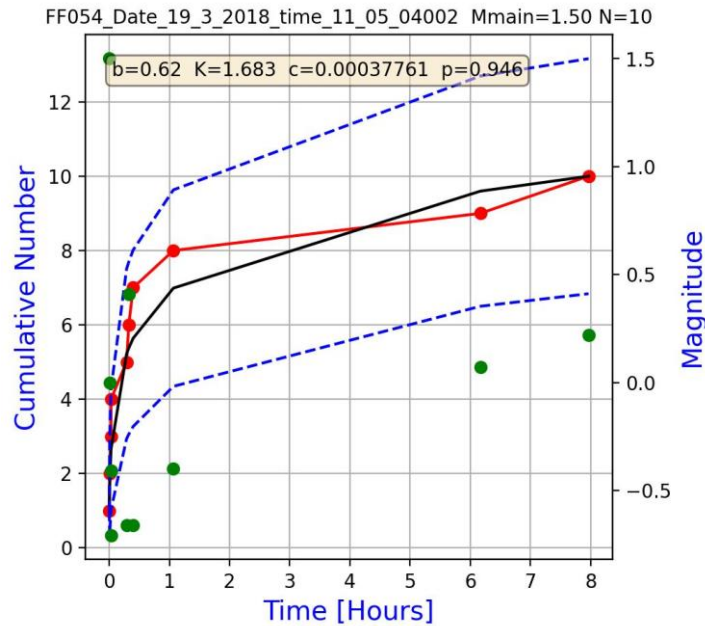


Fig.4.42 Cumulative curves of the aftershocks in time: thick line – model cumulative numbers after the identified best fit MOF model; dashed lines – error bounds; red circles – real cumulative numbers

Sq.No	Date	Time	X	Y	Z	M main	Vol	b	K	p	c	Ta [h]	Ra [m]	M2	N	dl2 [m]	dt2 [h]
55	'22.3.2018'	'03:45:50.852'	-6296.7	2781.1	-1099.3	2.28	GMZ_Bl_26-30	0.82	24.71	0.81	0.000138	9	200	1	85	66.54	0.01

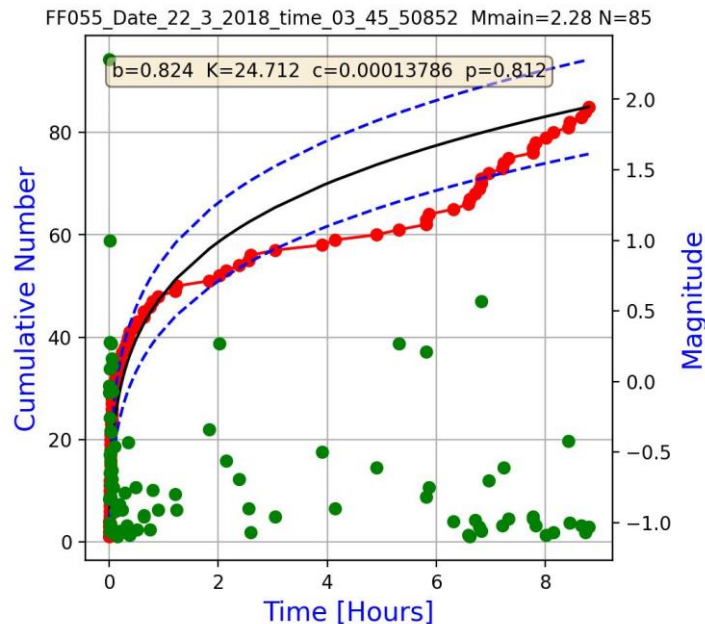


Fig.4.43 Cumulative curves of the aftershocks in time: thick line – model cumulative numbers after the identified best fit MOF model; dashed lines – error bounds; red circles – real cumulative numbers

Sq.No	Date	Time	X	Y	Z	M main	Vol	b	K	p	c	Ta [h]	Ra [m]	M2	N	dl2 [m]	dt2 [h]
56	'27.4.2018'	'06:19:59.886'	-6273	2580	-1092	1.66	GMZ_BI_26-30	1.18	26.21	0.60	0.000113	9	200	0	42	85.04	1.82

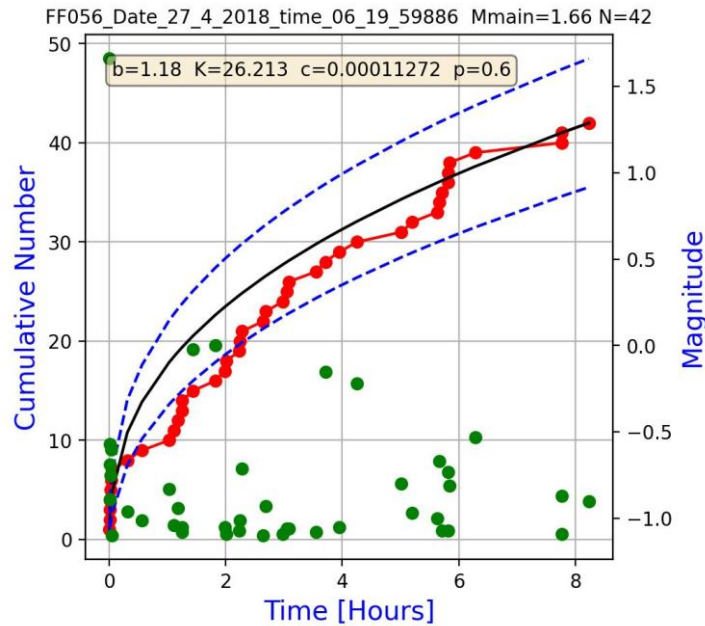


Fig.4.44 Cumulative curves of the aftershocks in time: thick line – model cumulative numbers after the identified best fit MOF model; dashed lines – error bounds; red circles – real cumulative numbers

Sq.No	Date	Time	X	Y	Z	M main	Vol	b	K	p	c	Ta [h]	Ra [m]	M2	N	dl2 [m]	dt2 [h]
60	'26.7.2018'	'08:49:45.927'	-6284	2654.6	-1192.6	1.67	GMZ_BI_26-30	1.16	308.35	1.20	2.000000	15	200	1.17	71	66.32	9.98

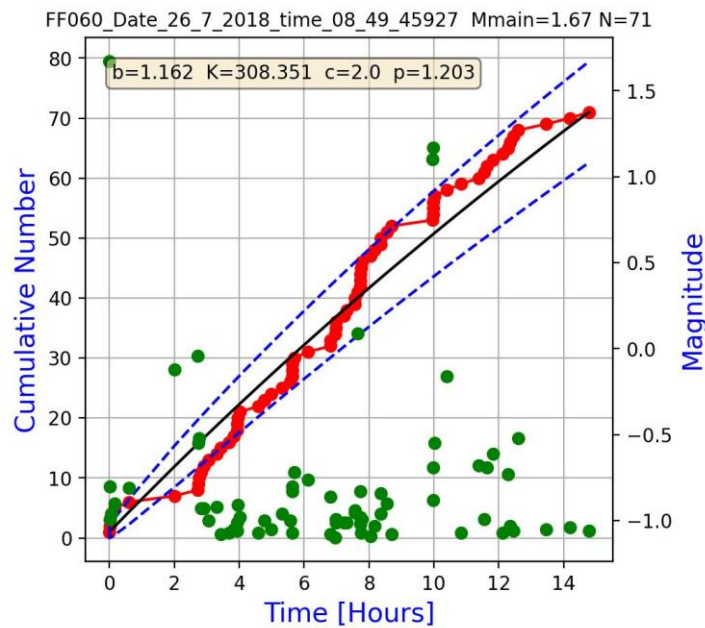


Fig.4.45 Cumulative curves of the aftershocks in time: thick line – model cumulative numbers after the identified best fit MOF model; dashed lines – error bounds; red circles – real cumulative numbers

Sq.No	Date	Time	X	Y	Z	M main	Vol	b	K	p	c	Ta [h]	Ra [m]	M2	N	dl2 [m]	dt2 [h]
61	'15.9.2018'	'02:40:06.819'	-6571.1	3680.8	-1064.3	1.51	GMZ_BI_38	0.41	2.84	0.72	0.000155	6	200	0.27	6	50.28	0.11

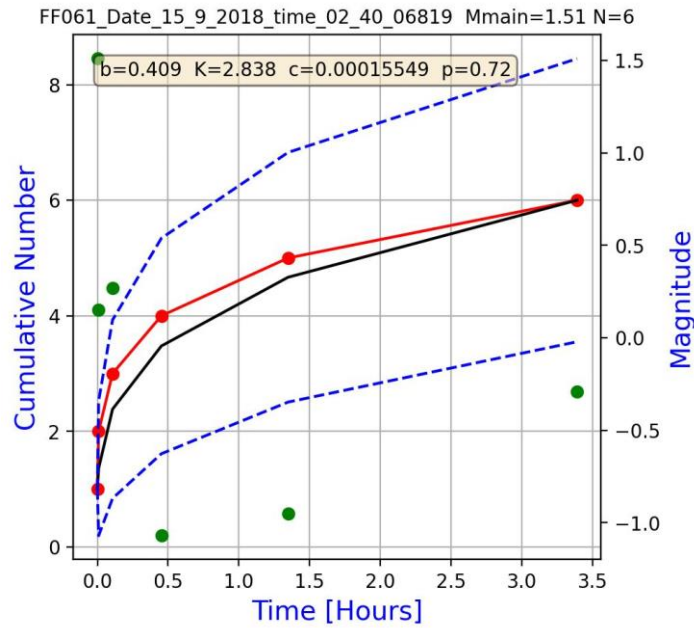


Fig.4.46 Cumulative curves of the aftershocks in time: thick line – model cumulative numbers after the identified best fit MOF model; dashed lines – error bounds; red circles – real cumulative numbers

Sq.No	Date	Time	X	Y	Z	M main	Vol	b	K	p	c	Ta [h]	Ra [m]	M2	N	dl2 [m]	dt2 [h]
62	'8.10.2018'	'17:08:14.094'	-6307.5	3246	-1035	1.65	GMZ_BI_34_v2	0.78	1.97	1.43	0.002297	9	150	0.52	57	43.27	0.86

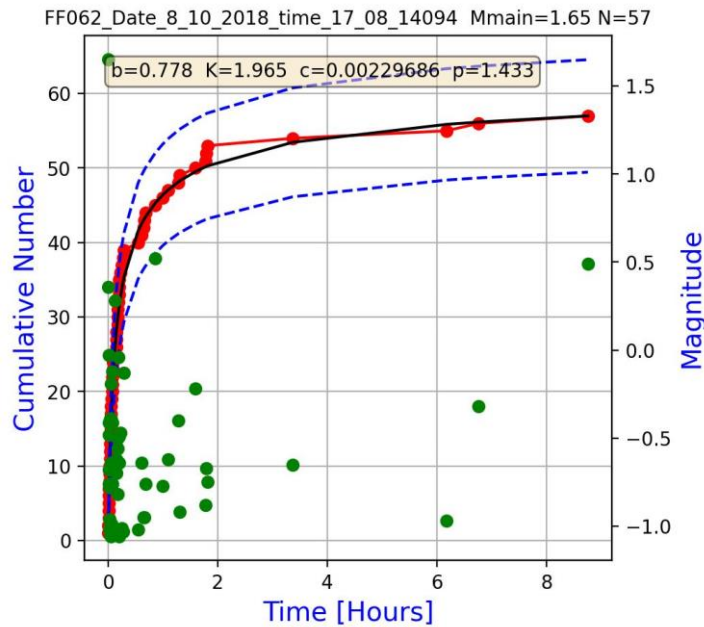


Fig.4.47 Cumulative curves of the aftershocks in time: thick line – model cumulative numbers after the identified best fit MOF model; dashed lines – error bounds; red circles – real cumulative numbers

Sq.No	Date	Time	X	Y	Z	M main	Vol	b	K	p	c	Ta [h]	Ra [m]	M2	N	dl2 [m]	dt2 [h]
63	'14.11.2018'	'02:53:53.823'	-6505.7	3818.4	-1055.7	1.5	GMZ_BI_38	0.65	6.89	1.05	0.000305	9	200	0.83	61	135.62	0.01

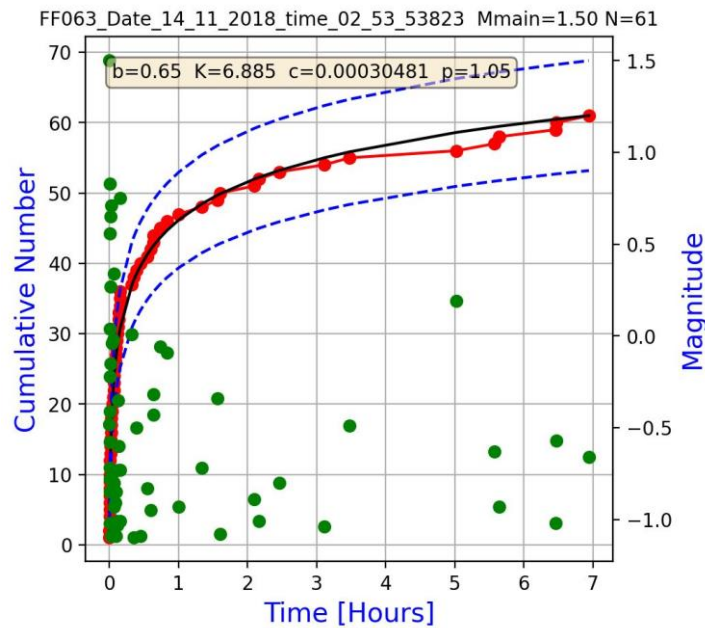


Fig.4.48 Cumulative curves of the aftershocks in time: thick line – model cumulative numbers after the identified best fit MOF model; dashed lines – error bounds; red circles – real cumulative numbers

Sq.No	Date	Time	X	Y	Z	M main	Vol	b	K	p	c	Ta [h]	Ra [m]	M2	N	dl2 [m]	dt2 [h]
64	'20.11.2018'	'01:21:12.132'	-6259.3	1872.4	-998.8	1.96	GMZ_BI_15-26	0.45	1.60	0.86	0.000179	9	175	0.37	7	65.30	6.55

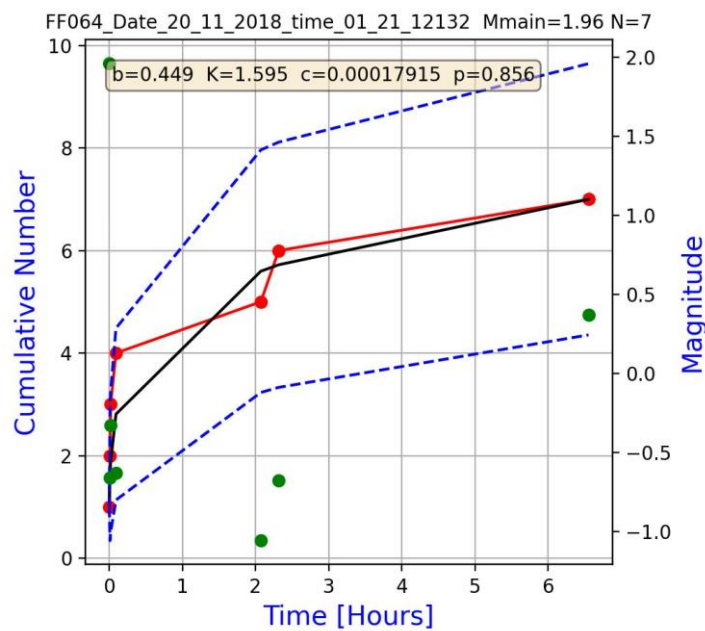


Fig.4.49 Cumulative curves of the aftershocks in time: thick line – model cumulative numbers after the identified best fit MOF model; dashed lines – error bounds; red circles – real cumulative numbers

Sq.No	Date	Time	X	Y	Z	M main	Vol	b	K	p	c	Ta [h]	Ra [m]	M2	N	dI2 [m]	dt2 [h]
65	'13.1.2019'	'03:43:02.700'	-6294.4	2782.4	-1099.4	1.79	GMZ_BI_26-30	1.01	14.97	0.84	0.000134	9	200	0.81	58	96.02	0.11

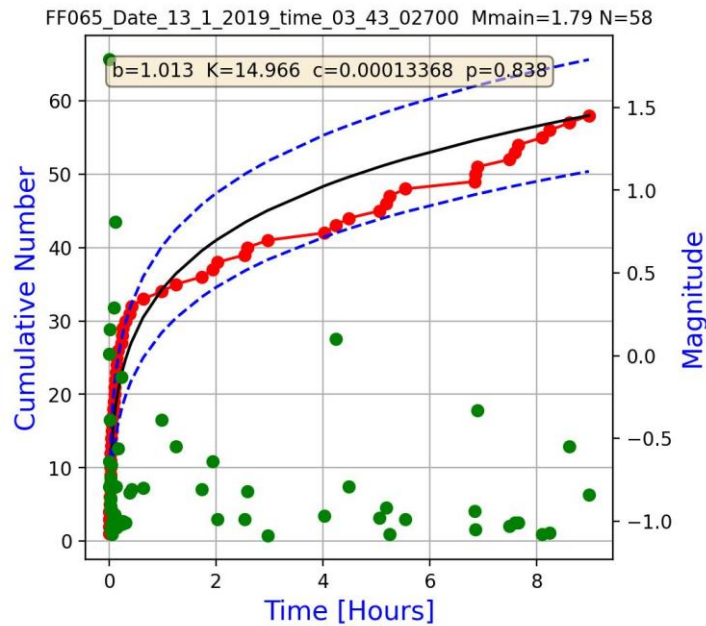


Fig.4.50 Cumulative curves of the aftershocks in time: thick line – model cumulative numbers after the identified best fit MOF model; dashed lines – error bounds; red circles – real cumulative numbers

Sq.No	Date	Time	X	Y	Z	M main	Vol	b	K	p	c	Ta [h]	Ra [m]	M2	N	dI2 [m]	dt2 [h]
66	'30.1.2019'	'21:02:53.948'	-6420.9	3369.8	-1112.5	2.3	GMZ_BI_34_v2	0.95	41.42	0.76	0.000172	42	250	0.52	175	224.06	0.01

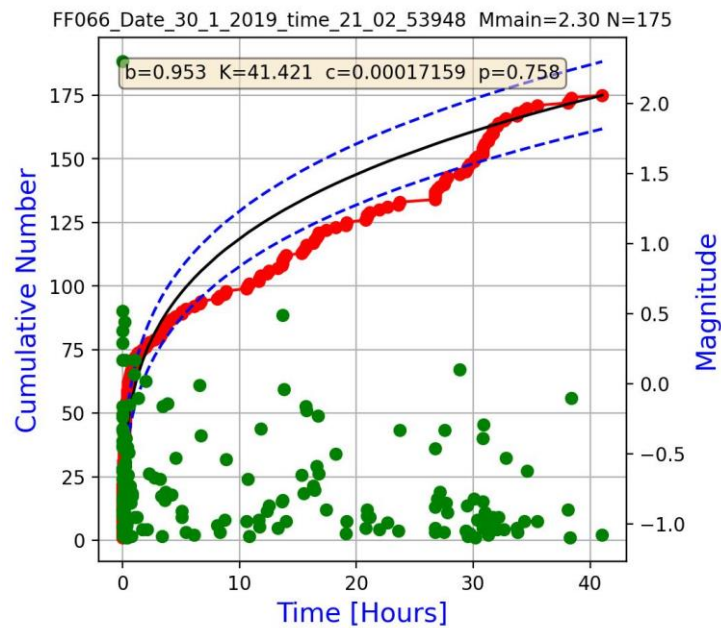


Fig.4.51 Cumulative curves of the aftershocks in time: thick line – model cumulative numbers after the identified best fit MOF model; dashed lines – error bounds; red circles – real cumulative numbers

Sq.No	Date	Time	X	Y	Z	M main	Vol	b	K	p	c	Ta [h]	Ra [m]	M2	N	dl2 [m]	dt2 [h]
67	'13.3.2019'	'10:04:20.393'	-6287.2	2751.2	-1153.4	1.69	GMZ_BI_26-30	0.90	4.39	0.90	0.000203	9	175	0.09	21	70.14	0.09

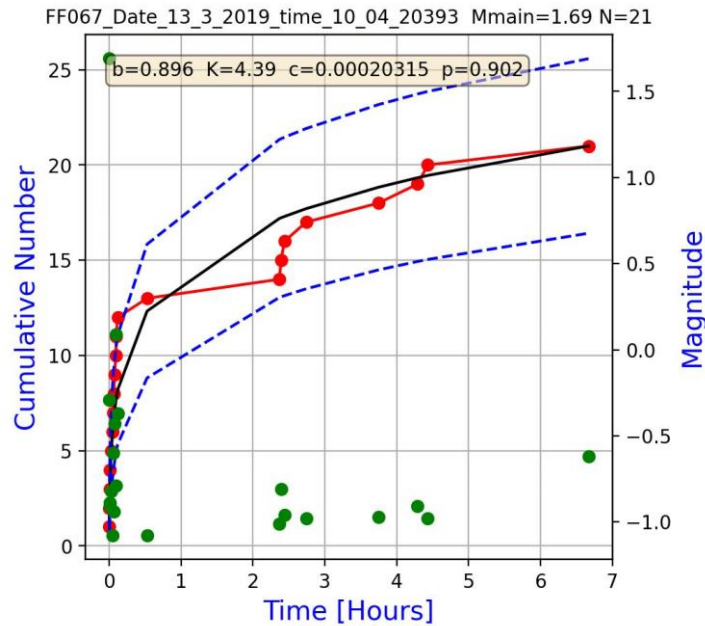


Fig.4.52 Cumulative curves of the aftershocks in time: thick line – model cumulative numbers after the identified best fit MOF model; dashed lines – error bounds; red circles – real cumulative numbers

Sq.No	Date	Time	X	Y	Z	M main	Vol	b	K	p	c	Ta [h]	Ra [m]	M2	N	dl2 [m]	dt2 [h]
70	'23.5.2019'	'01:31:36.184'	-6212.1	986.6	-975.8	1.65	GMZ_BI_04-12	1.05	10.65	0.62	0.000012	6	200	0.09	17	63.70	0.00

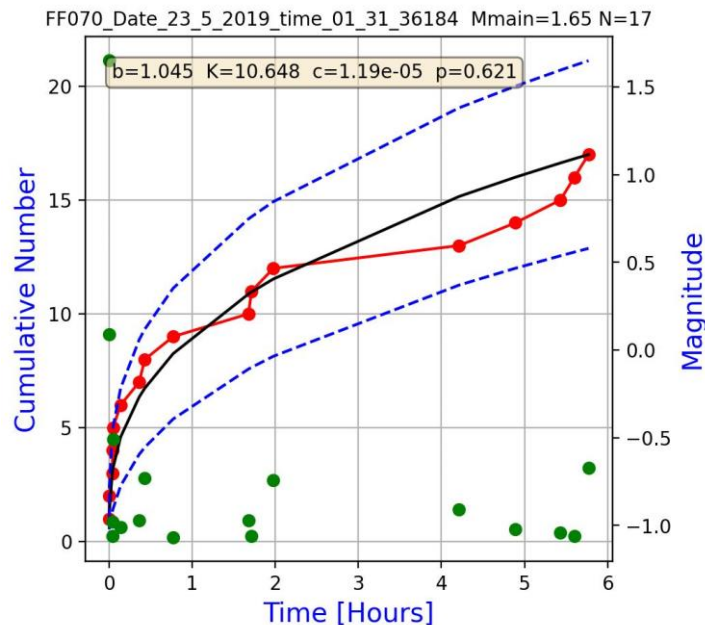


Fig.4.53 Cumulative curves of the aftershocks in time: thick line – model cumulative numbers after the identified best fit MOF model; dashed lines – error bounds; red circles – real cumulative numbers

Sq.No	Date	Time	X	Y	Z	M main	Vol	b	K	p	c	Ta [h]	Ra [m]	M2	N	dl2 [m]	dt2 [h]
71	'18.8.2019'	'20:04:44.133'	-6403.3	2265.7	-1049	1.6	GMZ_BI_15-26	0.79	6.97	0.61	0.001285	9	175	-0.26	11	44.48	5.27

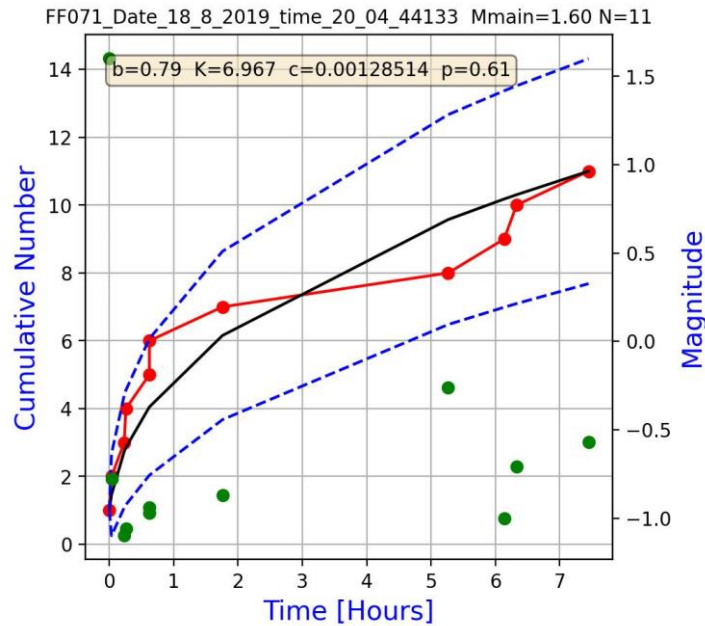


Fig.4.54 Cumulative curves of the aftershocks in time: thick line – model cumulative numbers after the identified best fit MOF model; dashed lines – error bounds; red circles – real cumulative numbers

Sq.No	Date	Time	X	Y	Z	M main	Vol	b	K	p	c	Ta [h]	Ra [m]	M2	N	dl2 [m]	dt2 [h]
72	'25.9.2019'	'11:22:29.943'	-6555.4	3835.3	-1152.9	1.81	GMZ_BI_38	0.67	4.29	0.92	0.000727	9	125	0.62	20	99.76	0.06

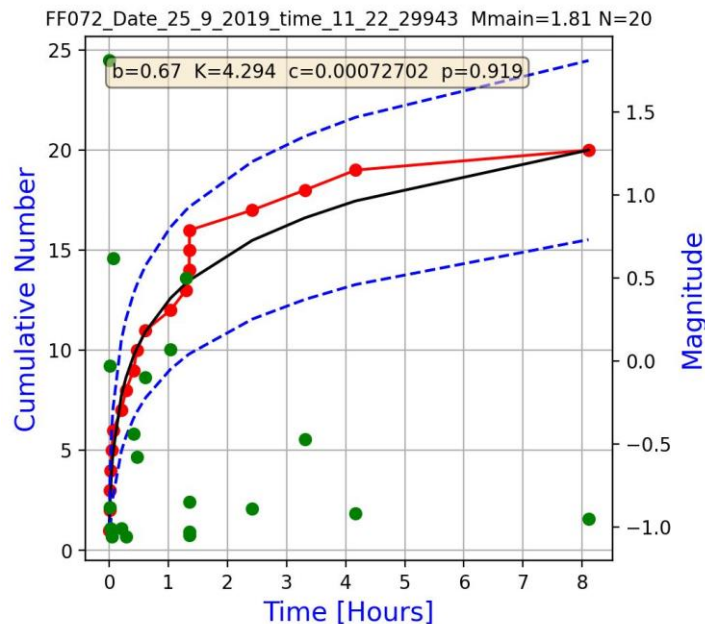


Fig.4.55 Cumulative curves of the aftershocks in time: thick line – model cumulative numbers after the identified best fit MOF model; dashed lines – error bounds; red circles – real cumulative numbers

Sq.No	Date	Time	X	Y	Z	M main	Vol	b	K	p	c	Ta [h]	Ra [m]	M2	N	dl2 [m]	dt2 [h]
73	'30.10.2019'	'01:32:08.388'	-6477.3	3582.8	-1050.3	1.55	GMZ_BI_34_v2	0.84	4.06	0.77	0.000155	18	200	0	14	105.81	0.90

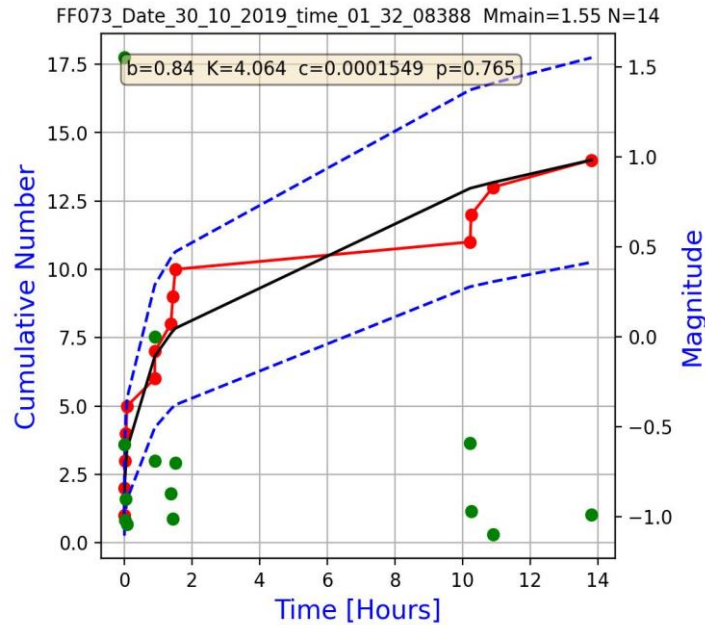


Fig.4.56 Cumulative curves of the aftershocks in time: thick line – model cumulative numbers after the identified best fit MOF model; dashed lines – error bounds; red circles – real cumulative numbers

Sq.No	Date	Time	X	Y	Z	M main	Vol	b	K	p	c	Ta [h]	Ra [m]	M2	N	dl2 [m]	dt2 [h]
74	'10.11.2019'	'01:32:54.938'	-6288.9	2614.7	-1203.4	2.46	GMZ_BI_26-30	0.89	12.08	1.00	0.001112	27	200	0.75	83	111.34	19.04

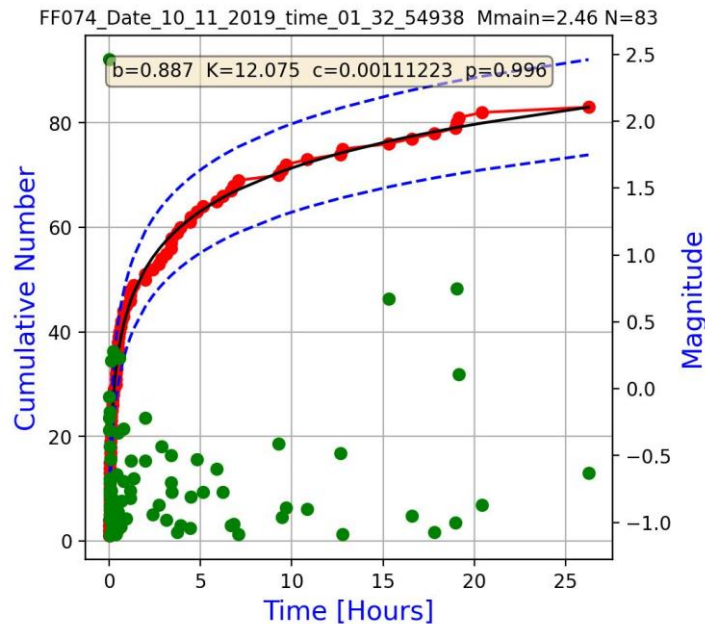


Fig.4.57 Cumulative curves of the aftershocks in time: thick line – model cumulative numbers after the identified best fit MOF model; dashed lines – error bounds; red circles – real cumulative numbers

Sq.No	Date	Time	X	Y	Z	M main	Vol	b	K	p	c	Ta [h]	Ra [m]	M2	N	dl2 [m]	dt2 [h]
75	'30.11.2019'	'02:35:11.712'	-6277.6	1171.7	-969.8	1.71	GMZ_BI_12-15	0.50	42.12	0.60	2.000000	6	100	0.13	7	13.72	2.79

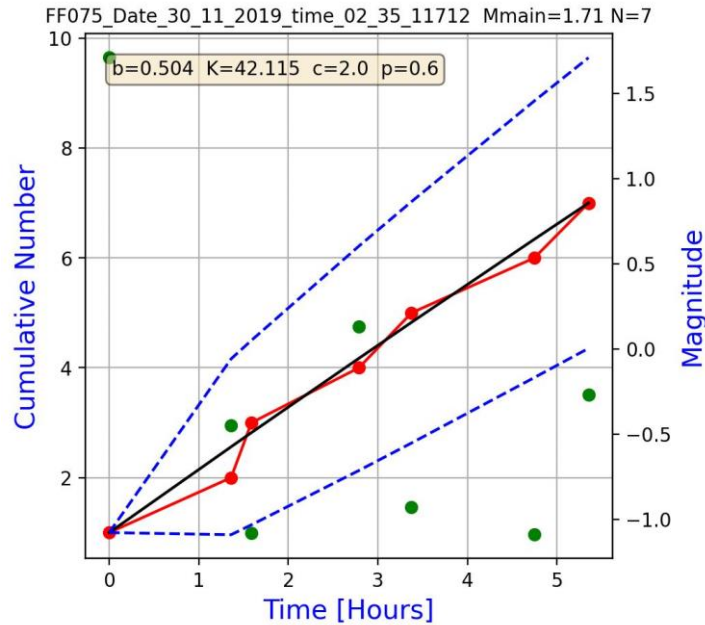


Fig.4.58 Cumulative curves of the aftershocks in time: thick line – model cumulative numbers after the identified best fit MOF model; dashed lines – error bounds; red circles – real cumulative numbers

Sq.No	Date	Time	X	Y	Z	M main	Vol	b	K	p	c	Ta [h]	Ra [m]	M2	N	dl2 [m]	dt2 [h]
76	'9.12.2019'	'08:53:20.342'	-6258.1	3207.3	-1037.6	1.6	GMZ_BI_34_v2	0.80	4.22	0.82	0.000049	9	125	-0.18	12	57.53	1.82

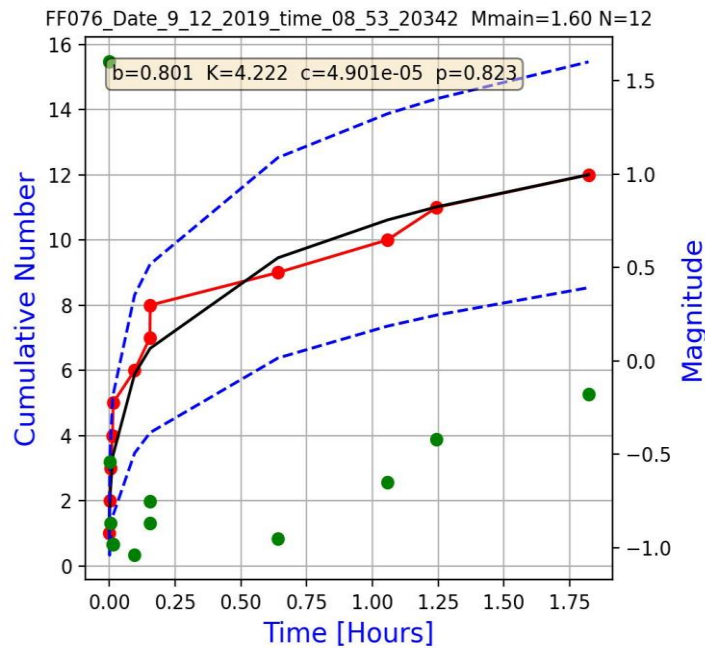


Fig.4.59 Cumulative curves of the aftershocks in time: thick line – model cumulative numbers after the identified best fit MOF model; dashed lines – error bounds; red circles – real cumulative numbers

Sq.No	Date	Time	X	Y	Z	M main	Vol	b	K	p	c	Ta [h]	Ra [m]	M2	N	dl2 [m]	dt2 [h]
77	'9.12.2019'	'12:42:48.653'	-6239.8	3327.9	-1099.7	2.18	GMZ_BI_34_v2	0.99	14.05	0.88	0.000332	18	250	0.46	67	144.82	0.01

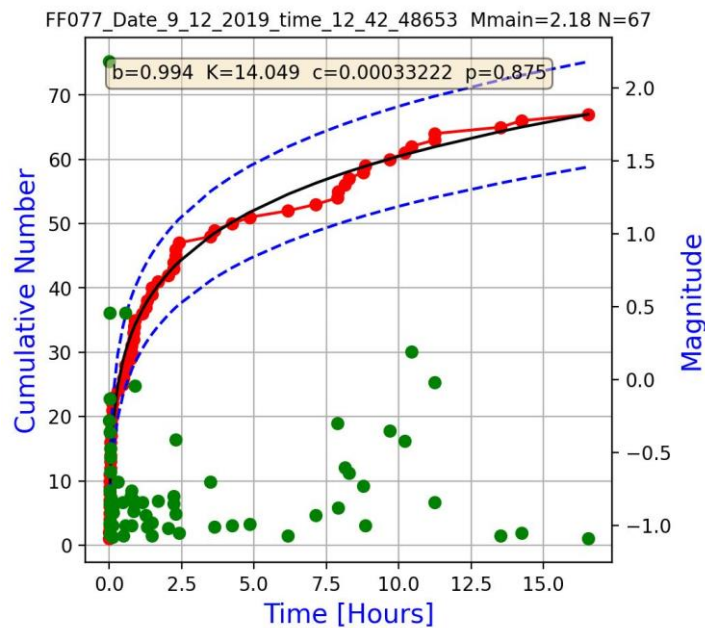


Fig.4.60 Cumulative curves of the aftershocks in time: thick line – model cumulative numbers after the identified best fit MOF model; dashed lines – error bounds; red circles – real cumulative numbers

Sq.No	Date	Time	X	Y	Z	M main	Vol	b	K	p	c	Ta [h]	Ra [m]	M2	N	dl2 [m]	dt2 [h]
78	'26.12.2019'	'15:48:13.612'	-6434.6	3424.2	-1162.6	1.92	GMZ_BI_34_v2	0.76	67.36	0.60	0.000125	9	225	0.23	42	61.75	0.33

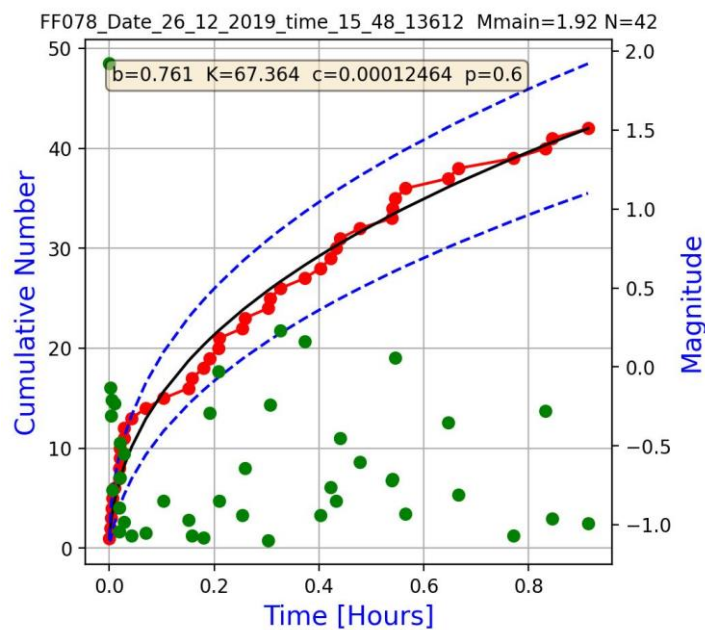


Fig.4.61 Cumulative curves of the aftershocks in time: thick line – model cumulative numbers after the identified best fit MOF model; dashed lines – error bounds; red circles – real cumulative numbers

Sq.No	Date	Time	X	Y	Z	M main	Vol	b	K	p	c	Ta [h]	Ra [m]	M2	N	dl2 [m]	dt2 [h]
79	'26.12.2019'	'16:46:49.878'	-6296.7	2775.5	-1138.2	1.6	GMZ_BI_26-30	0.57	17.27	0.60	2.000000	21	100	-0.18	6	36.86	0.00

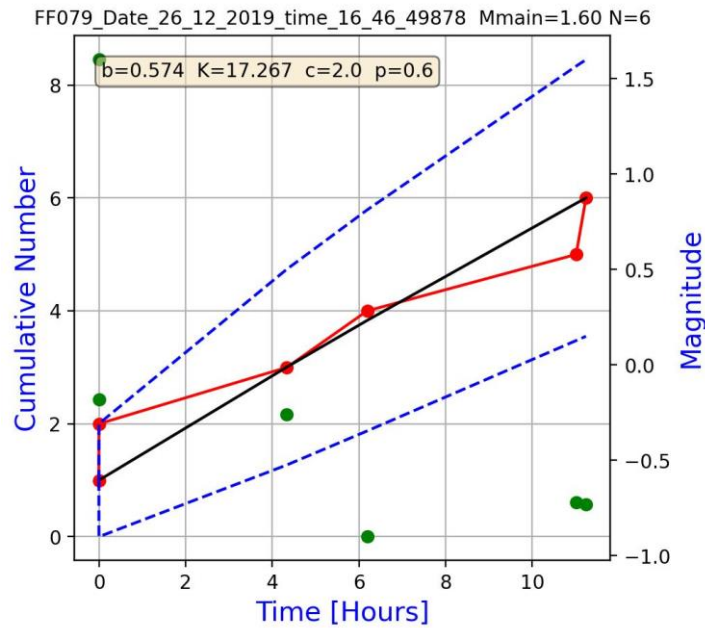


Fig.4.62 Cumulative curves of the aftershocks in time: thick line – model cumulative numbers after the identified best fit MOF model; dashed lines – error bounds; red circles – real cumulative numbers

Sq.No	Date	Time	X	Y	Z	M main	Vol	b	K	p	c	Ta [h]	Ra [m]	M2	N	dl2 [m]	dt2 [h]
81	'28.3.2020'	'18:23:46.584'	-6323.8	3569.3	-993	1.92	GMZ_BI_34_v2	0.68	6.53	0.81	0.000056	30	300	1.11	31	249.82	0.75

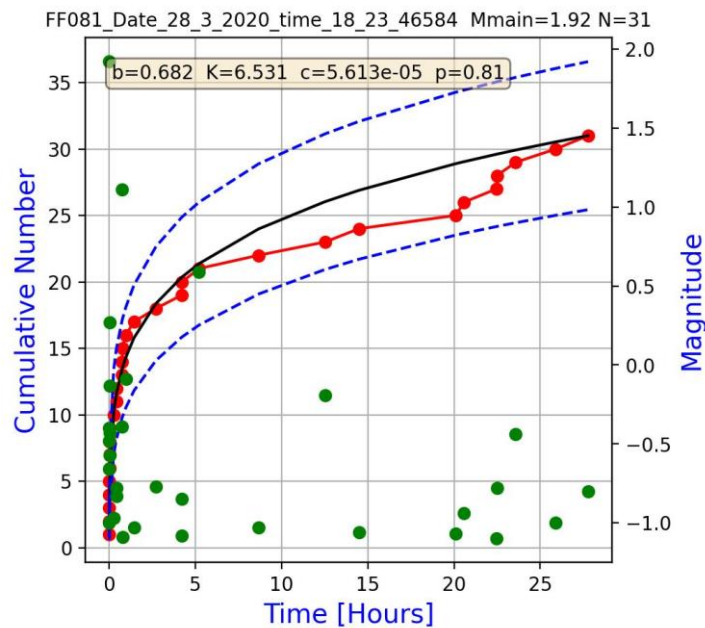


Fig.4.63 Cumulative curves of the aftershocks in time: thick line – model cumulative numbers after the identified best fit MOF model; dashed lines – error bounds; red circles – real cumulative numbers

Sq.No	Date	Time	X	Y	Z	M main	Vol	b	K	p	c	Ta [h]	Ra [m]	M2	N	dl2 [m]	dt2 [h]
83	'19.4.2020'	'23:00:08.655'	-6178.4	2412.8	-1123.8	1.67	GMZ_BI_15-26	0.67	5.39	0.60	0.000757	9	175	-0.16	7	153.22	4.27

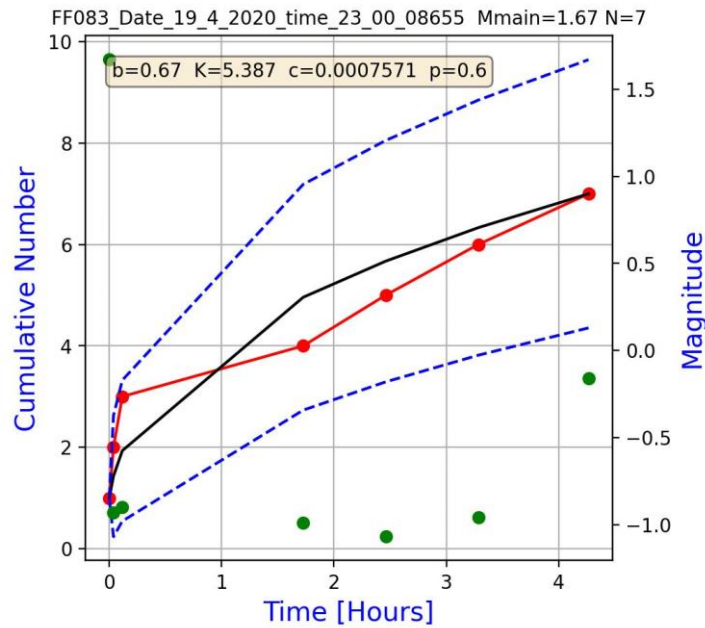


Fig.4.64 Cumulative curves of the aftershocks in time: thick line – model cumulative numbers after the identified best fit MOF model; dashed lines – error bounds; red circles – real cumulative numbers

Sq.No	Date	Time	X	Y	Z	M main	Vol	b	K	p	c	Ta [h]	Ra [m]	M2	N	dl2 [m]	dt2 [h]
84	'13.5.2020'	'19:22:25.329'	-6333.2	2197.6	-1012.9	1.58	GMZ_BI_15-26	0.75	2.95	0.95	0.000272	9	150	0.32	17	41.64	0.04

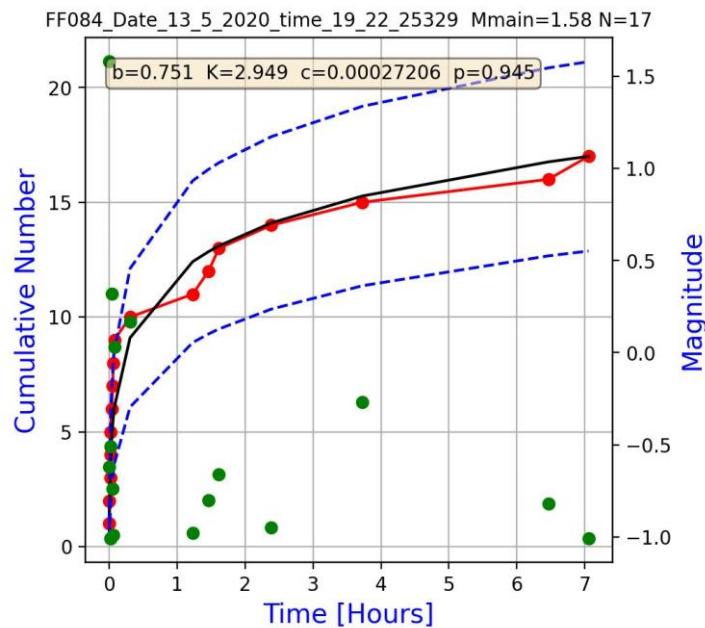


Fig.4.65 Cumulative curves of the aftershocks in time: thick line – model cumulative numbers after the identified best fit MOF model; dashed lines – error bounds; red circles – real cumulative numbers

Sq.No	Date	Time	X	Y	Z	M main	Vol	b	K	p	c	Ta [h]	Ra [m]	M2	N	dl2 [m]	dt2 [h]
85	'18.5.2020'	'03:11:51.880'	-6326.3	2140.7	-1148.4	3.24	GMZ_BI_15-26	0.97	189.04	0.95	0.007776	60	300	1.41	1001	215.66	16.38

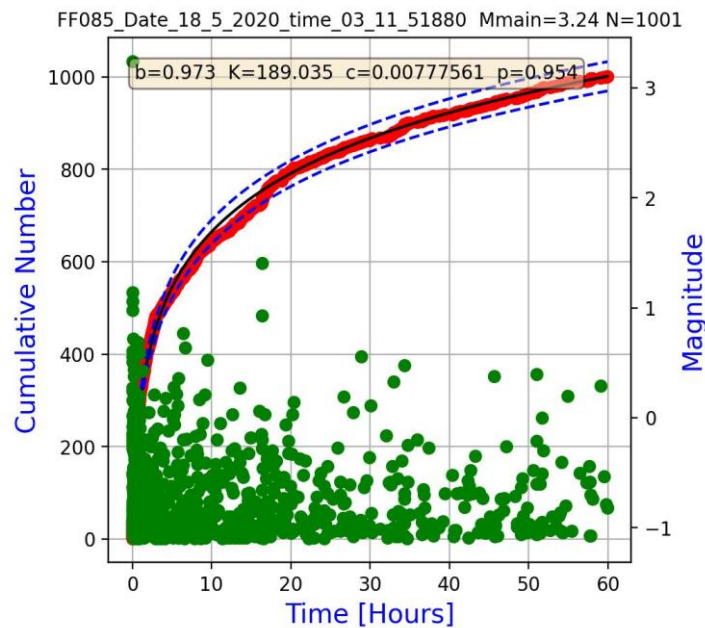


Fig.4.66 Cumulative curves of the aftershocks in time: thick line – model cumulative numbers after the identified best fit MOF model; dashed lines – error bounds; red circles – real cumulative numbers

Sq.No	Date	Time	X	Y	Z	M main	Vol	b	K	p	c	Ta [h]	Ra [m]	M2	N	dl2 [m]	dt2 [h]
86	'22.5.2020'	'01:20:00.642'	-6220.8	949.9	-987.9	1.99	GMZ_BI_04-12	0.66	3.48	0.91	0.001200	6	125	-0.06	14	46.03	0.05

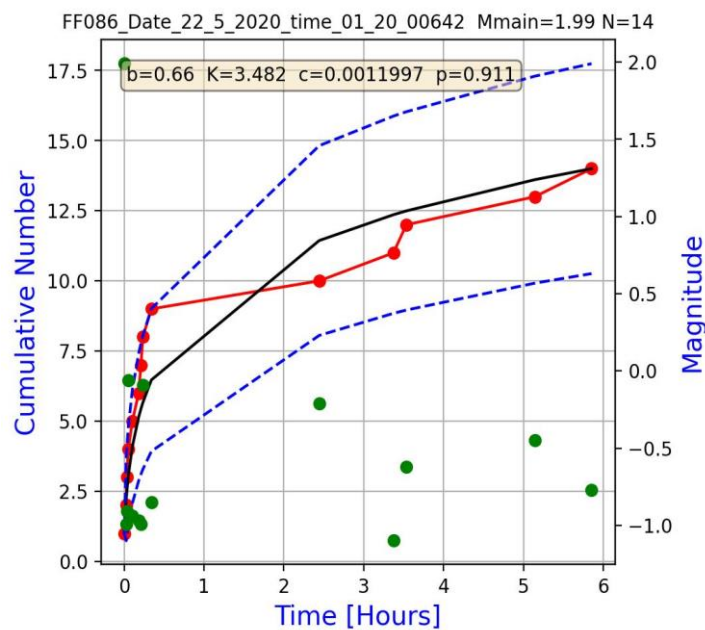


Fig.4.67 Cumulative curves of the aftershocks in time: thick line – model cumulative numbers after the identified best fit MOF model; dashed lines – error bounds; red circles – real cumulative numbers

Sq.No	Date	Time	X	Y	Z	M main	Vol	b	K	p	c	Ta [h]	Ra [m]	M2	N	dI2 [m]	dt2 [h]
87	'23.5.2020'	'17:59:36.431'	-6277.6	1848	-1122.2	1.51	GMZ_BI_15-26	0.78	13.15	0.60	0.000026	12	175	1.19	25	81.99	3.54

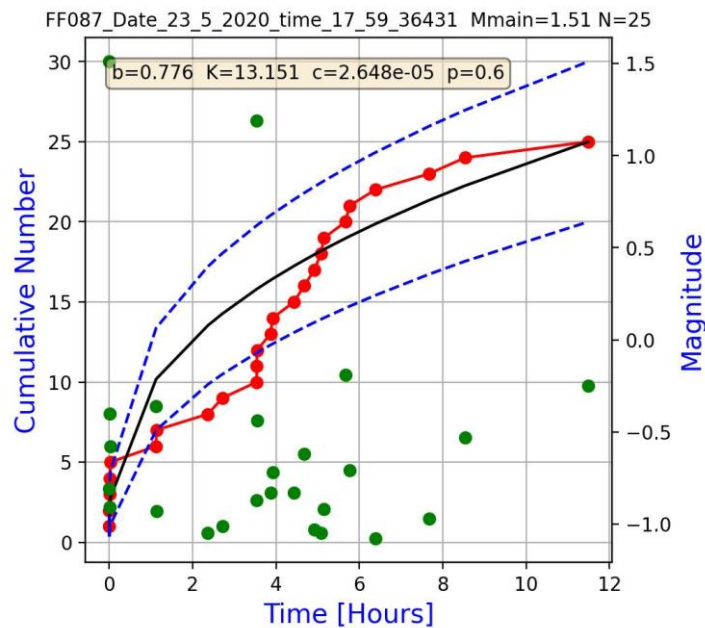


Fig.4.68 Cumulative curves of the aftershocks in time: thick line – model cumulative numbers after the identified best fit MOF model; dashed lines – error bounds; red circles – real cumulative numbers

Sq.No	Date	Time	X	Y	Z	M main	Vol	b	K	p	c	Ta [h]	Ra [m]	M2	N	dI2 [m]	dt2 [h]
88	'27.5.2020'	'01:21:11.163'	-6240.7	961.3	-973.9	1.81	GMZ_BI_04-12	1.13	9.32	0.60	0.000152	15	125	-0.24	19	113.74	0.01

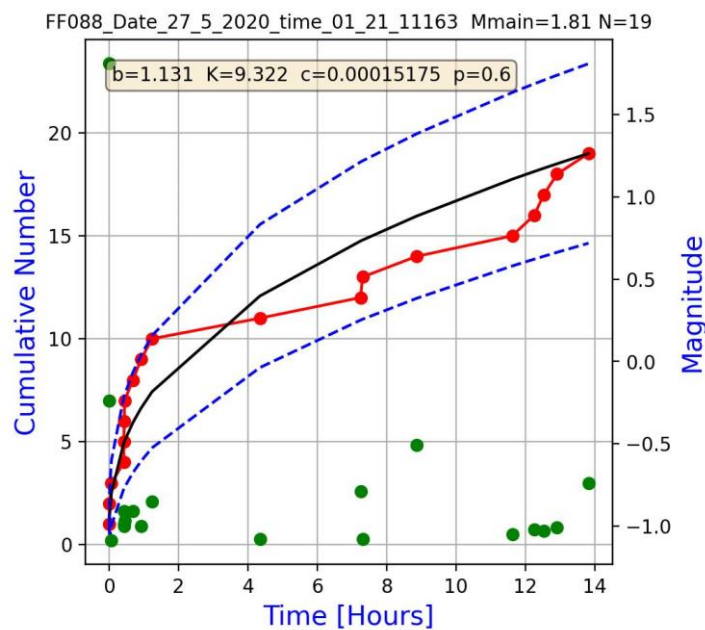


Fig.4.69 Cumulative curves of the aftershocks in time: thick line – model cumulative numbers after the identified best fit MOF model; dashed lines – error bounds; red circles – real cumulative numbers

Sq.No	Date	Time	X	Y	Z	M main	Vol	b	K	p	c	Ta [h]	Ra [m]	M2	N	dl2 [m]	dt2 [h]
89	'26.7.2020'	'04:01:37.731'	-6318.3	1298.4	-1007.1	1.58	GMZ_BI_12-15	0.71	2.62	0.99	0.000183	6	125	0.66	15	22.26	0.02

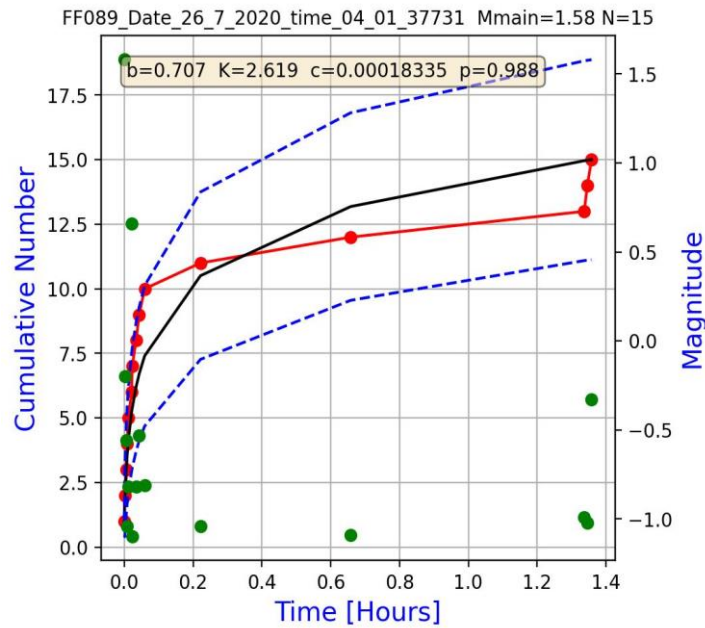


Fig.4.70 Cumulative curves of the aftershocks in time: thick line – model cumulative numbers after the identified best fit MOF model; dashed lines – error bounds; red circles – real cumulative numbers

Sq.No	Date	Time	X	Y	Z	M main	Vol	b	K	p	c	Ta [h]	Ra [m]	M2	N	dl2 [m]	dt2 [h]
90	'30.7.2020'	'16:18:41.994'	-6310.1	1240.3	-999	1.87	GMZ_BI_12-15	1.00	3.38	1.25	0.002529	9	125	0.2	43	7.90	0.10

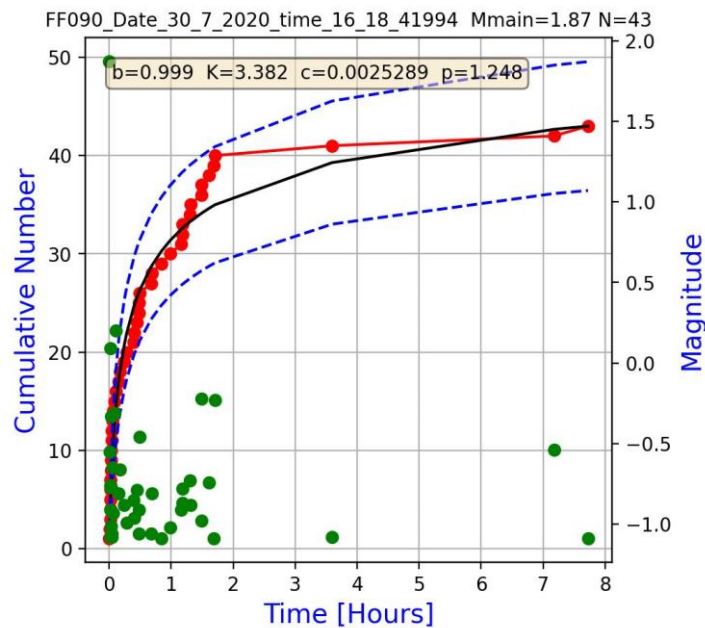


Fig.4.71 Cumulative curves of the aftershocks in time: thick line – model cumulative numbers after the identified best fit MOF model; dashed lines – error bounds; red circles – real cumulative numbers

Sq.No	Date	Time	X	Y	Z	M main	Vol	b	K	p	c	Ta [h]	Ra [m]	M2	N	dl2 [m]	dt2 [h]
91	'1.10.2020'	'23:38:50.439'	-6391.4	3283.9	-1131.6	1.94	GMZ_BI_34_v2	0.72	7.96	0.69	0.000029	18	150	-0.27	22	69.96	11.51

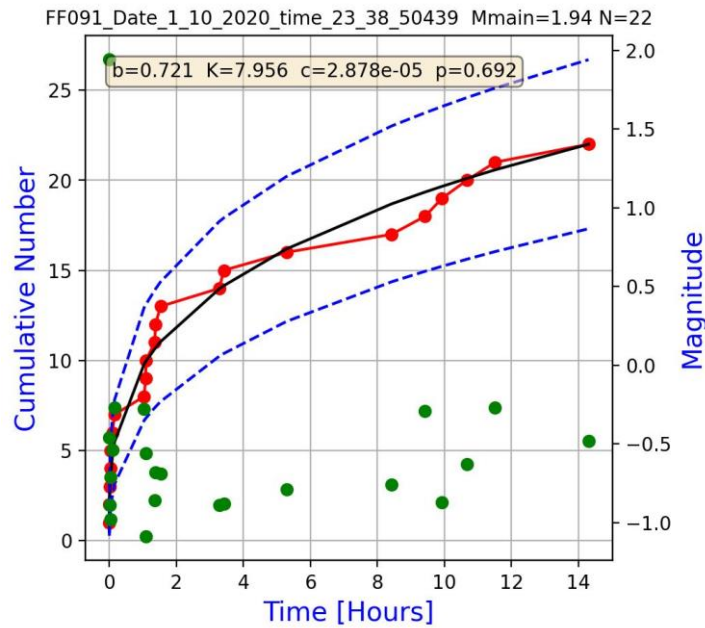


Fig.4.72 Cumulative curves of the aftershocks in time: thick line – model cumulative numbers after the identified best fit MOF model; dashed lines – error bounds; red circles – real cumulative numbers

Sq.No	Date	Time	X	Y	Z	M main	Vol	b	K	p	c	Ta [h]	Ra [m]	M2	N	dl2 [m]	dt2 [h]
92	'3.10.2020'	'03:08:40.090'	-6446.3	3376.6	-1100.4	1.71	GMZ_BI_34_v2	0.77	5.50	0.82	0.000142	12	225	-0.14	20	117.70	0.02

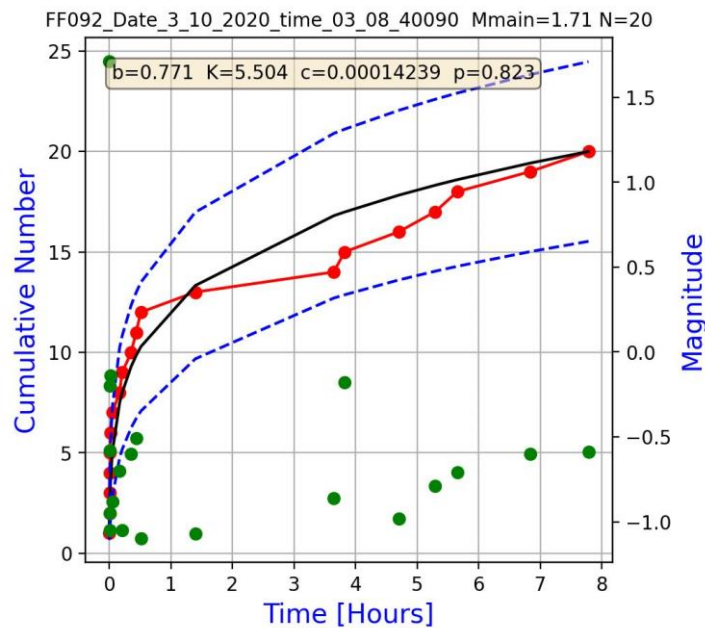


Fig.4.73 Cumulative curves of the aftershocks in time: thick line – model cumulative numbers after the identified best fit MOF model; dashed lines – error bounds; red circles – real cumulative numbers

Sq.No	Date	Time	X	Y	Z	M main	Vol	b	K	p	c	Ta [h]	Ra [m]	M2	N	dI2 [m]	dt2 [h]
94	'5.3.2021'	'15:19:44.523'	-6336.3	3236.4	-1152.7	1.82	GMZ_Bl_34_v2	0.65	7.91	0.84	0.000068	9	175	0.87	33	111.91	8.95

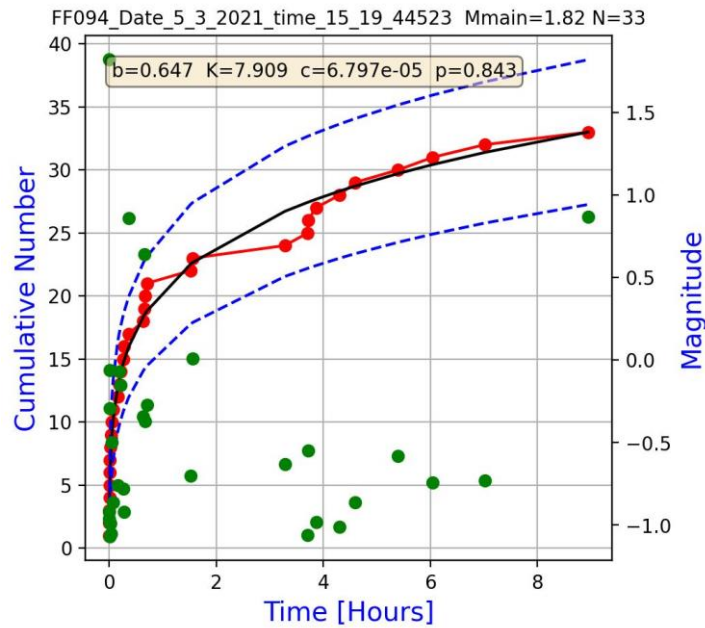


Fig.4.74 Cumulative curves of the aftershocks in time: thick line – model cumulative numbers after the identified best fit MOF model; dashed lines – error bounds; red circles – real cumulative numbers

Sq.No	Date	Time	X	Y	Z	M main	Vol	b	K	p	c	Ta [h]	Ra [m]	M2	N	dI2 [m]	dt2 [h]
95	'21.4.2021'	'16:15:40.251'	-6451.2	3284.3	-1188	1.57	GMZ_Bl_34_v2	0.59	16.46	2.00	0.435973	12	125	1.03	21	14.95	4.69

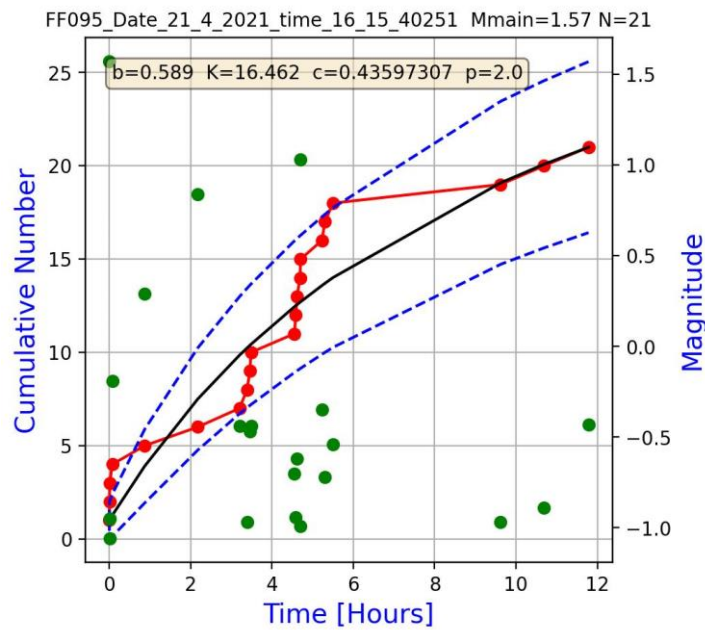


Fig.4.75 Cumulative curves of the aftershocks in time: thick line – model cumulative numbers after the identified best fit MOF model; dashed lines – error bounds; red circles – real cumulative numbers

Sq.No	Date	Time	X	Y	Z	M main	Vol	b	K	p	c	Ta [h]	Ra [m]	M2	N	dl2 [m]	dt2 [h]
96	'14.6.2021'	'18:59:44.210'	-6556.9	3547.5	-1118.7	1.6	GMZ_BI_34_v2	0.58	18.95	0.60	0.000725	9	200	0.73	8	126.96	0.43

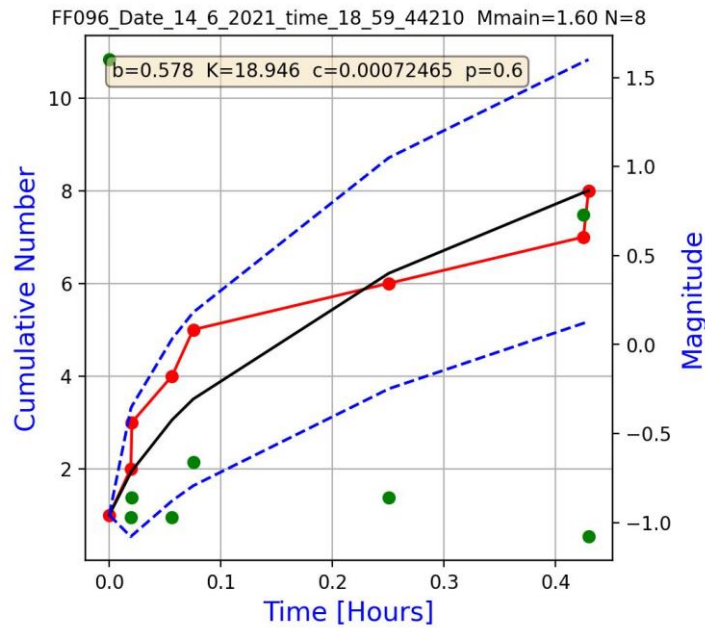


Fig.4.76 Cumulative curves of the aftershocks in time: thick line – model cumulative numbers after the identified best fit MOF model; dashed lines – error bounds; red circles – real cumulative numbers

Sq.No	Date	Time	X	Y	Z	M main	Vol	b	K	p	c	Ta [h]	Ra [m]	M2	N	dl2 [m]	dt2 [h]
97	'2.7.2021'	'18:57:15.561'	-6287.7	1725.8	-1044.7	1.57	GMZ_BI_15-26	0.37	0.60	2.00	0.072006	9	200	0.39	8	117.01	0.76

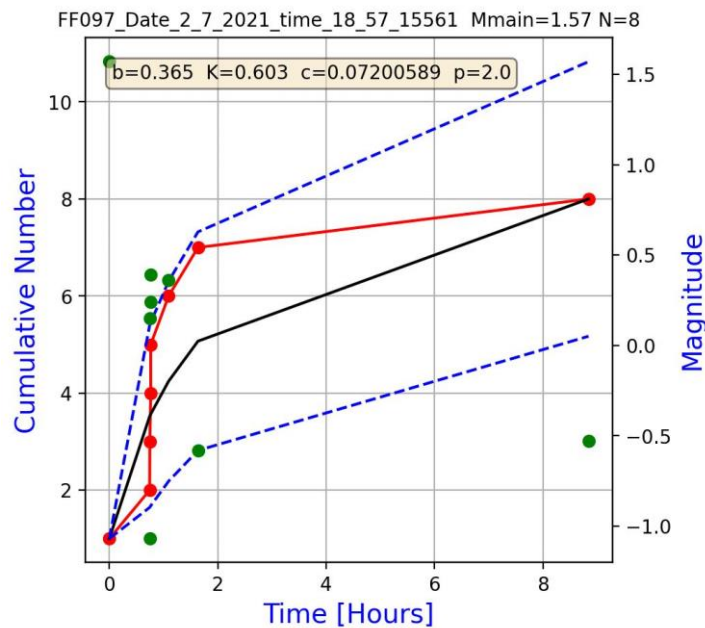


Fig.4.77 Cumulative curves of the aftershocks in time: thick line – model cumulative numbers after the identified best fit MOF model; dashed lines – error bounds; red circles – real cumulative numbers

Sq.No	Date	Time	X	Y	Z	M main	Vol	b	K	p	c	Ta [h]	Ra [m]	M2	N	dl2 [m]	dt2 [h]
98	'19.8.2021'	'01:18:12.801'	-6341.3	1883.1	-1133	1.77	GMZ_BI_15-26	0.95	4.88	0.87	0.000193	21	175	0.33	24	41.50	12.31

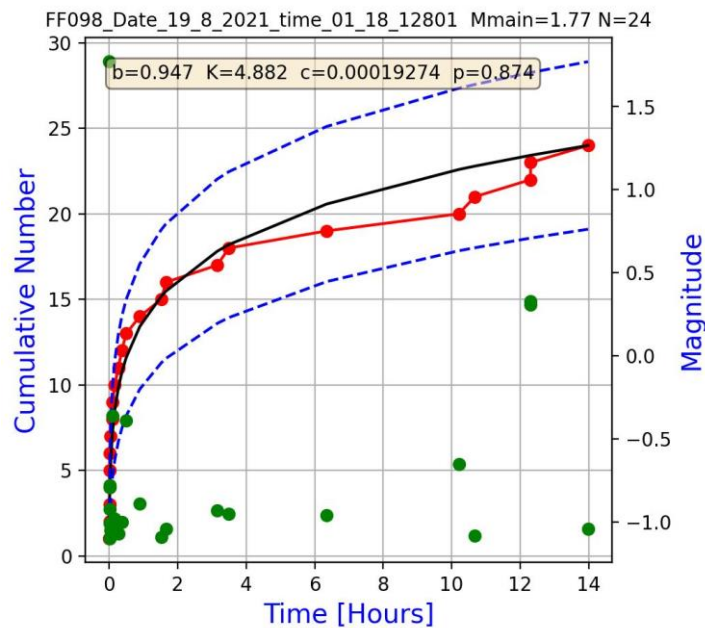


Fig.4.78 Cumulative curves of the aftershocks in time: thick line – model cumulative numbers after the identified best fit MOF model; dashed lines – error bounds; red circles – real cumulative numbers

Sq.No	Date	Time	X	Y	Z	M main	Vol	b	K	p	c	Ta [h]	Ra [m]	M2	N	dl2 [m]	dt2 [h]
100	'18.10.2021'	'01:31:03.246'	-6234.6	885.2	-1007	1.5	GMZ_BI_04-12	0.66	2.44	0.75	0.000057	6	125	-0.41	7	30.51	0.00

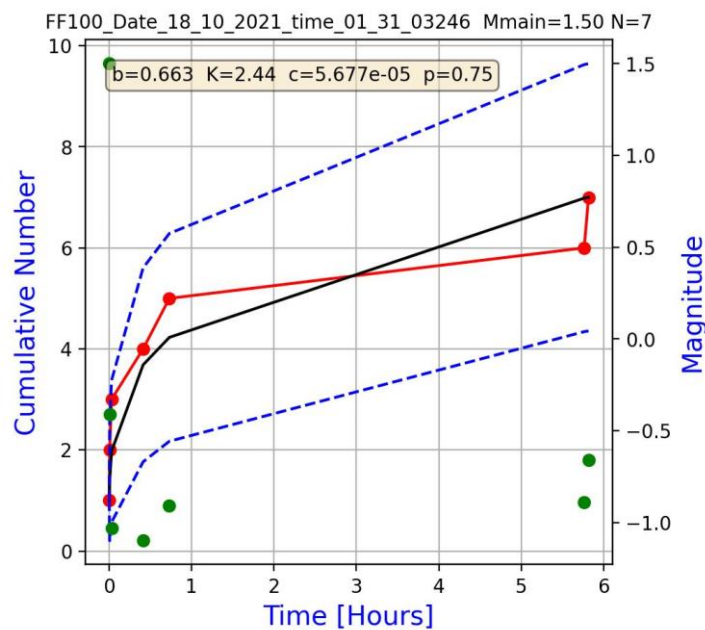


Fig.4.79 Cumulative curves of the aftershocks in time: thick line – model cumulative numbers after the identified best fit MOF model; dashed lines – error bounds; red circles – real cumulative numbers

Sq.No	Date	Time	X	Y	Z	M main	Vol	b	K	p	c	Ta [h]	Ra [m]	M2	N	dl2 [m]	dt2 [h]
101	'7.12.2021'	'16:49:17.635'	-6226.6	799.2	-1005.9	1.59	GMZ_BI_04-12	1.06	8.53	0.70	0.000073	6	125	-0.62	15	3.81	0.04

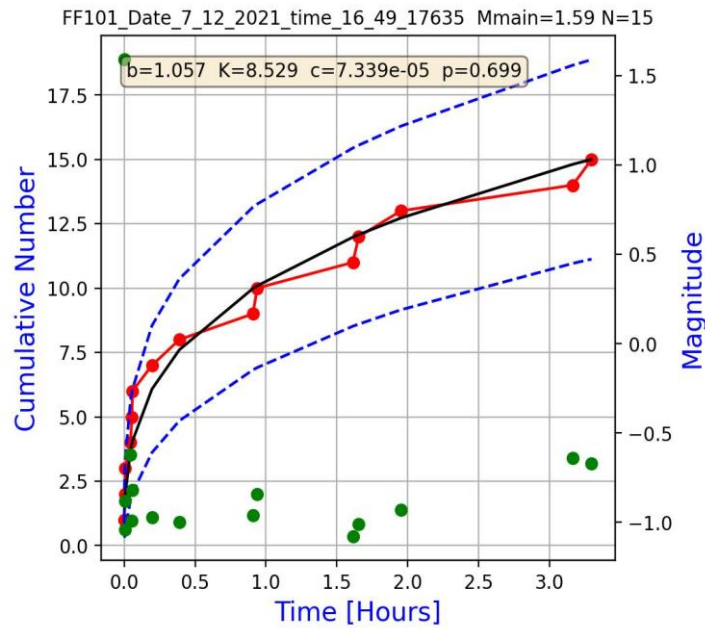


Fig.4.80 Cumulative curves of the aftershocks in time: thick line – model cumulative numbers after the identified best fit MOF model; dashed lines – error bounds; red circles – real cumulative numbers

Sq.No	Date	Time	X	Y	Z	M main	Vol	b	K	p	c	Ta [h]	Ra [m]	M2	N	dl2 [m]	dt2 [h]
102	'25.1.2022'	'12:01:53.771'	-6275.3	1768.2	-1038.3	1.73	GMZ_BI_15-26	1.10	6.64	1.12	0.000431	9	150	-0.09	77	30.53	0.03

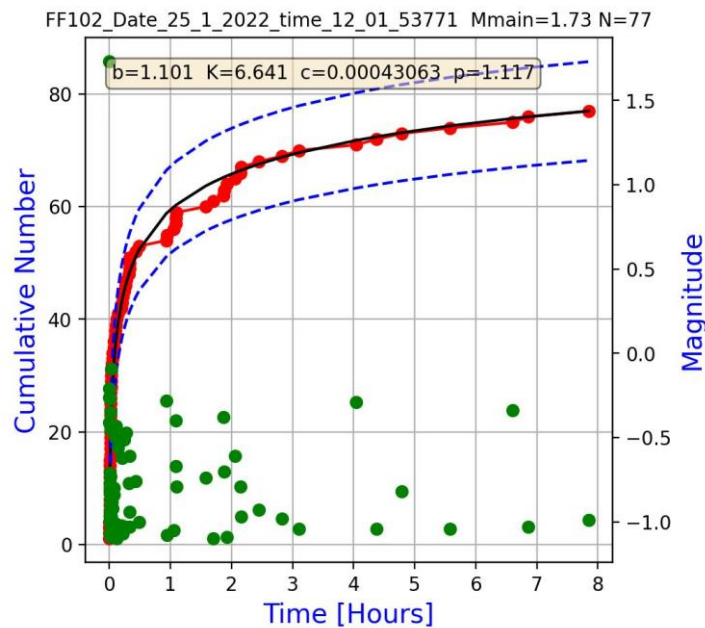


Fig.4.81 Cumulative curves of the aftershocks in time: thick line – model cumulative numbers after the identified best fit MOF model; dashed lines – error bounds; red circles – real cumulative numbers

Sq.No	Date	Time	X	Y	Z	M main	Vol	b	K	p	c	Ta [h]	Ra [m]	M2	N	dl2 [m]	dt2 [h]
103	'31.1.2022'	'05:01:00.502'	-6492.1	3540.6	-1128.1	1.96	GMZ_BI_34_v2	0.68	9.09	0.60	0.000011	9	175	0.61	15	32.68	0.87

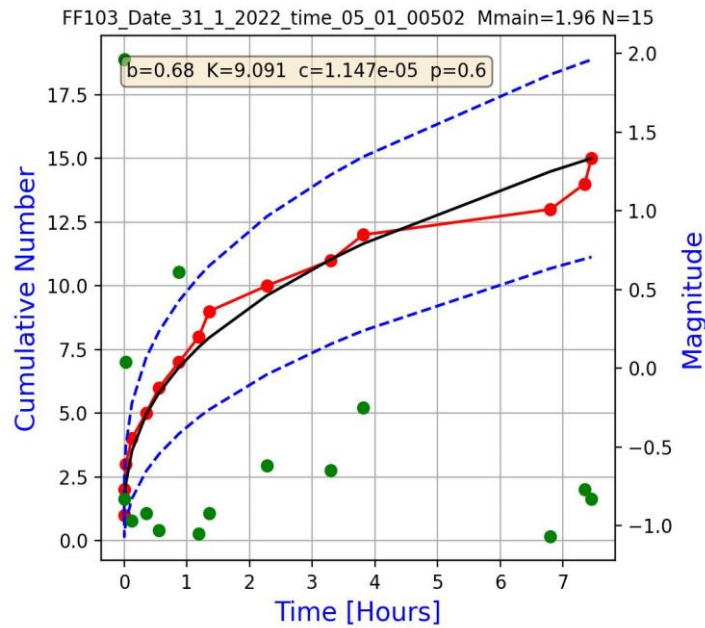


Fig.4.82 Cumulative curves of the aftershocks in time: thick line – model cumulative numbers after the identified best fit MOF model; dashed lines – error bounds; red circles – real cumulative numbers

Table 4.1 Trigger and aftershock sequence parameters. See details in text

Sq.No	Date	Time	X	Y	Z	M main	Vol	b	K	p	c	Ta [h]	Ra [m]	M2	N	dl2 [m]	dt2 [h]
1	'11.1.2015'	'01:33:10.526'	-6544.9	4023	-989.8	1.6	GMZ_BI_38	0.94	19.86	0.60	0.769145	60	300	0.42	35	104.31	18.40
2	'17.1.2015'	'01:49:21.085'	-6541.6	3984.5	-1019.8	1.66	GMZ_BI_38	0.60	2.90	1.10	0.000304	9	225	0.14	29	75.88	0.25
3	'17.1.2015'	'03:35:14.579'	-6380.5	3980.4	-1012.5	1.8	GMZ_BI_38	0.63	6.32	0.91	0.000083	27	250	0.64	41	208.76	1.44
4	'4.3.2015'	'16:44:53.156'	-6217.6	2624.9	-1000.8	1.6	GMZ_BI_26-30	0.63	10.67	0.71	0.000122	9	225	1.24	23	108.79	1.69
5	'18.3.2015'	'01:46:47.964'	-6488.5	4515.3	-996.2	1.58	GMZ_BI_41	0.77	11.52	0.60	0.000359	48	300	0.26	35	194.50	24.50
6	'25.3.2015'	'13:29:34.315'	-6290.3	2581.2	-1144.4	1.59	GMZ_BI_26-30	0.74	0.84	1.16	0.000341	6	125	-0.43	10	75.78	0.00
7	'25.3.2015'	'14:02:00.734'	-6298	2566.8	-1118.2	1.65	GMZ_BI_26-30	0.83	19.99	0.69	0.000040	18	175	0.84	56	53.74	0.10
8	'28.3.2015'	'20:48:46.008'	-6359.9	2178.2	-1201.2	1.66	GMZ_BI_15-26	0.64	5.63	0.72	0.000047	9	125	0.5	14	33.22	0.14
9	'9.4.2015'	'01:33:56.941'	-6191	2501.7	-1122.4	1.92	GMZ_BI_26-30	0.63	0.45	1.17	0.000188	9	125	-0.14	9	42.93	0.32
10	'15.4.2015'	'01:58:39.523'	-6185.6	2704.5	-996.4	1.64	GMZ_BI_26-30	0.61	4.33	0.65	0.000096	6	150	0.02	7	52.99	3.23
11	'31.5.2015'	'03:03:08.345'	-6346.1	2197.2	-1216.1	1.57	GMZ_BI_15-26	0.69	46.93	0.60	2.000000	6	125	-0.46	8	22.18	3.81
12	'22.7.2015'	'04:15:07.227'	-6250.8	2546.7	-1026	1.84	GMZ_BI_26-30	0.82	5.32	0.81	0.000077	12	225	0.38	20	64.92	5.45
13	'16.8.2015'	'19:59:09.589'	-6440.5	3358.1	-1143.3	1.58	GMZ_BI_34_v2	1.05	35.90	0.63	2.000000	24	175	0.16	21	105.17	14.70
16	'10.9.2015'	'08:51:45.498'	-6303.2	2635.3	-1127.1	2.1	GMZ_BI_26-30	0.69	11.72	0.92	0.000536	15	150	0.66	54	91.35	6.22
17	'10.9.2015'	'16:17:26.345'	-6286.4	2627.6	-1120.9	1.62	GMZ_BI_26-30	0.81	8.18	0.91	0.000469	12	175	0.14	39	121.50	0.06
18	'17.9.2015'	'13:30:33.860'	-6319.3	2595.2	-1198.6	2.14	GMZ_BI_26-30	0.84	24.10	0.98	0.000748	45	275	0.79	176	222.72	19.36
19	'24.9.2015'	'00:04:52.980'	-6301	2916	-1116	2.09	GMZ_BI_26-30	0.77	15.70	0.79	0.000082	18	200	0.45	61	67.06	0.00
20	'13.10.2015'	'22:19:44.791'	-6322.1	2381.1	-1027.1	1.68	GMZ_BI_15-26	0.48	5.93	0.60	0.000354	9	175	0.93	10	66.47	1.58
25	'15.3.2016'	'03:50:28.289'	-6565.8	4150.6	-1077.8	1.86	GMZ_BI_38	0.70	0.92	1.13	0.001001	9	175	-0.27	10	77.78	0.13
26	'7.4.2016'	'01:36:57.699'	-6551.8	4508.8	-1123.2	2.4	GMZ_BI_41	0.72	6.53	0.82	0.001759	21	225	0.01	23	116.20	0.06

27	'3.5.2016'	'07:29:06.907'	-6555	4047.5	-1088.6	2.05	GMZ_BI_38	0.82	12.89	0.74	0.000084	15	275	0.2	37	134.27	1.40
28	'19.5.2016'	'19:03:59.971'	-6299.4	2670.8	-1007.4	1.51	GMZ_BI_26-30	0.47	2.91	1.00	0.053993	9	150	-0.19	5	85.82	3.89
29	'22.5.2016'	'02:31:16.146'	-6406.1	3355.1	-1127.3	1.88	GMZ_BI_34_v2	0.75	23.22	0.78	0.000065	24	225	1.12	92	88.98	0.02
31	'26.5.2016'	'21:59:36.899'	-6426.1	3475	-1081.1	1.55	GMZ_BI_34_v2	0.72	34.63	0.82	0.000105	36	250	1.18	167	30.52	0.01
33	'22.7.2016'	'10:59:35.670'	-6300	2569.5	-1070.8	2.52	GMZ_BI_26-30	0.86	25.64	0.88	0.000377	60	300	0.59	158	119.87	18.97
34	'13.8.2016'	'11:52:45.992'	-6462.5	3472.3	-1072.4	1.96	GMZ_BI_34_v2	0.67	6.97	0.77	0.000163	9	200	0.38	21	141.39	0.11
35	'25.8.2016'	'09:59:31.061'	-6264.4	1263.1	-1128.4	1.61	GMZ_BI_12-15	1.25	230.60	0.60	1.050746	6	200	-0.4	53	81.13	0.75
36	'20.9.2016'	'05:47:51.609'	-6367.6	2918.1	-1168.4	2.13	GMZ_BI_26-30	0.81	26.85	0.82	0.000328	24	250	0.9	114	191.56	0.26
37	'24.9.2016'	'08:11:27.279'	-6278.5	2168.8	-1020.8	1.88	GMZ_BI_15-26	0.93	4.34	0.89	0.000076	24	175	-0.31	25	102.25	17.37
38	'1.10.2016'	'05:58:22.947'	-6661.9	4111.5	-1106.5	1.75	GMZ_BI_38	0.63	21.91	0.66	0.000107	12	275	1.34	49	219.73	7.09
39	'6.11.2016'	'06:52:15.830'	-6388.4	3386.5	-1114.5	1.58	GMZ_BI_34_v2	0.93	33.69	0.60	0.000078	21	200	1	78	89.01	2.27
41	'26.12.2016'	'03:31:24.239'	-6424.9	3440.3	-1077.2	1.91	GMZ_BI_34_v2	0.70	5.62	1.15	0.000851	9	175	0.46	66	164.00	0.34
42	'17.1.2017'	'07:16:03.212'	-6339.2	3011.6	-1153.9	1.51	GMZ_BI_26-30	0.98	12.75	0.75	0.000096	12	150	-0.08	39	37.92	0.23
43	'20.1.2017'	'03:52:06.529'	-6181.5	1997.1	-1020.2	1.87	GMZ_BI_15-26	0.69	9.67	0.66	0.000080	33	225	0.92	29	80.42	4.95
45	'11.2.2017'	'05:40:12.759'	-6423.4	3316.8	-1123.5	1.75	GMZ_BI_34_v2	0.66	7.43	0.92	0.000205	9	225	0.84	39	42.45	0.00
46	'2.4.2017'	'19:42:37.152'	-6333.1	2923.1	-1129.4	1.89	GMZ_BI_26-30	0.84	10.91	0.60	0.000233	9	125	-0.03	18	72.23	6.31
47	'10.5.2017'	'04:54:33.435'	-6460.3	3447.1	-1147.1	2.05	GMZ_BI_34_v2	1.12	72.29	0.62	0.000077	48	275	0.58	238	91.33	0.00
50	'24.9.2017'	'05:48:57.552'	-6539.6	4017.7	-1099	1.56	GMZ_BI_38	0.53	5.45	0.69	0.000011	9	125	0.29	8	71.09	0.30
51	'27.10.2017'	'22:51:15.302'	-6564.8	4580	-1163.1	1.64	GMZ_BI_41	0.66	2.09	0.97	0.001423	9	175	-0.1	11	19.27	0.01
52	'4.11.2017'	'13:14:44.823'	-6319.1	2543.3	-1210.9	1.69	GMZ_BI_26-30	0.63	1.66	1.06	0.000140	9	150	0.26	17	56.84	0.26
53	'28.12.2017'	'09:15:37.747'	-6556.5	4567.5	-1149.2	1.54	GMZ_BI_41	0.57	4.93	0.61	0.000257	36	150	0.33	14	41.48	0.54
54	'19.3.2018'	'11:05:04.002'	-6480.7	4662.7	-1161.3	1.5	GMZ_BI_41	0.62	1.68	0.95	0.000378	9	175	0.41	10	136.03	0.32
55	'22.3.2018'	'03:45:50.852'	-6296.7	2781.1	-1099.3	2.28	GMZ_BI_26-30	0.82	24.71	0.81	0.000138	9	200	1	85	66.54	0.01
56	'27.4.2018'	'06:19:59.886'	-6273	2580	-1092	1.66	GMZ_BI_26-30	1.18	26.21	0.60	0.000113	9	200	0	42	85.04	1.82
60	'26.7.2018'	'08:49:45.927'	-6284	2654.6	-1192.6	1.67	GMZ_BI_26-30	1.16	308.35	1.20	2.000000	15	200	1.17	71	66.32	9.98
61	'15.9.2018'	'02:40:06.819'	-6571.1	3680.8	-1064.3	1.51	GMZ_BI_38	0.41	2.84	0.72	0.000155	6	200	0.27	6	50.28	0.11
62	'8.10.2018'	'17:08:14.094'	-6307.5	3246	-1035	1.65	GMZ_BI_34_v2	0.78	1.97	1.43	0.002297	9	150	0.52	57	43.27	0.86
63	'14.11.2018'	'02:53:53.823'	-6505.7	3818.4	-1055.7	1.5	GMZ_BI_38	0.65	6.89	1.05	0.000305	9	200	0.83	61	135.62	0.01
64	'20.11.2018'	'01:21:12.132'	-6259.3	1872.4	-998.8	1.96	GMZ_BI_15-26	0.45	1.60	0.86	0.000179	9	175	0.37	7	65.30	6.55
65	'13.1.2019'	'03:43:02.700'	-6294.4	2782.4	-1099.4	1.79	GMZ_BI_26-30	1.01	14.97	0.84	0.000134	9	200	0.81	58	96.02	0.11
66	'30.1.2019'	'21:02:53.948'	-6420.9	3369.8	-1112.5	2.3	GMZ_BI_34_v2	0.95	41.42	0.76	0.000172	42	250	0.52	175	224.06	0.01
67	'13.3.2019'	'10:04:20.393'	-6287.2	2751.2	-1153.4	1.69	GMZ_BI_26-30	0.90	4.39	0.90	0.000203	9	175	0.09	21	70.14	0.09
70	'23.5.2019'	'01:31:36.184'	-6212.1	986.6	-975.8	1.65	GMZ_BI_04-12	1.05	10.65	0.62	0.000012	6	200	0.09	17	63.70	0.00
71	'18.8.2019'	'20:04:44.133'	-6403.3	2265.7	-1049	1.6	GMZ_BI_15-26	0.79	6.97	0.61	0.001285	9	175	-0.26	11	44.48	5.27
72	'25.9.2019'	'11:22:29.943'	-6555.4	3835.3	-1152.9	1.81	GMZ_BI_38	0.67	4.29	0.92	0.000727	9	125	0.62	20	99.76	0.06
73	'30.10.2019'	'01:32:08.388'	-6477.3	3582.8	-1050.3	1.55	GMZ_BI_34_v2	0.84	4.06	0.77	0.000155	18	200	0	14	105.81	0.90
74	'10.11.2019'	'01:32:54.938'	-6288.9	2614.7	-1203.4	2.46	GMZ_BI_26-30	0.89	12.08	1.00	0.001112	27	200	0.75	83	111.34	19.04
75	'30.11.2019'	'02:35:11.712'	-6277.6	1171.7	-969.8	1.71	GMZ_BI_12-15	0.50	42.12	0.60	2.000000	6	100	0.13	7	13.72	2.79
76	'9.12.2019'	'08:53:20.342'	-6258.1	3207.3	-1037.6	1.6	GMZ_BI_34_v2	0.80	4.22	0.82	0.000049	9	125	-0.18	12	57.53	1.82
77	'9.12.2019'	'12:42:48.653'	-6239.8	3327.9	-1099.7	2.18	GMZ_BI_34_v2	0.99	14.05	0.88	0.000332	18	250	0.46	67	144.82	0.01
78	'26.12.2019'	'15:48:13.612'	-6434.6	3424.2	-1162.6	1.92	GMZ_BI_34_v2	0.76	67.36	0.60	0.000125	9	225	0.23	42	61.75	0.33
79	'26.12.2019'	'16:46:49.878'	-6296.7	2775.5	-1138.2	1.6	GMZ_BI_26-30	0.57	17.27	0.60	2.000000	21	100	-0.18	6	36.86	0.00
81	'28.3.2020'	'18:23:46.584'	-6323.8	3569.3	-993	1.92	GMZ_BI_34_v2	0.68	6.53	0.81	0.000056	30	300	1.11	31	249.82	0.75
83	'19.4.2020'	'23:00:08.655'	-6178.4	2412.8	-1123.8	1.67	GMZ_BI_15-26	0.67	5.39	0.60	0.000757	9	175	-0.16	7	153.22	4.27
84	'13.5.2020'	'19:22:25.329'	-6333.2	2197.6	-1012.9	1.58	GMZ_BI_15-26	0.75	2.95	0.95	0.000272	9	150	0.32	17	41.64	0.04
85	'18.5.2020'	'03:11:51.880'	-6326.3	2140.7	-1148.4	3.24	GMZ_BI_15-26	0.97	189.04	0.95	0.007776	60	300	1.41	1001	215.66	16.38

86	'22.5.2020'	'01:20:00.642'	-6220.8	949.9	-987.9	1.99	GMZ_BI_04-12	0.66	3.48	0.91	0.001200	6	125	-0.06	14	46.03	0.05
87	'23.5.2020'	'17:59:36.431'	-6277.6	1848	-1122.2	1.51	GMZ_BI_15-26	0.78	13.15	0.60	0.000026	12	175	1.19	25	81.99	3.54
88	'27.5.2020'	'01:21:11.163'	-6240.7	961.3	-973.9	1.81	GMZ_BI_04-12	1.13	9.32	0.60	0.000152	15	125	-0.24	19	113.74	0.01
89	'26.7.2020'	'04:01:37.731'	-6318.3	1298.4	-1007.1	1.58	GMZ_BI_12-15	0.71	2.62	0.99	0.000183	6	125	0.66	15	22.26	0.02
90	'30.7.2020'	'16:18:41.994'	-6310.1	1240.3	-999	1.87	GMZ_BI_12-15	1.00	3.38	1.25	0.002529	9	125	0.2	43	7.90	0.10
91	'1.10.2020'	'23:38:50.439'	-6391.4	3283.9	-1131.6	1.94	GMZ_BI_34_v2	0.72	7.96	0.69	0.000029	18	150	-0.27	22	69.96	11.51
92	'3.10.2020'	'03:08:40.090'	-6446.3	3376.6	-1100.4	1.71	GMZ_BI_34_v2	0.77	5.50	0.82	0.000142	12	225	-0.14	20	117.70	0.02
94	'5.3.2021'	'15:19:44.523'	-6336.3	3236.4	-1152.7	1.82	GMZ_BI_34_v2	0.65	7.91	0.84	0.000068	9	175	0.87	33	111.91	8.95
95	'21.4.2021'	'16:15:40.251'	-6451.2	3284.3	-1188	1.57	GMZ_BI_34_v2	0.59	16.46	2.00	0.435973	12	125	1.03	21	14.95	4.69
96	'14.6.2021'	'18:59:44.210'	-6556.9	3547.5	-1118.7	1.6	GMZ_BI_34_v2	0.58	18.95	0.60	0.000725	9	200	0.73	8	126.96	0.43
97	'2.7.2021'	'18:57:15.561'	-6287.7	1725.8	-1044.7	1.57	GMZ_BI_15-26	0.37	0.60	2.00	0.072006	9	200	0.39	8	117.01	0.76
98	'19.8.2021'	'01:18:12.801'	-6341.3	1883.1	-1133	1.77	GMZ_BI_15-26	0.95	4.88	0.87	0.000193	21	175	0.33	24	41.50	12.31
100	'18.10.2021'	'01:31:03.246'	-6234.6	885.2	-1007	1.5	GMZ_BI_04-12	0.66	2.44	0.75	0.000057	6	125	-0.41	7	30.51	0.00
101	'7.12.2021'	'16:49:17.635'	-6226.6	799.2	-1005.9	1.59	GMZ_BI_04-12	1.06	8.53	0.70	0.000073	6	125	-0.62	15	3.81	0.04
102	'25.1.2022'	'12:01:53.771'	-6275.3	1768.2	-1038.3	1.73	GMZ_BI_15-26	1.10	6.64	1.12	0.000431	9	150	-0.09	77	30.53	0.03
103	'31.1.2022'	'05:01:00.502'	-6492.1	3540.6	-1128.1	1.96	GMZ_BI_34_v2	0.68	9.09	0.60	0.000011	9	175	0.61	15	32.68	0.87

Table 4.2 Average MOF parameters, b-value and average sequence duration (Tav) and aftershock zone radius (Rav)

Vol.	b-av	St.d. b	K-av	St.d. K	c-av	St.d. c	p-av	St.d. p	Nc	Tav	Rav
GMZ_BI_38	0.66	0.14	8.43	6.95	0.0772	0.2307	0.85	0.19	10	16.50	215.00
GMZ_BI_41	0.67	0.07	5.35	3.57	0.0008	0.0006	0.79	0.16	5	24.60	205.00
GMZ_BI_15-26	0.73	0.20	21.69	47.70	0.1488	0.5138	0.86	0.36	14	16.29	178.57
GMZ_BI_26-30	0.80	0.17	25.65	60.86	0.1765	0.5628	0.86	0.18	23	16.17	183.70
GMZ_BI_12-15	0.86	0.28	69.68	94.27	0.7634	0.8326	0.86	0.27	4	6.75	137.50
GMZ_BI_04-12	0.91	0.21	6.88	3.29	0.0003	0.0005	0.72	0.11	5	7.80	140.00
GMZ_BI_34_v2	0.78	0.15	20.25	19.90	0.1163	0.4313	0.85	0.32	21	18.29	203.57
All	0.77	0.17	22.56	33.79	0.1833	0.3675	0.83	0.23	82	15.20	180.48

Except Table 4.1 (mofall.txt file from the ForA1.0 software) in which the MOF and some other parameters of the aftershock sequences are provided, the software also calculates the average parameter values for each studied volume and for Kiruna mine as a whole (Table 4.2 – vmofall.txt file from the ForA1.0 software).

The results saved in Table 4.2 deliver the opportunity to see the spatial distribution of the aftershock sequence parameters along the GMZ volumes of Kiruna mine. No big variation is observed of the MOF model p-value except for the GMZ_BI_04-12 volume where the p-value is considerably smaller. The ratio of small to strong events (b-value) shows greater variation with a minimum value for GMZ_BI_38 volume and maximum one for GMZ_BI_38 volume. For a better interpretation of these results, however, one needs more data about the GMZ volumes describing not only seismicity.

4.2 Examples of the distribution analysis of distances between aftershocks hypocenters [\(bck\)](#)

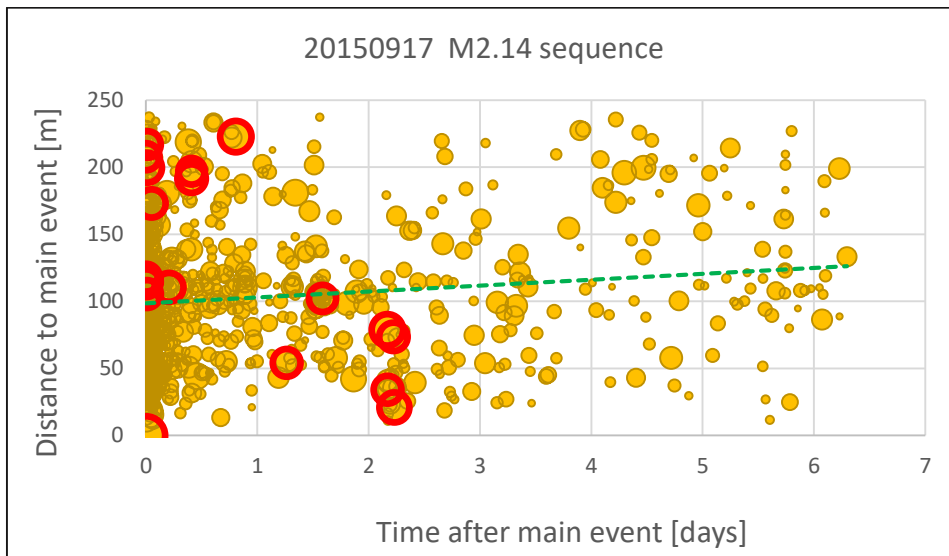


Fig.4.83 Temporal evolution of distances between the hypocenter of each aftershock and the main event hypocenter. Circle size corresponds to event magnitude. Red circles denote events with magnitudes $M \geq 0$.

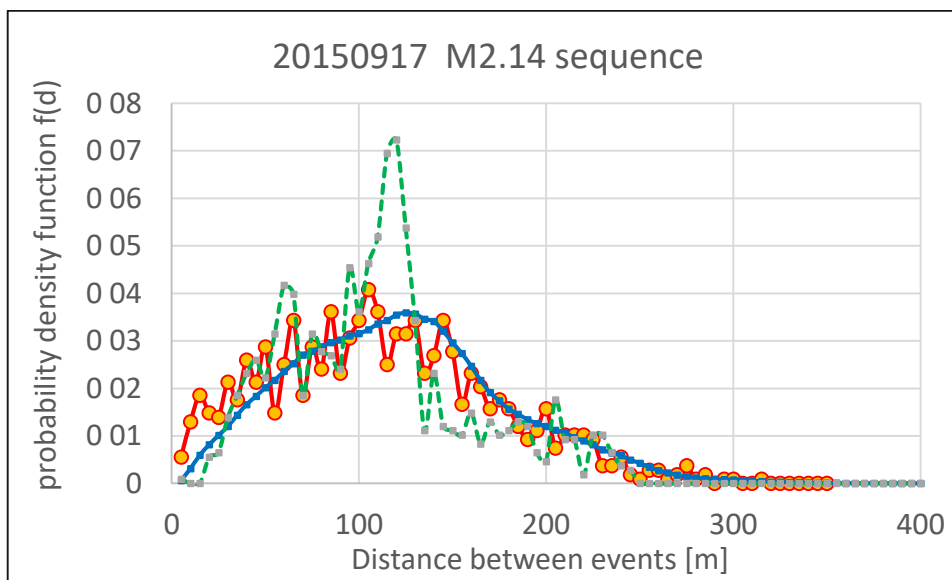


Fig.4.84 Distribution of distances between hypocenters of aftershocks: thick blue line – distribution of all possible distances between different events; red line with points – distribution of distances between subsequent events; green dashed line – distribution of distances between the trigger and the aftershocks

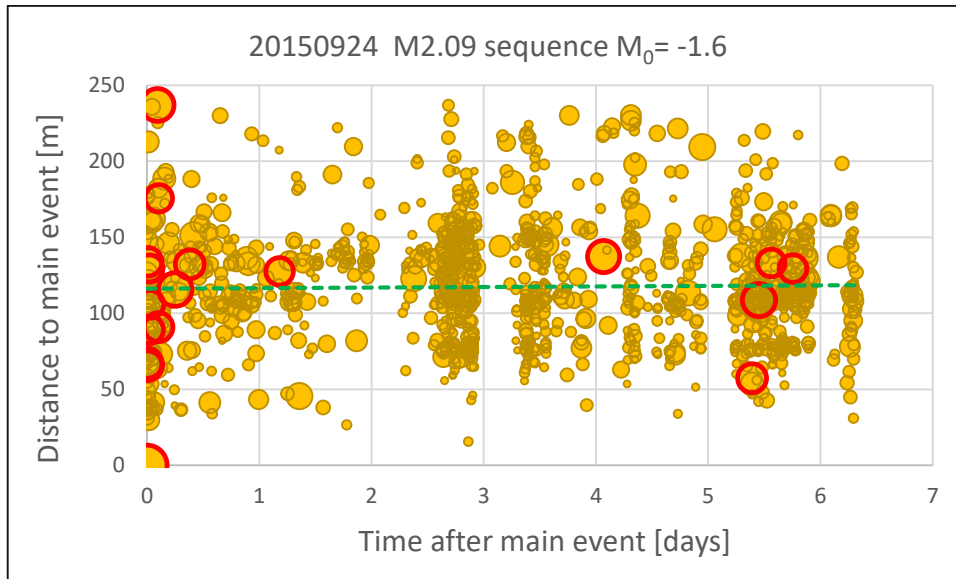


Fig.4.85 Temporal evolution of distances between the hypocenter of each aftershock and the main event hypocenter. Circle size corresponds to event magnitude. Red circles denote events with magnitudes $M \geq 0$.

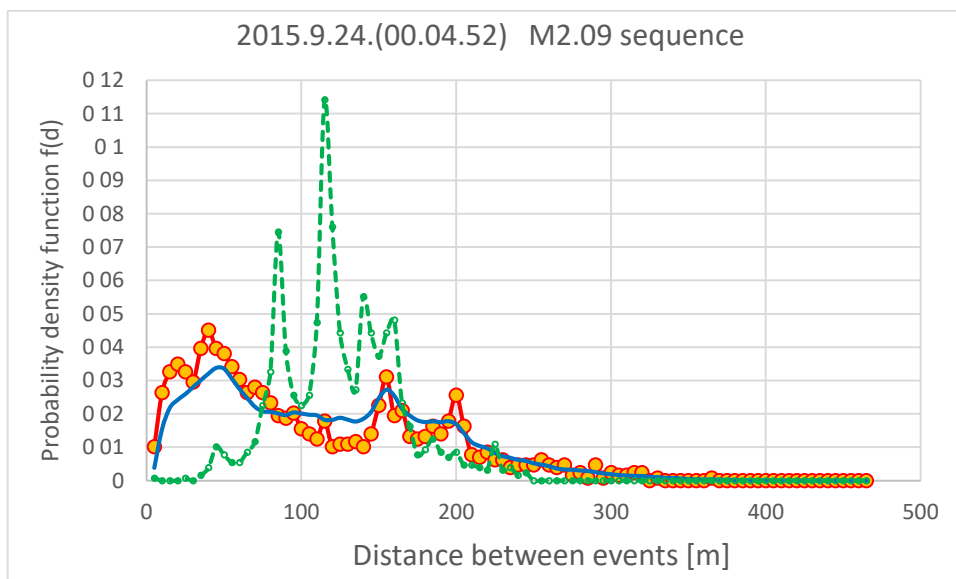


Fig.4.86 Notation as in Fig.4.84

As mentioned in chapter 3.3, the distances between aftershock hypocenters could carry information about stress redistribution after a trigger event, possible processes of hypocenter diffusion or sub-clustering etc. To identify similar non-random features, it is necessary to develop a reference distribution that models the null hypothesis of independence in the realization of aftershocks in space.

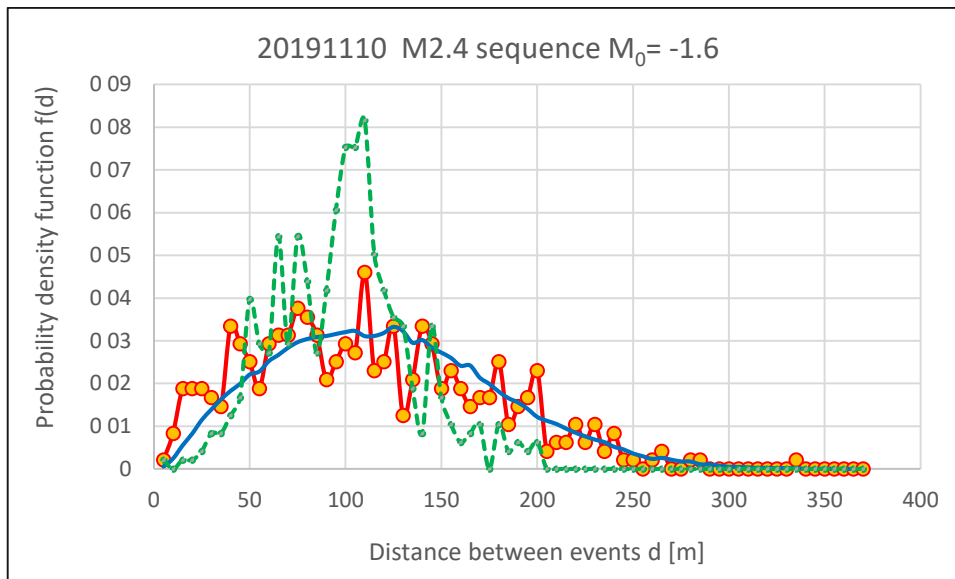


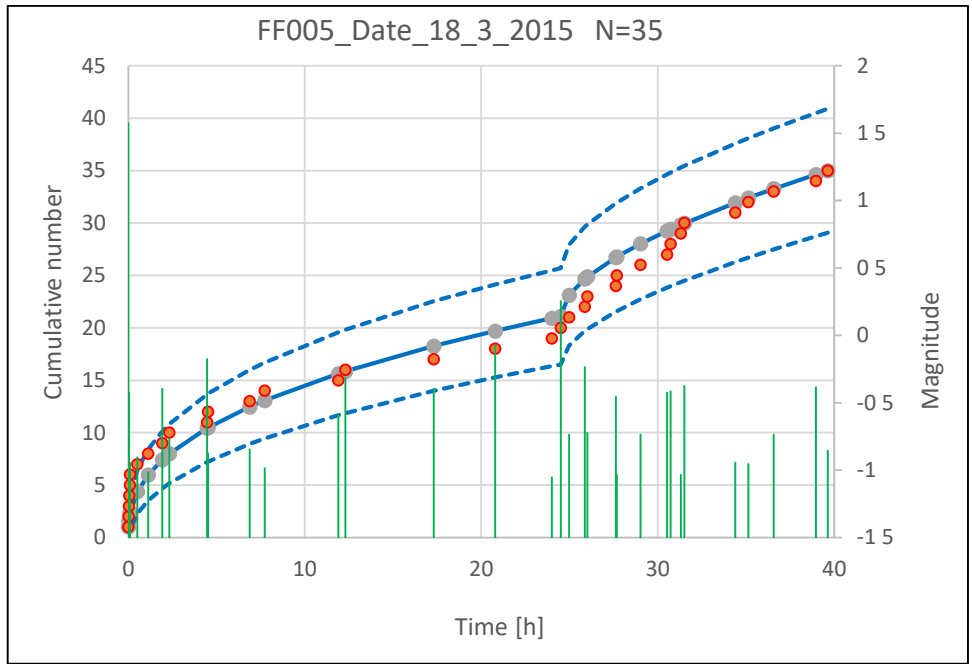
Fig.4.87 Distribution of distances between hypocenters of aftershocks: thick blue line – distribution of all possible distances between different events; red line with points – distribution of distances between subsequent events; green dashed line – distribution of distances between the trigger and the aftershocks

My suggestion is that we could apply the distance distribution between all possible hypocenters as such a model of the null hypothesis. Deviations of the real distance distribution (to trigger hypocenter or between subsequent aftershocks) could point to important characteristics of the aftershock process.

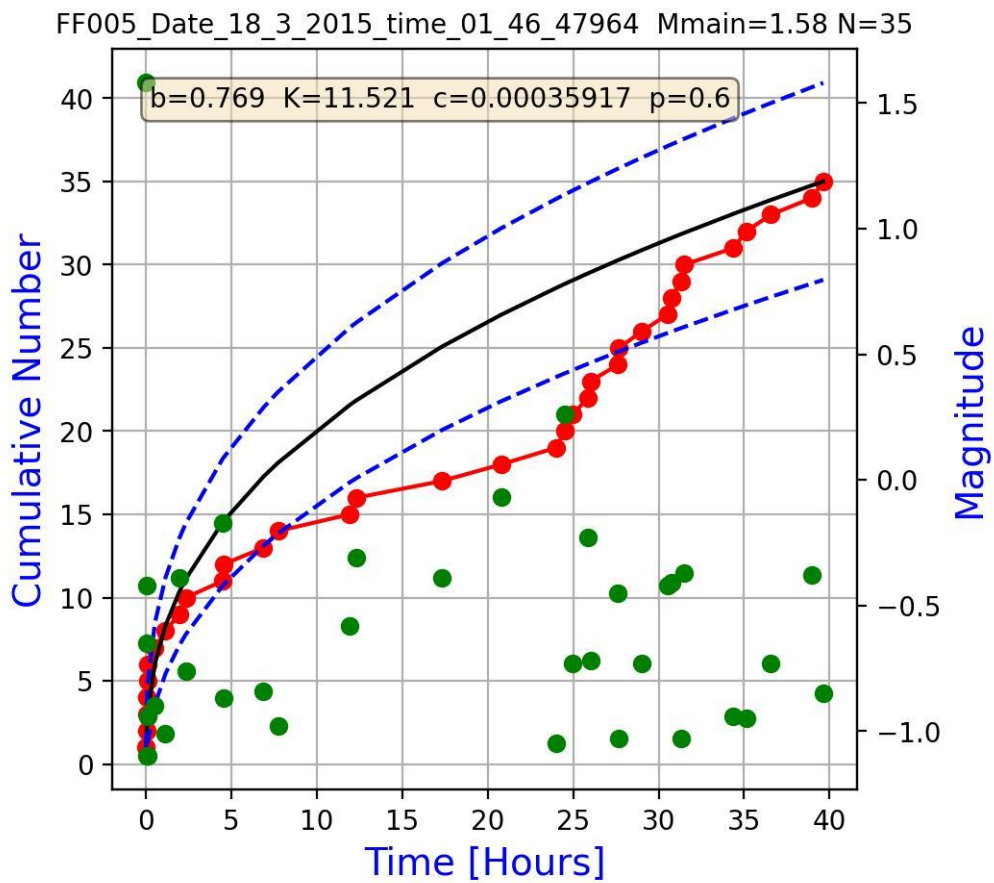
In this chapter I provide the results from the distance analysis of several aftershock sequences in Kiruna mine their choice made so that there could be enough events in each sequence. If, for example we examine Fig.4.86 and Fig.4.87, a significant deviation can be identified between the distance distribution between trigger and aftershocks for the range 90-140 m (green dashed line compared to thick blue line). A possible cause of these results could be the existence of a secondary cluster of aftershocks at a distance around the observed range.

4.3 RETAS model example [\(bck\)](#)

If one examines the plots of the cumulative curves after the MOF model for each aftershock sequence (Fig.4.1 to Fig.4.82) it can be seen that in some cases the MOF model does not provide a good fit of the aftershock evolution in time. This is often related to sequences which are more complex and form secondary clusters in time. In this chapter I have presented an example of how another model (RETAS) can be applied more successfully to capture how aftershock rate changes in time.



a)



b)

Fig.4.88 Demonstration of two stochastic models applied to model the temporal distribution of one and the same aftershock sequence: a) RETAS model; b) MOF model

In fact, the studied sequence (see Fig.4.88) was modeled by both the RETAS and the MOF models. It can be seen that the RETAS model fitted the real data much better than the MOF one (compare Fig.4.88a to Fig.4.88b). As mentioned before, however, there are some problems to use RETAS for operational purposes as it is not adequate for quick estimation of the duration of a starting aftershock sequence.

In fact, several aftershock sequences from Kiruna mine have been previously analyzed statistically and modeled by the RETAS model (including MOF as one of its versions. Below follows some info about these sequences and the results from their analysis were presented by Gospodinov in an internal report (2020).

M2.05 Aftershock sequence of 2015-9-10, started at 8:51:45

M2.14 Aftershock sequence of 2015-9-17, started at 13:30:33

M2.09 Aftershock sequence of 2015-9-24, started at 00:04:52.

M2.14 Aftershock sequence of 2019-12-26, started at 15:48:13

M2.41 Aftershock sequence of 2019-11-10, started at 1:32:54

4.4. Statistical relations between the aftershock sequence parameters [\(bck\)](#)

One of the advantages of the ForA1.0 software is that it offers the possibility for quick analysis of a big number of aftershock sequences (N=103 in our case).

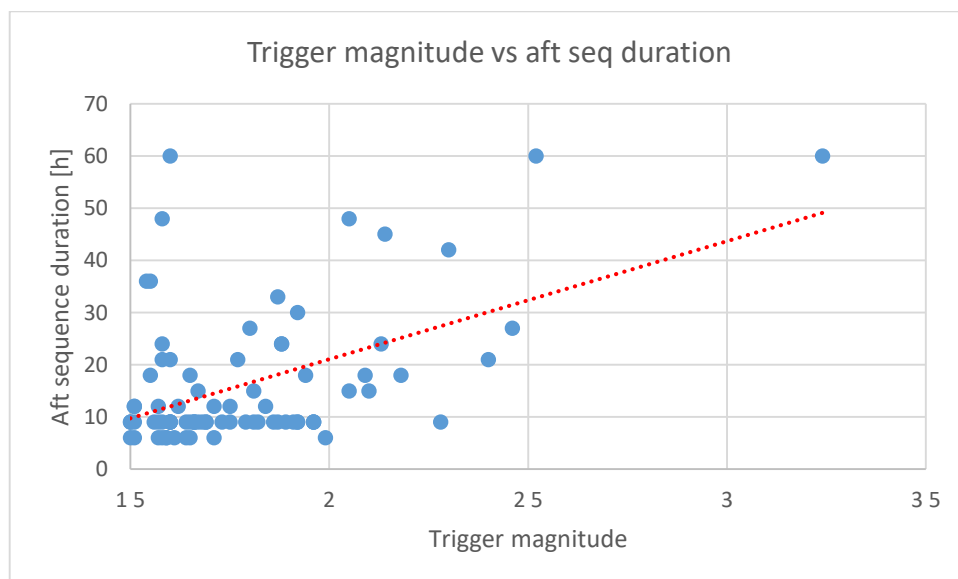


Fig.4.89 Correlation between the trigger magnitude and aftershock sequence duration.

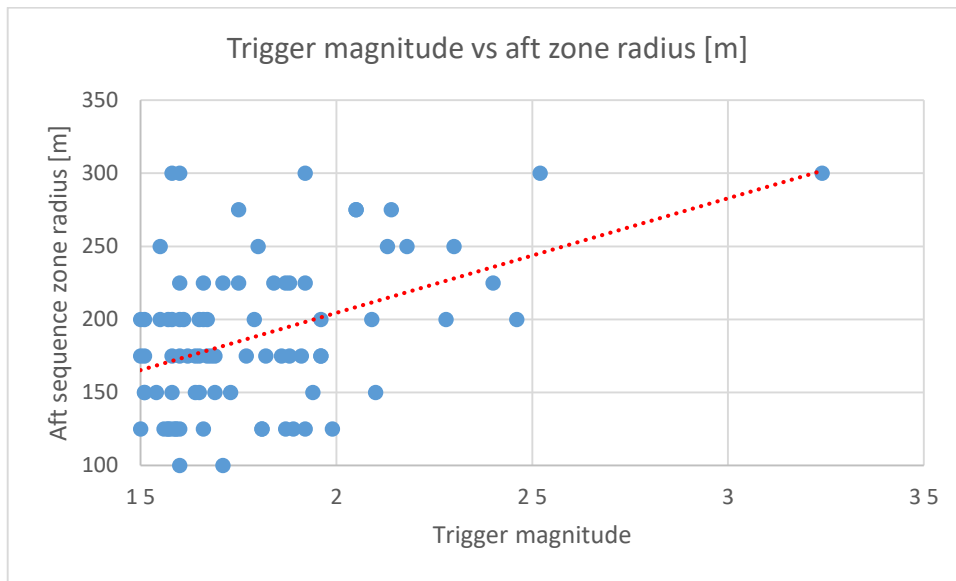


Fig.4.90 Correlation between the trigger magnitude and the aftershock zone radius.

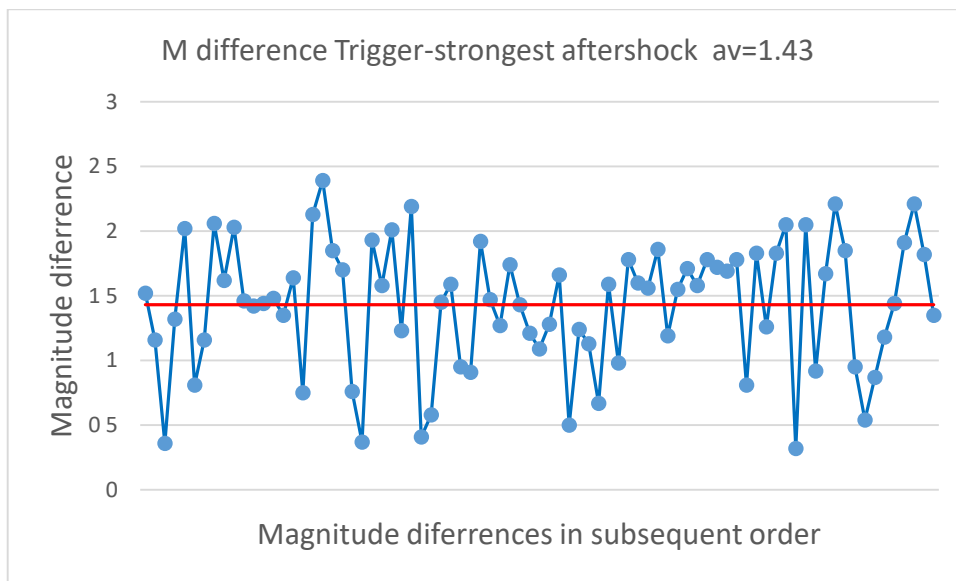


Fig.4.91 Differences between the trigger magnitude and the strongest aftershock magnitude. The average value is 1.43

Within minutes the program provides a number of parameters of the different sequences (see Table 4.1). Then one can easily examine the correlation between the parameters. I have presented the results from similar analyses on Fig.4.89 to Fig 4.93.

It could be expected that the aftershock sequence duration and the zone radius would expand with the trigger magnitude increase and the results on Fig.4.89, 4,90 do support this expectation for Kiruna mine (this is not so for Malmberget mine, Sweden).

The observed correlations allow to estimate the duration and the aftershock zone radius of a starting new sequence immediately after the trigger magnitude is known.

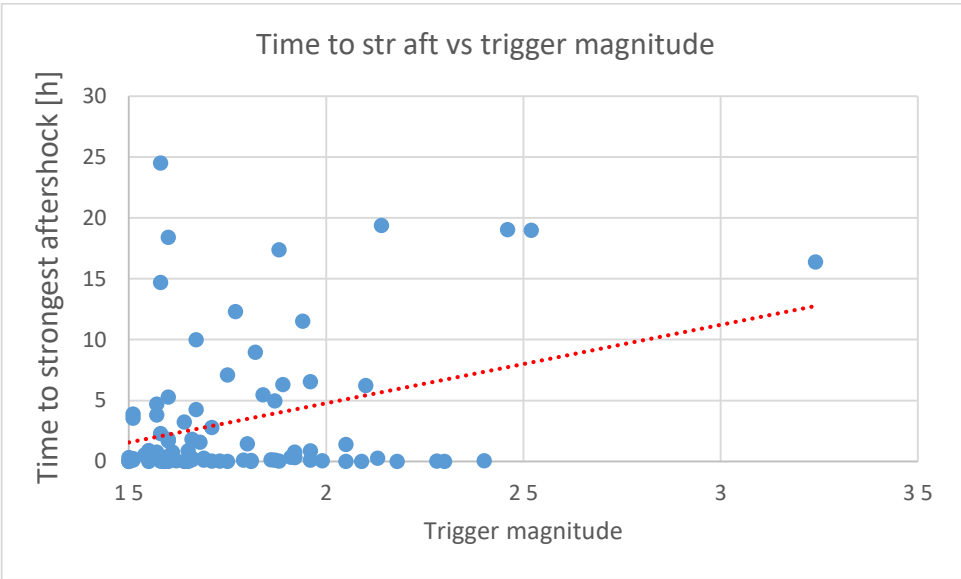


Fig.4.92 Correlation between the trigger magnitude and the time to the strongest aftershock.

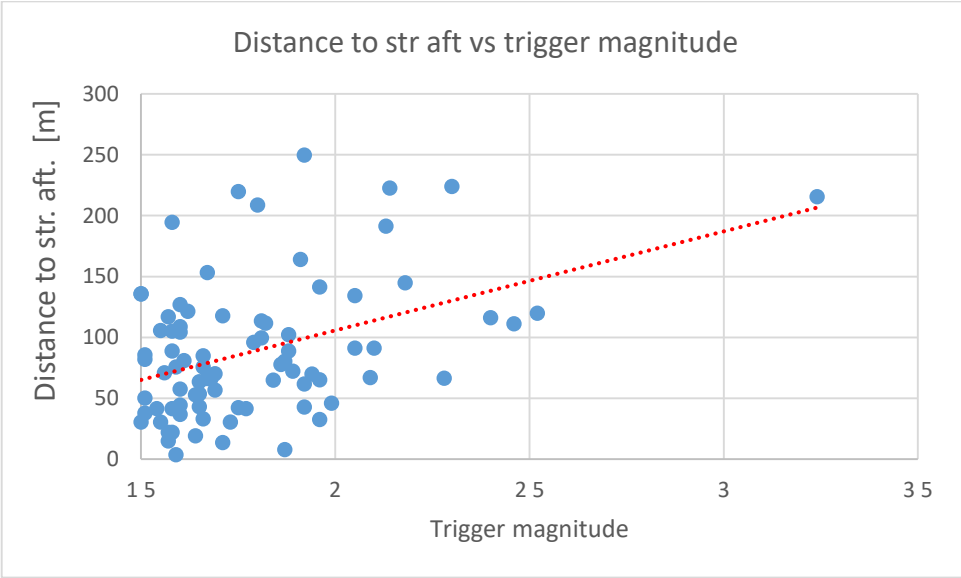


Fig.4.93 Correlation between the trigger magnitude and the distance to the strongest aftershock.

Certain correlation was found both between the trigger magnitude and the time and distance to the strongest aftershock (Fig.4.92, 4.93). The results on Fig.4.91 show an average magnitude difference between the trigger magnitude and the one of the

strongest aftershock of around 1.43. This value is quite somewhat different from the value of 1.2 which is valid for crustal earthquakes after the so called Bath's law (Bath, 1965).

A more detailed analysis of the correlation between the aftershock parameters displayed in Fig.4.89 to 4.93 is presented for separate volumes in Appendix B.

5. Forecasting the aftershock rate and occurrence probability evolution [\(bck\)](#)

One of the major goals of the current project was to develop algorithms and corresponding software by which to verify the possibility to apply stochastic models for re-entry protocol purposes in real time. The general approach to solving this task is based on the following steps:

- a) the software keeps track of each incoming earthquake in real time.
- b) if its magnitude is less than the trigger threshold magnitude (in our case $M=1.5$), the event is saved in the background events file.
- c) If the magnitude $M \geq 1.5$ the system enters an alarm state
 - The rate and the occurrence probability evolutions are plotted after the MOF model with average MOF parameters, estimated on previous aftershock sequences
 - An estimate of the starting sequence duration is provided, based on the time at which certain value of the decay rate is reached
 - A 3D spatial plot is also started which at the beginning contains only the trigger event hypocenter and later all future aftershock hypocenters are included.
 - The ForA1.0 software starts compiling the new aftershocks in a new file (new directory also)
 - When the number of events of the new sequence reaches $N=20$ (40, 60, ...), the software performs recalculation of the MOF parameters, re-plotting the evolution curves hence providing new estimate of the aftershock sequence duration
 - If it turns out that the new series has less than 20 events, the first evolution plot, based on averaged parameters will remain until the end of the alarm state.
 - To define the spatio-temporal boundaries of the new series, which is relevant when a decision has to be made about the re-entry time, the user can use alternatively the average duration and radius values (plotted on the software window) or the duration estimate provided by the stochastic model.
 - When the number of events is less than 20, it is recommended to use the average values because the initial random model, based on average MOF parameters, can give quite different results from those for the specific series.
 - The sequence ends after the average duration time is over.



Fig.5.1 Demonstration of the directory containing the plots from the subsequent rate evolution forecasts after the simulation file

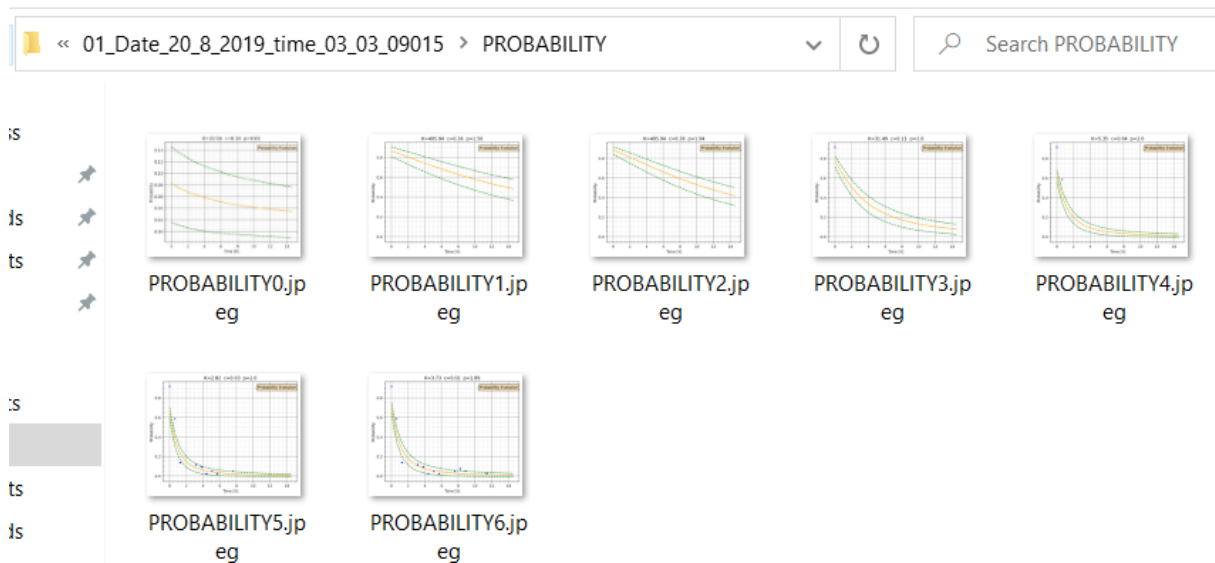


Fig.5.2 Demonstration of the directory containing the plots from the subsequent occurrence probability forecasts after the simulation file

In a real-time case, as the sequence could last for hours, there will be enough time for the user to arrange the evolution and the 3D windows on the monitor. As we used a simulation file to stand for a new aftershock sequence, the whole procedure is over within seconds, so the user has little time to do that arrangement.

On the other hand, all forecasting rate and probability windows are saved in separate directories (see ForA1.0 user's guide for more details – Appendix A), so

that the user can look at them retrospectively after the sequence is over (see Fig.5.1, 5.2)

6. Software [\(bck\)](#)

I first attempted to use the ZMAP software (Wiemer, 2001) to solve part of my tasks but it is developed to analyze specifically crustal seismicity and I could not apply it to mining seismicity. FORTRAN language was first used to program nearly all algorithms needed.

6.1 mXrap [\(bck\)](#)

The mXrap is a basic software applied in both Malmberget and Kiruna mines to deal with different aspects of mining seismicity. After I got access to it I used this software a lot for different purposes. Firstly, this was the software by which I prepared and exported the initial data catalog. What is more, I utilized it during the entire period of the project work for comparison purposes while elaborating the ForA1.0 modules.

6.2 ForA1.0 [\(bck\)](#)

The ForA1.0 software (Fig.6.1) is a package of software modules written in PYTHON (one unit in FORTRAN) which can tackle the following tasks:

- Error checking – reading the initial catalog and verifying it for some errors (empty lines, empty fields etc.)
- Initial aftershock sequence identification on user defined aftershock sequence duration and zone radius.

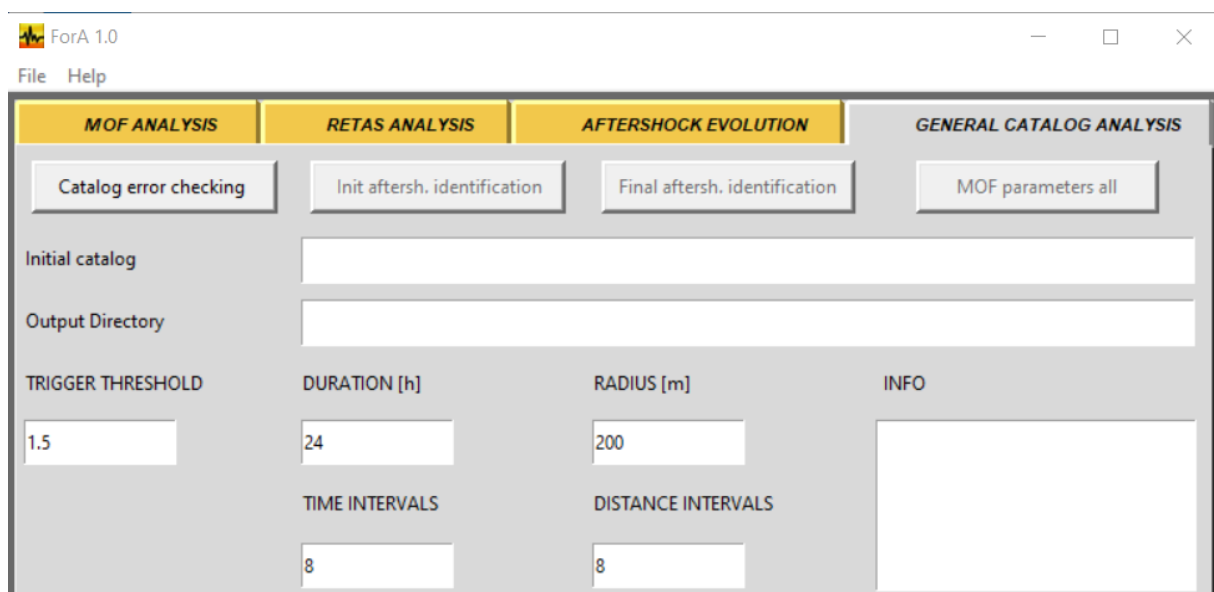


Fig.6.1 Basic view of the ForA1.0 software

- Final aftershock sequence identification after an algorithm based on background seismicity
- Analyzing all identified sequences by the MOF model and plotting the results
- Saving the obtained parameters for the analyzed sequences
- Calculating and saving the average parameter values for the different mine volumes and for the entire mine
- Forecasting and plotting the rate evolution of a starting aftershock sequence
- Forecasting and plotting the occurrence probability evolution of strong aftershocks
- Plotting the spatial evolution (hypocenters) of a new aftershock sequence

Much more details about ForA1.0 are provided in the user's guide (Appendix A) in the chapter below (chapter 8).

7. Comments and outlook [\(bck\)](#)

From the beginning, the work on the current project was focused on several directions. The first of them was the choice and compiling of the initial data catalog and the activities related to this field were described in chapter 2. What I would like to point out as a conclusion about his part of the work, is the importance of the data unification, data format and lack of errors. The procedures here will not have to be repeated often as new aftershock sequences have to be added to the database to be worth performing a new analysis. That provides enough time and motivation to thoroughly analyze and prepare the initial data.

The methodology chapter (Chapter 3) presents all the algorithms and methods which were applied for the aftershock sequences initial and final identification and the stochastic models which were used to depict the energy and temporal aftershock distributions. The approach to calculate the occurrence probability evolution of strong aftershocks with time was also applied. After the initial sequence identification on a user defined spatio-temporal filter, the final identification was performed on an algorithm which keeps a track when and how far from the trigger hypocenter the aftershock rate reaches the background seismicity level. The stochastic model which has been applied to model subsequently the temporal distribution of all identified aftershock sequences, was the MOF model which was chosen because it can be used to estimate sequence duration after the rate decays to a predefined level. The Gutenberg-Richter law formed the necessary basis for modelling of the aftershock magnitude distribution and hence for the occurrence probability calculation of strong aftershocks.

The presented methods for the rate and occurrence probability estimation were implied in the developed ForA1.0 software. If the software could have access to the data for the occurring new events from the mine, it would start its 'Aftershock evolution' module after a new sequence begins (new trigger) and evolution plots would be shown of both rate and probability, plotting also the subsequent hypocenters of new aftershocks. These evolution plots will first be based on the average MOF parameters obtained from all analyzed previous sequences and then will be recalculated after each new 20 aftershocks. Forecasted estimates of the ongoing sequence duration will be provided after each re-calculation together with the average aftershock zone radius to

help the staff in Kiruna mine make their decisions about the needed activities in the mine.

As there is no access to the ongoing seismic activity of Kiruna mine, the software was set to test the above options by using a sample file (one of the aftershock sequences with other events) by which to simulate the current seismicity reading the events one by one until the trigger is recognized. Then the 'Aftershock evolution' module runs and the rate and probability evolution plots are presented.

Generally, the fulfilled analysis of the Kiruna mine seismicity revealed some specific features. A considerable number of sequences (~ 37%) are not well fitted by the MOF model either due to slow or non-decaying behavior or to the existence of secondary clustering of the aftershocks. This could, however, lead to poor forecast success in the case of a new aftershock sequence.

A characteristic feature of Kiruna mine aftershock activity turns to be the often identified abrupt start of the aftershock sequence with no or very small rate decay at the beginning. That surely means that the forecasted sequence duration on MOF parameters, determined after data from the beginning of the series, will be overestimated. This effect was also found in the simulation file analysis 'evolproba.csv' (see Fig.4.32), which was applied for the rate and probability simulation in the ForA1.0 software. There is a number of other sequences which exhibit similar behavior like having a high rate (higher than predicted by the MOF model) at the start of the corresponding sequence (see, for example, Fig.4.4, 4.6, 4.8, 4.10, 4.12, 4.15, 4.27, 4.29, 4.33, 4.50, 4.52, 4.65, 4.67, 4.70 etc.). If a new aftershock sequence starts in real time and it has similar characteristics, it is quite probable that the duration estimate based on the MOF model, will be overestimated at the beginning of the sequence. In similar cases it would be the user's responsibility to choose between the MOF forecasted sequence duration and the average duration value of all sequences in Kiruna mine, both provided by the ForA1.0 software.

Summarizing the experience, I gained during the implementation of this project, I could classify possible future activities in this direction into the following groups:

Research – the present analysis revealed that in some cases of more complex aftershock sequences a more sophisticated model is better to be applied and in fact the RETAS model has been successfully used to model an aftershock sequence in Kiruna mine (Dineva et al., 2022). The latter model, however, is not appropriate for determining the duration of the aftershock sequence. In fact, it could be used to model

general seismicity in the mine but considering the software and the data volume problems we faced even with only aftershocks, modelling general seismicity could be a very hard task.

The magnitude and the temporal aftershock distributions were modeled in this project by the Gutenberg-Richter and by the MOF models but no model was offered for the spatial distribution which was analyzed only empirically. That is why it seems appropriate to propose and use models for the analysis of the spatial distribution of aftershocks. Ogata & Zhuang (2006) offer a spatio-temporal ETAS model which could be verified on mining seismicity and for deeper analysis of distances between aftershock hypocenters one could use the approach developed by Gospodinov (2004) and Gospodinov & Christoskov (1988).

In this project the work was focused only on the study of rate changes of mining seismicity and the possible use of the results for re-entry considerations. The interrelation of different parameters associated to activities in the mine, however, are much more complex and it seems necessary to consider them, too. That can be done in a more general approach when re-entry is concerned by using more modern methods (regression, AI methods etc.).

Practical issues – the developed ForA1.0 software offers a tool for automatic forecasting of the rate and occurrence probability evolution after a trigger event occurs and a new aftershock sequence begins. The software is set to work with no more than N=999 trigger events (sequences) in the initial catalog file. This tool is useful but not a complete solution for solving all issues related to mine re-entry and the final decision must be made by the appropriate mine personnel. The software is dependent on the user defined choice of a number of parameter values such as: initial aftershock sequence duration and zone radius; number of intervals for the final identification algorithm; minimum magnitude of strong aftershocks for probability evolution; rate and occurrence probability values at which the ‘alarm’ can be considered over and re-entry permitted etc. We have chosen some of these values on the basis of our experience but the optimal selection should be based on additional information from the mine.

8. Appendix A (ForA1.0 user's guide) [\(bck\)](#)

ForA USER'S GUIDE

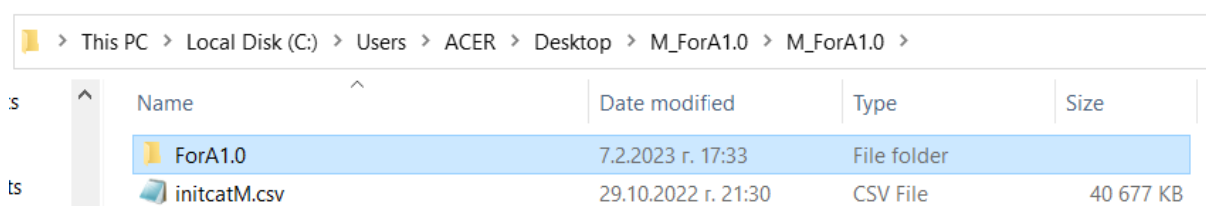
Contents

1. General Catalog Analysis	85
1.1 Catalog error checking	86
1.2 Init aftershock identification	87
1.3 Final aftershock identification	88
1.4 MOF parameters all	91
2. Aftershock Evolution	94
2.1 Aftershock rate evolution	96
2.2 Occurrence probability evolution	97
2.3 Spatial evolution	97
3. MOF Analysis	97
4. RETAS Analysis	97
5. A very short ForA1.0 user's guide:	

For the implementation the main goal of forecasting the space, rate and occurrence probability evolution of the aftershock process immediately after a trigger, one has to follow certain sequential steps to prepare the results needed for the execution of the final software module. ForA1.0 software was developed for recalling the tasks of the current project. Among its main options are the possibility to identify aftershock sequences from a general catalog with many sequences, to analyze and model all identified sequences and to obtain different parameters like the b-value, MOF parameters K, c, p , time duration and spatial radius of each sequence. The software also provides the average values of these parameters for the entire zone of the investigated volumes or for each volume separately. These software options analyze the set of sequences somewhat automatically, thus avoiding the need to refer to each series individually and the analysis is done much faster. The software is set to work with no more than $N=999$ triggers (sequences) in the initial catalog.

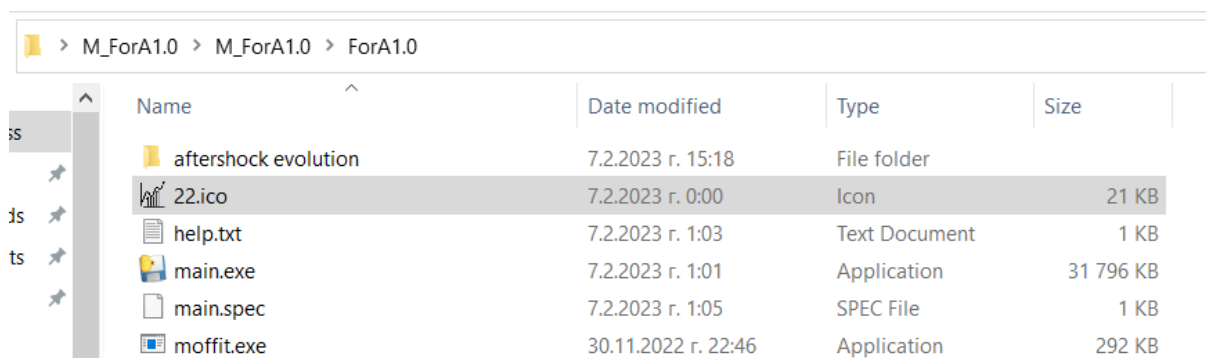
1. General Catalog Analysis [\(up\)](#)

After unzipping the installing file M_ForA1.0.zip one gets access to the following files and directories (Fig.A1). The file *kirinit.csv* (for Malmberget mine the file is *initcatM.csv*) is the initial catalog exported from mXrap which contains all seismic events from Kiruna mine following the chosen filters (Mo, time period, chosen volumes etc.). This is the initial file on which all further analysis will be based. It may have another name and be in another directory (it will be later selected for the software execution).



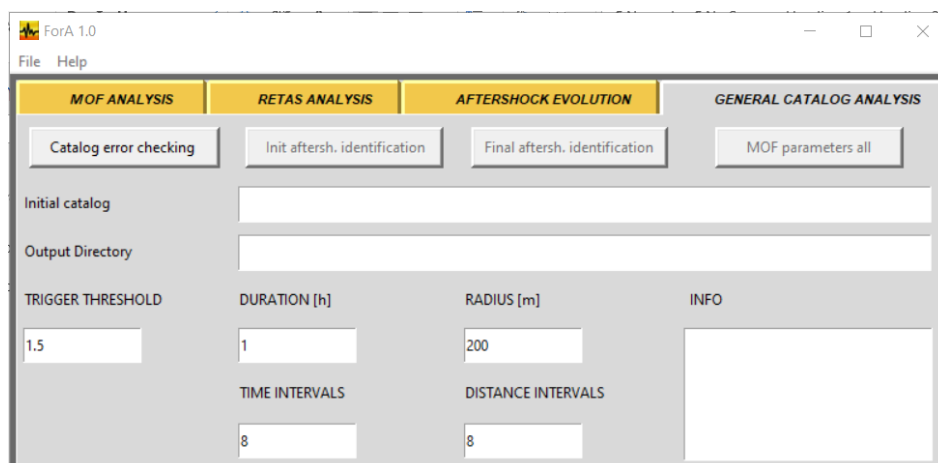
Name	Date modified	Type	Size
ForA1.0	7.2.2023 r. 17:33	File folder	
initcatM.csv	29.10.2022 r. 21:30	CSV File	40 677 KB

Fig.A1 Directory and file structure immediately after unzipping the installing file



Name	Date modified	Type	Size
aftershock evolution	7.2.2023 r. 15:18	File folder	
22.ico	7.2.2023 r. 0:00	Icon	21 KB
help.txt	7.2.2023 r. 1:03	Text Document	1 KB
main.exe	7.2.2023 r. 1:01	Application	31 796 KB
main.spec	7.2.2023 r. 1:05	SPEC File	1 KB
moffit.exe	30.11.2022 r. 22:46	Application	292 KB

Fig.A2 Structure of the ForA1.0 directory



ForA 1.0

File Help

MOF ANALYSIS **RETAS ANALYSIS** **AFTERSHOCK EVOLUTION** **GENERAL CATALOG ANALYSIS**

Buttons: Catalog error checking, Init aftersh. identification, Final aftersh. identification, MOF parameters all

Initial catalog: []

Output Directory: []

TRIGGER THRESHOLD: 1.5

DURATION [h]: 1

RADIUS [m]: 200

TIME INTERVALS: 8

DISTANCE INTERVALS: 8

INFO: []

Fig.A3 Starting window of the ForA1.0 software

The ForA1.0 directory contains the following files (Fig.A2) to be considered. The *moffit.exe* file is an executable file, written and compiled in FORTRAN. It is called by the main Python program and the user doesn't have to interact with it.

The *help.pdf* file contains the ForA1.0 user's guide. The executable file to run ForA1.0 is *main.exe*. There is also a directory 'aftershock evolution' in which all results from the software module 'aftershock evolution' will be saved. The considered files in the ForA1.0 directory should be in one directory while the directory may have another name and be in another directory (it will be later selected for the software execution).

1.1 Catalog error checking [\(up\)](#)

After starting ForA1.0 (run *main.exe*) a window will be opened similar to the one on Fig.A3 (if another option is selected (in grey), please select 'General Catalog Analysis'). To select the initial catalog file one should click in the 'Initial catalog' window and then select the file through 'File -> OPEN FILE' which in this case is `C:/Users/ACER/Desktop/M_ForA1.0/M_ForA1.0/initcatM.csv`.

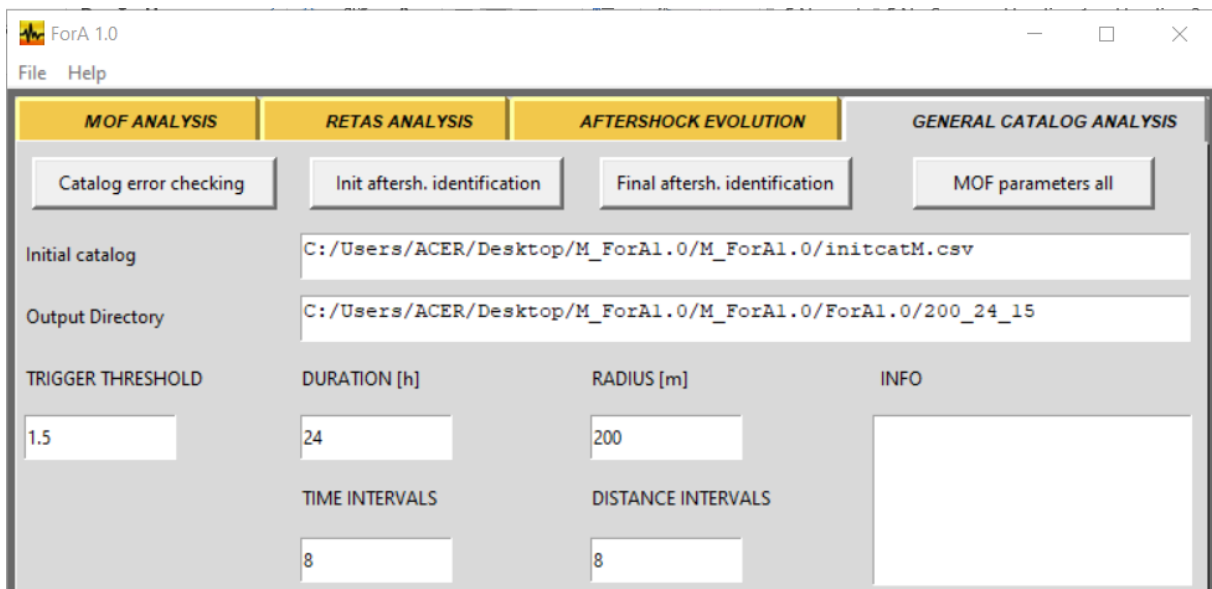


Fig.A4 Choosing the initial catalog file and output directory for 'Catalog error checking' and 'Init aftersh. identification'

Then an output directory should be selected for the sub-directories with the aftershock sequences. Click in 'Output directory' and select one through 'File -> SELECT OUTPUT DIRECTORY FOR CATALOG ANALYSIS'.

The output directory should be created in advance outside ForA1.0

In this case I created a directory (it will be empty at the beginning) C:/Users/ACER/Desktop/M_ForA1.0/M_ForA1.0/ForA1.0/200_24_15 for the output of the aftershock sequences,

The directory name was chosen to carry info about the user chosen aftershock zone radius (200 m by default), time duration (24 hours by default) and min trigger threshold (by default $M=1.5$) (Fig.A4). These default values can be changed by entering different values in the corresponding windows. I also created another output directory 300_600_15 in which to save the results from the initial catalog analysis for different user defined radius (300 m) and duration (60 hours)

The first option to use after selecting the initial catalog is 'Catalog error checking'. The module checks for some errors in the initial catalog – empty row or empty fields which could sometimes appear for different reasons. If an error is found, the number of the row is printed in the 'INFO' window. The errors should be corrected outside the program and the file selected again for analysis. If no errors were found, the message 'NO ERRORS' is written in the 'INFO' window.

The 'Catalog error checking' option is not obligatory but it is advisable. It is recommended to check the initial catalog for errors in advance before providing it to ForA1.0 for analysis.

1.2 Init aftershock identification [\(up\)](#)

In case of no errors one can run the 'Init aftersh. analysis' module (see Fig.A4). The windows 'TIME INTERVALS' and 'DISTANCE INTERVALS' are out of use, so it is not necessary to change the default values there.

After running the module, the program identifies all aftershock sequences following each trigger event ($M \geq 1.5$) according to the user defined spatio-temporal filter (Fig.A4). The program also creates a subdirectory in the selected output directory for each sequence (see Fig.A5) where it saves a file with the identified trigger and aftershocks (the directory name and the file name are after the trigger date and time of occurrence).

By this the initial aftershock identification after the user defined filter (200 m x 24 hours in this case) is completed and a message 'AFTERSHOCK IDENTIFICATION COMPLETED' appears in the 'INFO' window. It takes about one minute to identify 67 sequences out of around 500000 events in the initial catalog (average PC functionality; WINDOWS 10).

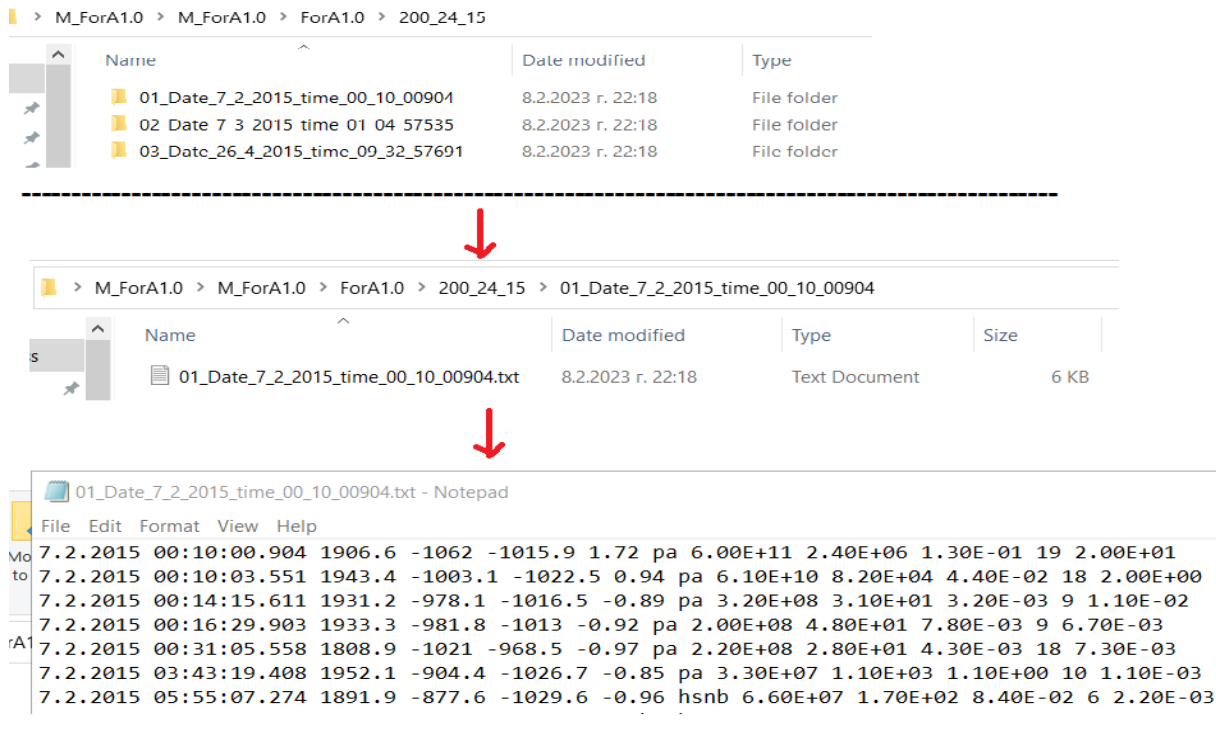


Fig.A5 Results from the execution of the 'Init aftersh. identification' module. (see explanations in text)

1.3 Final aftershock identification [\(up\)](#)

To apply the 'Final aftersh. Analysis' module it is obligatory to have applied the 'Init aftersh. identification' module first. This is so because the execution of the 'Final aftersh. Analysis' is based on the analysis of each initially identified aftershock sequence. The algorithm of final aftershock identification is developed after these main assumptions:

- The aftershock zone is modeled in space as a sphere whose center coincides with the trigger hypocenter
- Aftershock density decreases with the increase of the distance between aftershock hypocenters and the trigger
- Aftershock rate decreases with the increase of the time period between aftershock occurrence and the trigger occurrence

The above suppositions seem quite reasonable as this has been the case with many aftershock sequences, both crustal and in mines. Basing on these hypotheses one could consider the final radius of the aftershock zone to be the one for which aftershock hypocenter density decays to background density, calculated for the same sphere on events before the sequence has started (Fig.A6a). The algorithm to perform the final identification is demonstrated graphically on Fig.A6a where the darker color denotes higher density and the sequence radius is the one for which densities (colors), both for aftershocks and for background events coincide (dashed line).

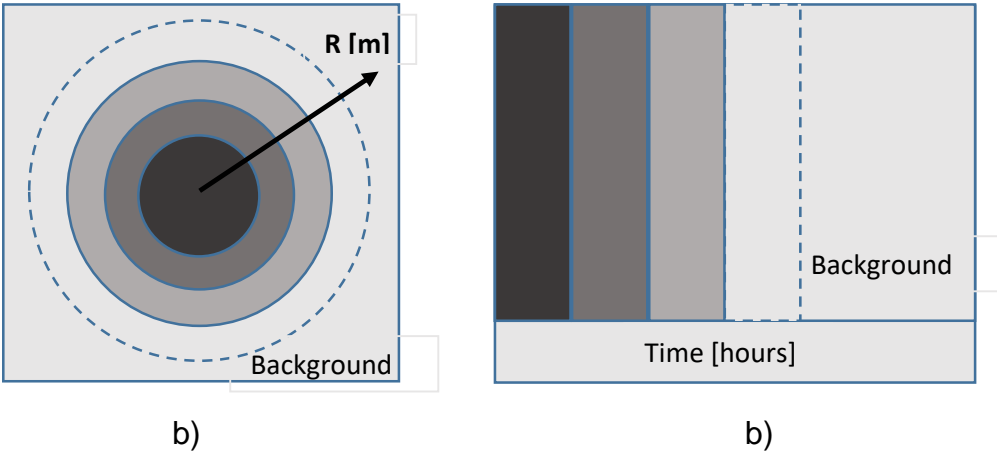


Fig.A6 Demonstration of the algorithm on which final aftershock identification is based: a) in space; b) in time (see details in text)

> This PC > Desktop > M_ForA1.0 > M_ForA1.0 > ForA1.0 > 200_24_15 > 01_Date_7_2_2015_time_00_10_00904

Name	Date modified	Type	Size
01_Date_7_2_2015_time_00_10_00904.txt	8.2.2023 r. 22:18	Text Document	6 KB
FF01_Date_7_2_2015_time_00_10_00904.txt	9.2.2023 r. 15:10	Text Document	6 KB
PARAMETER.txt	9.2.2023 r. 15:10	Text Document	1 KB

PARAMETER.txt - Notepad

```
File Edit Format View Help
New distance- 200
New time- 24.0
```

Fig.A7 File structure of a certain trigger sub-directory containing the initial and the final aftershock sequences identified. 'PARAMETER.txt' file saves the final radius [m] and duration [h]

A similar approach is applied for the final estimation of the aftershock sequence duration. It is considered that the time when the aftershock rate (number per unit interval) decays to the background rate (for the same space volume) marks the duration of the sequence (coinciding colors on Fig.A6b)

So, what the 'Final aftersh. Analysis' module does is to open the initial aftershock sequence for a specific trigger, to analyze it following the above algorithm and to provide a final aftershock sequence saved as a text file in the same directory for this sequence (Fig.A7). 'FF' is added to the initial file name to make difference between the initial and the final file.

A file named saves the final radius [m] and duration [h]. All this is done by the module for every sequence and the corresponding final sequences are saved in the different sub-directories.

It is important to note that one should be careful about selecting the output directory where the 'Init aftersh. identification' has been run before executing the 'Final aftersh. Analysis' module.

It is also significant to make the right choice of the number of distance intervals ('DISTANCE INTERVALS' window) by which to divide the user defined radius and the number of time intervals ('TIME INTERVALS' window) by which to divide the user defined duration for the final identification. If, for example, one chooses 8 distance intervals and 8 time intervals (as by default), that means that the distance interval length for radius $R=200$ m will be 25 m and the time interval for duration of 24 hours will be 3 hours. These intervals (25 m and 3 h) turn to be reasonable as for many sequences the number of aftershocks is no more than 20-30 events and smaller intervals could lead to fewer events in an interval. If, on the opposite, the intervals are much bigger, we could lose some details of the distributions. This means that if the user defined radius is set to 300 m it would be reasonable to number of distance intervals to 12 so that the interval length is again 25 m etc. These considerations are only advisable and not obligatory.

This module takes some more time to process the aftershock sequence (67 in this case) which is around 7-8 minutes.

1.4 MOF parameters all [\(up\)](#)

The 'MOF parameters all' should be run after executing the first two modules - 'Init aftersh. identification' and 'Final aftersh. Analysis'.



Name	Date modified	Type	Size
01_Date_7_2_2015_time_00_10_00904.txt	8.2.2023 r. 22:18	Text Document	6 KB
FF01_Date_7_2_2015_time_00_10_00904.jpeg	9.2.2023 r. 16:43	JPEG File	107 KB
FF01_Date_7_2_2015_time_00_10_00904.txt	9.2.2023 r. 15:10	Text Document	6 KB
PARAMETER.txt	9.2.2023 r. 15:10	Text Document	1 KB

Fig.A8 File structure of a certain trigger sub-directory after saving the cumulative curve MOF plot (.jpeg)

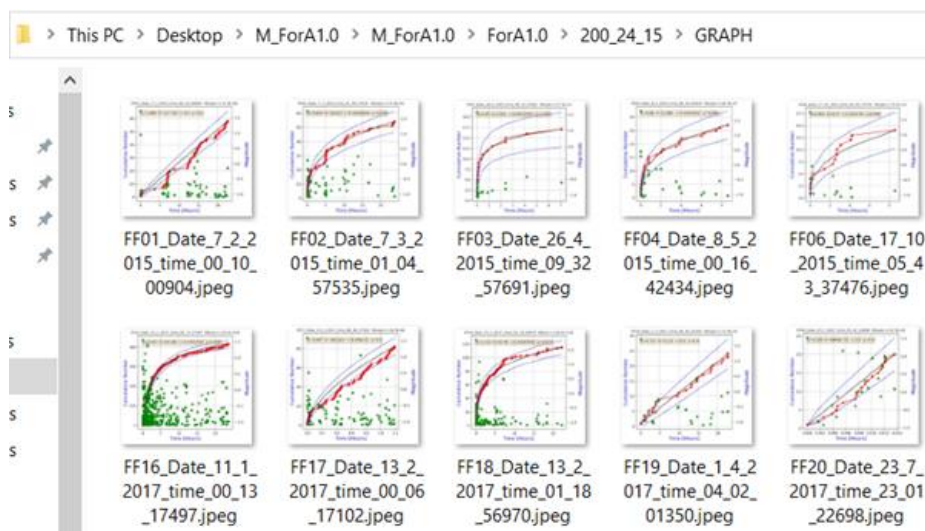


Fig.A9 Directory 'GRAPH' with all cumulative curve MOF plots for the different sequences

Now that one has the final aftershock sequence for each trigger, 'MOF parameters all' allows the program to open each final sequence, determine the b-value and estimating the MLE (Maximum Likelihood Estimates) K, c and p-values of the MOF model for it. A cumulative distribution curve is plotted after the estimated MOF values and the plot is saved in the corresponding subdirectory.

Now each directory for the different sequences contains the initial sequence, the final sequence and the cumulative MOF plot for the final sequence (Fig.A8). Except being

saved in its specific directory, each cumulative MOF curve is also save in a common directory 'GRAPH' (Fig.A9). This provides great convenience in to quickly browse, compare and analyze the results on the plots.

The execution of the current version of the 'MOF parameters all' module is associated with a disadvantage, related to the use of FORTRAN module moffit.exe which is called by the main Python program. This operation causes the appearance of successive flickering FORTRAN console windows for around 30 s which is embarrassing but this problem will be soon solved.

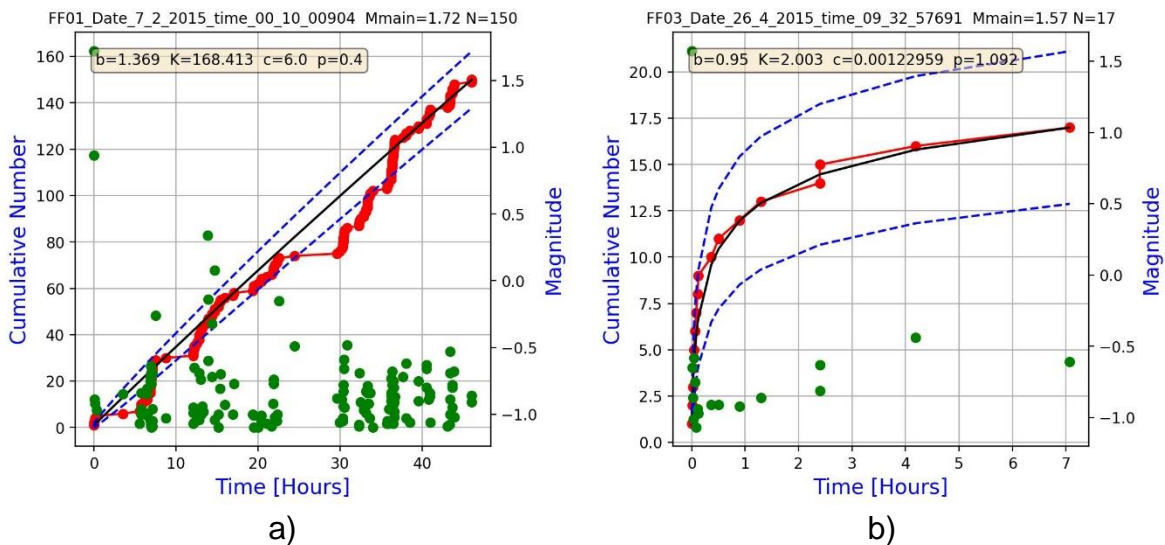


Fig.A10 Illustration of the cumulative MOF plots for two of the sequences. There are similar plots for all sequences with event number $N \geq 5$: a) 'bad' fit – the sequence is not with a decaying rate at all and K, c, p values are far from 'normal'; b) 'good' fit

On the other hand, the 'MOF parameters all' module saves all estimated parameters (b-value, MOF parameters, duration zone radius etc.) in a file mofall.txt. The information in this file could be very useful for further analysis and searching for statistical relationships between the various parameters of the aftershock series. 'MOF parameters all' also calculates and saves in file vmofall.txt the averaged values of some of the aftershock sequence parameters and the corresponding standard deviations for further use in the 'Aftershock evolution' module (Fig.A12).

Among other columns in the mofall.txt file, column 'M' contains the estimated final duration for each sequence, column 'N' refers to the final radius, 'O' – strongest aftershock magnitude, 'P' – events number, 'Q' – distance to strongest aftershock and 'R' – time to strongest aftershock.

	A	B	C	D	E	F	G	H	I	J	K	L	M	N	O	P	Q	R
1	Sq.No	Date	Time	X	Y	Z	M main	Vol	b	K	p	c	Ta [h]	Ra [m]	M2	N	dl2 [m]	dt2 [h]
2	1	'7.2.2015'	'00:10:00.	1906.6	-1062	-1015.9	1.72	pa	1.369	168.413	0.4	6	51	275	0.94	150	69.76396	0.000735
3	2	'7.3.2015'	'01:04:57.	2339.5	-1085.4	-1039.3	1.75	vr	0.923	15.702	0.717	0.00034	9	150	0.12	37	76.94186	0.051938
4	3	'26.4.2015'	'09:32:57.	1890.4	-900.4	-1040.4	1.57	hsnb	0.95	2.003	1.092	0.00123	9	125	-0.44	17	35.90557	4.189256
5	4	'8.5.2015'	'00:16:42.	2013.2	-976.6	-1034.6	1.82	pa	0.68	11.865	0.694	0.000109	9	150	0.45	27	58.54947	0.001844
6	6	'17.10.20.'	'05:43:37.	1802.6	-591.6	-1030.5	1.75	de	0.801	8.13	0.596	2.42E-05	9	225	-0.05	14	59.70142	0.166667
7	7	'30.11.20.'	'08:32:03.	1340.9	-169.2	-1050.3	1.61	biotit	1.127	17.321	0.687	4.73E-05	21	150	0.12	51	11.39737	2.483019
8	8	'13.12.20.'	'00:37:26.	879.5	-1610.8	-950.7	1.58	fa_ka	0.776	8.46	0.4	0.035104	15	225	0.06	10	106.025	1.314198
9	9	'19.3.2015'	'06:03:55.	1970.9	-963.4	-1040.5	1.62	pa	0.806	8.074	0.77	1.18E-05	21	125	0.95	30	38.57331	0.562528

Fig.A11 Contents of the mofall.txt file in the output directory. The file saves info about the trigger event and the sequence that followed it. See details in text

The completion of this module takes less than a minute. If for some reasons the program has been closed after some of the 'General Catalog Analysis' modules have been executed, after running ForA1.0 again the 'General Catalog Analysis' buttons will be deactivated. Choosing the output directory will activate them and one can continue executing the rest modules.

	A	B	C	D	E	F	G	H	I	J	K	L
1	Vol.	b-av	St.d. b	K-av	St.d. K	c-av	St.d. c	p-av	St.d. p	Nc	Tav	Rav
2	pa	0.8956	0.250026	126.442	168.7294	1.333491	2.347522	1.1358	0.943245	5	31.8	175
3	vr	0.873111	0.136734	65.84456	123.1383	0.735068	1.878439	0.881722	0.608023	18	18.66667	170.8333
4	fa_ka	0.8815	0.366883	23.49117	37.0265	1.008812	2.232156	0.7195	0.364901	6	11.5	204.1667
5	biotit	0.786357	0.229788	14993.22	28669.44	1.575755	2.477451	0.712071	0.318072	14	14.78571	157.1429
6	de	0.7886	0.093839	10.026	13.05607	1.200389	2.399805	0.7992	0.265017	5	18	185
7	hsnb	0.762	0.136207	13.34617	15.49923	1.000223	2.235968	0.754833	0.258165	6	16	141.6667
8	All	0.831195	0.202246	2538.729	4837.815	1.14229	2.26189	0.833854	0.45957	54	18.45873	172.3016

Fig.A12 Contents of the vmofall.txt file in the output directory. The file saves the averaged values of some of the aftershock sequence parameters and the corresponding standard deviations for further use in the 'Aftershock evolution' module.

Generalizing the options of the 'General Catalog Analysis' modules of ForA1.0, it can be seen that they allow fulfilling a number of tasks (initial and final sequence identification, estimation of each sequence duration and zone radius, MOF parameter estimation and calculating average parameter values, plotting the results etc.) all performed within around 10 minutes.

2. Aftershock evolution [\(up\)](#)

The 'Aftershock evolution' modules of ForA1.0 aim at providing a forecast of the aftershock sequence duration and zone radius immediately after a strong event in the mine triggers the sequence. One way to do this is to use the averaged values of the durations and radiuses of all previous sequences in the mine which we already have and this approach was applied for the aftershock spatial zone estimation. Another methodology is based on the stochastic modelling of the aftershock temporal distribution. The Modified Omori Formula (MOF) model was chosen due to its simplicity and the possibility it provides to estimate sequence duration once the model parameters are known. It has to be noted that generally the 'Aftershock evolution' modules are intended to work in case the ForA1.6 software has access to each new event occurring in the mine. Up to now it is not known how that will be realized, so, the process of reading newly occurred events in the mine was simulated by subsequently reading events from a sample file one by one.

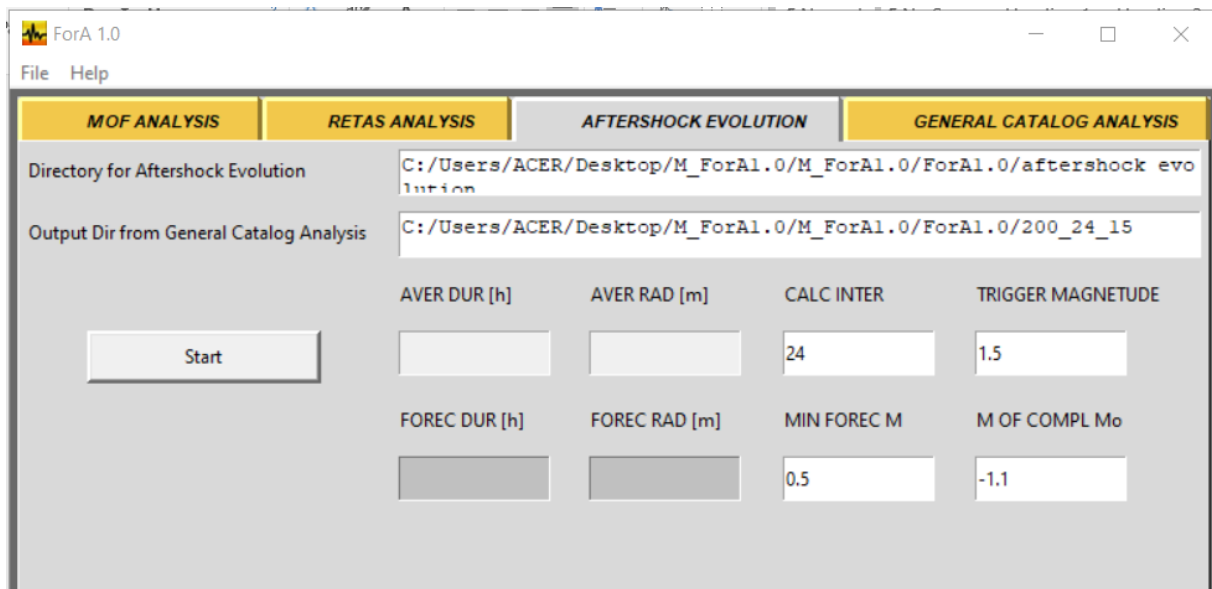


Fig.A13 'Aftershock evolution' window

This file contains only one trigger. The program reads the events one by one (simulating the process of newly occurred events in real time), saves each event in a file for background shocks and is activated for rate, probability and space evolution plotting immediately after a trigger ($M \geq 1.5$). In the current situation of using a sample simulation file, the 'Aftershock evolution' modules are executed simultaneously after clicking the 'Start' button (Fig.A13). Before doing it the user has to select the output

directory (the one used for 'General catalog analysis' where the vmofall.txt is) and a directory for the 'Aftershock evolution' results (it must have been created in advance).

In the 'CALC INTER' window the user has to choose the number of intervals for plotting the rate (and probability) evolution plot. The default value of 24 allows a sufficiently smooth curve to be obtained. The value of 0.5 in the 'MIN FOREC M' is the minimum magnitude of strong aftershocks whose occurrence probability is provided by the 'Aftershock probability evolution' module.

The 'M OF COMPL Mo' window shows the magnitude of completeness value which was already determined during the analysis of the initial catalog. After clicking the 'Start' button, the program reads the sample file, identifies the 'new' trigger and performs calculations and plotting of the rate and probability evolution windows with the increase of 'new' aftershocks. All this is done in a matter of seconds, a lot of plots appear and at the end the last (last updated) three plots remain (rate, probability, space) remain. All previous plots (for previous updates), however, are saved in separate directories: '3D_EVOLUTION' – space; 'EVOLUTION' – rate; 'PROBABILITY' – probability, for further posterior viewing and analyzing the subsequent windows of the sequence evolution. This can easily be done by, for example, starting a slide-show in each directory and following the update windows (one at each 20 events for rate and probability and a new plot for each new aftershock for space).

In the current situation of using a sample simulation file, all subsequent plots of the updated windows appear on the screen in a matter of seconds, each new one erasing the previous and leaving finally the plots of the last updates. In a real-time situation each updated plot will stay on the screen depending on the real aftershock rate of the ongoing sequence

All these three directories are in a directory after the name (date and time) of the new aftershock sequence where also all events of the new sequence are saved in a file. The plots on Fig.A14 display the case when all updated plots have already been shown and then saved in the corresponding directories and what is seen are final update plots. For a real time sequence the previous updated plots will also subsequently be shown on the screen.

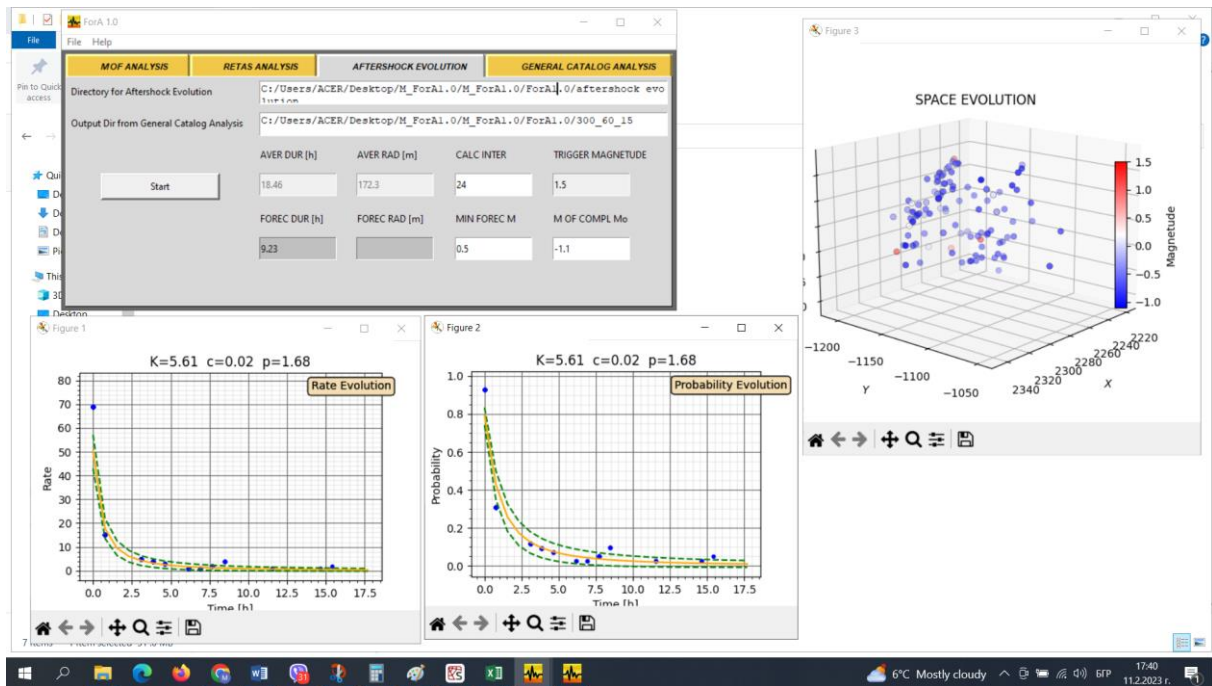


Fig.A14 Rate (down-left), probability (down-middle) and 3D spatial plots of the final updates of the ongoing aftershock sequence.

These final plots (Fig.A14) are interactive and zooming (also rotating for the 3D plot) can be performed. The simulation sample file is named *evolproba.csv* and is saved in the 'aftershock evolution' directory. It should be saved there and it should be under that name. If another sample file is to be verified its name should be changed to *evolproba.csv*.

2.1 Aftershock rate evolution [\(up\)](#)

The MOF model is most suitable for the so called 'normal' aftershock sequences in which there is no secondary triggering. The model specifies how the aftershock rate (number of aftershocks $n(t)$ per unit time) decreases with time t and is based on three parameters K , c and p (eq.1) which are specific for each sequence.

$$n(t) = \frac{K}{(t+c)^p} \quad (1)$$

Knowing these parameters allows to calculate (forecast) the aftershock rate evolution which can eventually be applied to estimate the sequence duration. As there are no any aftershocks immediately after a new trigger occurs the calculations by eq.1

are first performed using the averaged K, c, p values from the previous sequences calculated in 'General catalog analysis' and a plot of the rate decay with time is presented. Then recalculations are made after each new 20 aftershocks of the ongoing sequence and the updated rate evolution is presented again. The final plot of the rate evolution is shown on Fig.A14 (down-left).

2.2 Occurrence probability evolution [\(up\)](#)

Kknowing the rate evolution allows the calculation of the occurrence probability of at least one strong aftershock with a magnitude above a certain value. This value has been chosen to be $M=0.5$ following some experience cases which reveal that events stronger than this limit could have impact on the work safety in the mine and should be considered for re-entry concerns. The final evolution plot is presented on Fig.A14 (down-middle) and the previous plots are saved in the 'PROBABILITY' directory.

2.3 Spatial evolution [\(up\)](#)

The spatial evolution is exposed by subsequently plotting the hypocenters of the 'new' aftershocks and saving the plots in the '3D_EVOLUTION' directory. The last 3D plot presented on Fig.A14 (right) can be rotated to see details of the aftershock hypocenter distribution (events are colored according to their magnitude).

3. MOF analysis [\(up\)](#)

This module is not intended to be completed at this stage and may be developed in the future.

4. RETAS analysis [\(up\)](#)

This module is not intended to be completed at this stage and may be developed in the future.

5. A very short ForA1.0 user's guide: [\(up\)](#)

- Unzip
- Brows to main.exe and run it
- Select 'General Catalog Analysis'
- Click in the 'initial catalog' window and through 'File -> File open' select '*kirinit.csv*' (for Malmberget mine the files is 'initcatM.csv')
- Click in the 'Output directory' and select '200_24_15'
- Do not change selected values in the windows below
- Click 'Catalog error checking'
- If 'NO ERRORS' in the INFO window, click 'Init aftersh. identification'

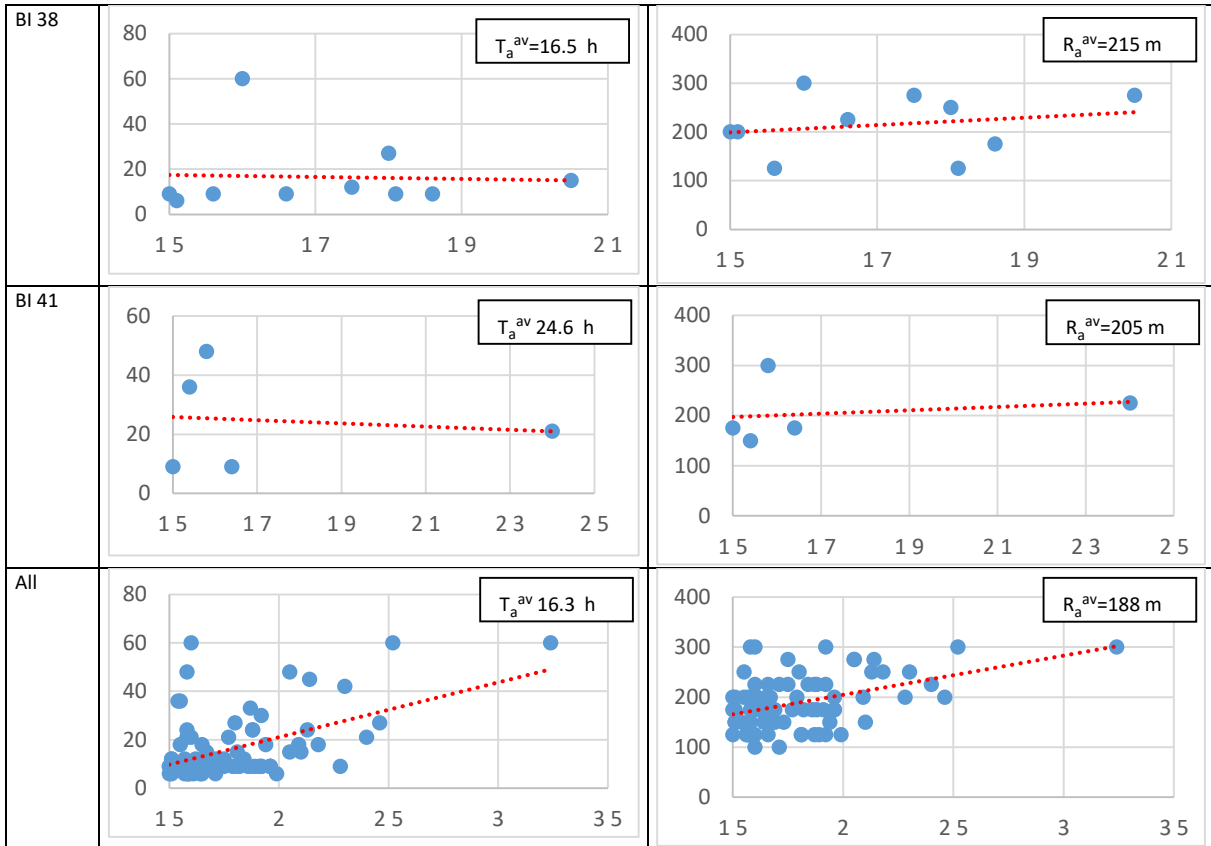
- the button remains pressed and when this module ends, the button pops up again (~ 1 minute) – separate directories are created in the '200_24_15' directory for each trigger (sequence) with a file containing the init sequence (200 m x 24 h)
- click on 'Final aftersh identification' – around 8 minutes. This module analyzes each initial sequence, identifies and saves the final sequence in the corresponding directory. A small file 'PARAMETER.txt' is also saved with the final sequence duration and radius
- click on 'MOF parameters all' – less than a minute with popping black windows – the module fits MOF model to each final sequence ($N > 5$), plots the cumulative curve with the MOF parameters in each corresponding directory. All plots are also saved in one common directory 'GRAPH' for easy browsing and analysis. Two files are also saved – mofall.txt and vmofall.txt with data about the aftershock sequences
- select 'Aftershock evolution'
- the module reads a simulation file 'evolproba.csv' row by row imitating sequential occurring of events and when it identifies a trigger, evolution forecasting is started (rate and probability) also 3D printing of the subsequent hypocenters. The subsequent results are plotted and saved correspondingly, the last updated plots remaining on the screen

Appendix B [\(bck\)](#)

Correlation between trigger magnitude and aftershock sequence duration and zone radius.

Table B1. Correlation between trigger magnitude and aftershock sequence duration T_a and zone radius R_a . Average values of T_a and R_a are also provided.

GMZ Vol	Correlation between the trigger magnitude and aftershock sequence duration T_a	Correlation between the trigger magnitude and the aftershock zone radius R_a
BI 04-12	<p>$T_a^{av}=7.8$ h</p>	<p>$R_a^{av}=140$ m</p>
BI 12-15	<p>$T_a^{av}=6.8$ h</p>	<p>$R_a^{av}=138$ m</p>
BI 15-26	<p>$T_a^{av}=16.3$ h</p>	<p>$R_a^{av}=179$ m</p>
BI 26-30	<p>$T_a^{av}=16.2$ h</p>	<p>$R_a^{av}=184$ m</p>
BI 34 v2	<p>$T_a^{av}=18.3$ h</p>	<p>$R_a^{av}=204$ m</p>



References

- Bath, M., 1965. Lateral inhomogeneities in the upper mantle. *Tectonophysics*, 2, 488–514.
- Christoskov, L. and Lazarov, R. (1981), *Basic considerations on earthquake catalog representativeness in the aspect of seismostatistical estimates (in Bulgaria)*, *Bulgar. Geophys. J. VII*, 3, 58–72.
- Dineva S, Boskovic M (2017) Evolution of seismicity at Kiirunavaara Mine. *Deep Mining 2017: Eighth International Conference on Deep and High Stress Mining – J Wesseloo (ed.)*, Australian Centre for Geomechanics. Perth. ISBN 978–0–9924810–6–3. https://papers.acg.uwa.edu.au/p/1704_07_Dineva/
- Dineva S, Dahner C, Malovichko D, Lund B, Gospodinov D, Piana Agostinetti N, Rudzinski L (2022) Analysis of the magnitude 4.2 seismic event on May 18, 2020 in the Kiirunavaara mine, Sweden, *Proceedings of RaSiM 10-Rockbursts and Seismicity in Mines*, April 24–29, 2022, Tucson, Arizona, 16 pp
- Duplancic, P. & Brady, B.H. 1999, "Characterization of caving mechanisms by analysis of seismicity and rock stress", 9th International Congress on Rock Mechanics, A.A. Balkema, pp. 1049.
- Gardner, J.; Knopoff, L. Is the sequence of earthquakes in Southern California, with aftershocks removed, Poissonian? *Bull. Seism. Soc. Am.* **1974**, *64*, 1363–1367.
- Estay, R., J. Vallejos, C. Pavez, and M. Brönnner, (2020), "A comparison of characteristic parameters of mining related and tectonic seismic aftershock sequences," *International Journal of Rock Mechanics and Mining Sciences*, vol. 128, p. 11, 2020.
- Gospodinov D., L.Christoskov, (1988), Model investigations of earthquake space distribution, *Proceed. of the XXI Gen.Ass. of ESC*, 23-27 August, 1988, Sofia, Bulgaria, pp.50-57.
- Gospodinov, D., (2004), Simulation of some point processes in aftershock analysis, *Proc. Intern. sympos. "Science & Education"*, October 1-3, Jambol, 2004, Vol.3, pp.109-115
- Gospodinov D., (2016), MODELLING THE ENERGY RELEASE PROCESS OF AFTERSHOCKS, *Bulletin of the Geological Society of Greece*, vol. L, 2016, EGE2016_paper_129, Print ISSN: 0438-9557, Online ISSN: 2529-1718, **DOI**: <https://doi.org/10.12681/bgsg.11840>
- Gospodinov, D., (2017), Spatio-temporal evolution of aftershock energy release following the 1989, MW6.9, LOMA Prieta earthquake in California *Acta Geophys.* 65: 565, journal ISSN : 1895-6572, journal e-ISSN : 1895-7455, <https://doi.org/10.1007/s11600-017-0038-5>
- Gospodinov D, Rotondi R (2006) Statistical analysis of triggered seismicity in the Kresna Region of SW Bulgaria (1904) and the Umbria-Marche Region of Central Italy (1997). *Pageoph* 163:1597–1615
- Gospodinov D, Vassilios K, Papadimitriou E, (2015) Seismicity rate modeling for prospective stochastic forecasting: the case of 2014 Kefalonia, Greece, seismic excitation. *Nat Hazard* 79(2) <https://doi.org/10.1007/s11069-015-1890-8>
- Gospodinov, D., Dineva, S. & Dahnér-Lindkvist, C. (2022) On the applicability of the RETAS model for forecasting aftershock probability in underground mines (Kiirunavaara Mine, Sweden). *J Seismol* , 26, pages 1023–1037 (2022). <https://doi.org/10.1007/s10950-022-10108-6>
- Gutenberg B, Richter CF (1944) Frequency of earthquakes in California. *Bull Seismol Soc Am* 34:185–188
- Harris PC, Wesseloo J (2015) mXrap software, version 5. Australian Centre for Geomechanics, The University of Western Australia. Perth. <http://www.mXrap.com>
- Jordan TH, et al. (2011) Operational earthquake forecasting; state of knowledge and guidelines for utilization, report by the International Commission on Earthquake Forecasting for Civil Protection. *Ann Geophys* 54 <https://doi.org/10.4401/ag-5350>
- Kubacki T, Koper KD, Pankow KL and McCarter MK (2014) Changes in mining-induced seismicity before and after the 2007 Crandall Canyon Mine collapse. *JGR Solid Earth* 119:4876–4889 <https://doi.org/10.1002/2014JB011037>
- Larsson K, (2004), Mining induced seismicity in Sweden, Licentiate thesis / Luleå University of Technology, 2004. p. 169, ISSN 1402-1757 ; 2004:80
- Malek F, Leslie I (2006) Using seismic data for rockburst re-entry protocol at INCO's Copper Cliff North Mine. In *Golden Rocks 2006, The 41st US Symposium on Rock Mechanics (USRMS)*, Paper ARMA/USRMS 06–1163. OnePetro
- Marzocchi W, Lombardi A-M (2009) Real-time forecasting following a damaging earthquake. *Geophys Res Lett.* <https://doi.org/10.1029/2009GL040233>
- Marzocchi W, Murru M, Lombardi A-M, Falcone G, Console R (2012) Daily earthquake forecasts during the May–June 2012 Emilia earthquake sequence (northern Italy). *Ann Geophys* 55:561–567

- McGarr A, Green RE (1978) Microtremor sequences and tilting in a deep mine. *Bull Seismol Soc Am* 66:1679–1697
- Nordström E, Dineva S, Nordlund E (2020) Back analysis of short-term seismic hazard indicators of larger seismic events in deep underground mines (Ikab, Kiirunavaara mine, Sweden). *Pure Appl Geophys* 177(2):763–785
- Ogata Y (1988) Statistical models for earthquake occurrences and residual analysis for point processes. *J Am Stat Assoc* 83:9–27
- Ogata Y, Zhuang J (2006) Space-time ETAS model and an improved extension. *Tectonophysics* 413:13–23
- Peresan, A.; Gentili, S. Identification and characterisation of earthquake clusters: A comparative analysis for selected sequences in Italy and adjacent regions. *Boll. Geofis. Teor. Appl.* **2020**, *61*, 57–80.
- Perman, Fredrik, Jonny Sjöberg and Thomas Wettainen. "Numerical Modeling of Mining-Induced Seismicity — Review and Case Study Example from the Malmberget Mine." (2013).
- Reasenbergh PA, Jones LM (1989) Earthquake hazard after a mainshock in California. *Science* 243(4895):1173–1176
- Reasenbergh P, Jones LM (1994) Earthquake aftershocks: update. *Science* 265:1251–1252
- Reasenbergh, P. Second-order moment of central California seismicity, 1969–1982. *J. Geophys. Res.* **1985**, *90*, 5479–5495.
- Spottiswoode S (2000) Aftershocks and foreshocks of mine seismic events. 3rd International Workshop on the Application of Geophysics to Rock and Soil Engineering, Geo-Eng2000, Melbourne, Australia
- Tierney SR, Morkel IG (2017) The optimisation and comparison of re-entry assessment methodologies for use in seismically active mines. In: J Wesseloo (ed.), *Proceedings of the Eighth International Conference on Deep and High Stress Mining*. Australian Centre for Geomechanics, Perth, pp. 183–196
- Umar, S B (2014) Rock Mass Behavior and Cap Rock Stability at the Malmberget Mine, LICENTIATE THESIS, Luleå University of Technology Department of Civil, Environmental and Natural Resources Engineering Division of Mining and Geotechnical Engineering, Printed by Luleå University of Technology, Graphic Production, 2014 ISSN 1402-1757, ISBN 978-91-7583-097-1 (print), ISBN 978-91-7583-098-8 (pdf)
- Umar, S.B., Sjöberg, J., and E. Nordlund. "Rock Mass Characterization and Conceptual Modeling of the Printzsköld Orebody of the Malmberget Mine." Paper presented at the 47th U.S. Rock Mechanics/Geomechanics Symposium, San Francisco, California, June 2013.
- Utsu T (1961) A statistical study of the occurrence of aftershocks. *Geophys Mag* 30:521–605
- Vallejos J & McKinnon S (2008) Guidelines for the development of re-entry protocols in seismically active mines. In *The 42nd US Rock Mechanics Symposium (USRMS)*. OnePetro
- Vallejos JA (2010) Analysis of seismicity in mines and development of re-entry protocols. PhD thesis, Queen's University, Canada
- Vallejos JA, Estay R (2018) Seismic parameters of mining induced aftershock sequences for re-entry protocol development. *Pageoph* 175:793. <https://doi.org/10.1007/s00024-017-1709-5>
- Vallejos JA, McKinnon SD (2009) Re-entry protocols for seismically active mines using statistical analysis of aftershock sequences. In: *Rock Engineering in Difficult Conditions*. Proceedings of the 20th Canadian Rock Mechanics Symposium, Toronto, Canada, paper 4028
- Vallejos JA, McKinnon SD (2011) Correlations between mining and seismicity for re-entry protocol development. *Int J Rock Mech Min Sci* 48:616–625. <https://doi.org/10.1016/j.ijrmms.2011.02.014>
- Wettainen, T. and Martinsson, J.. (2014) Estimation of future ground vibration levels in Malmberget town due to mining-induced seismic activity. *J. S. Afr. Inst. Min. Metall.* [online]. 2014, vol.114, n.10 [cited 2023-02-02], pp.835-843. Available from: <http://www.scielo.org.za/scielo.php?script=sci_arttext&pid=S2225-62532014001000013&lng=en&nrm=iso>. ISSN 2411-9717
- Wiemer S (2001) A software package to analyze seismicity: ZMAP. *Seismol Res Lett* 72:373–382
- Woodward K, (2015) Identification and Delineation of Mining Induced Seismic Responses, PhD thesis, School of Civil and Resource Engineering, University of Western Australia
- Woodward K, Wesseloo J (2015) Observed spatial and temporal behavior of seismic rock mass response to blasting. *J South Afr Inst Min Metall* 115(11):1044–1056
- Woodward KR, Potvin Y, Wesseloo J (2017) The spatial and temporal assessment of clustered and time-dependent seismic responses to mining. In J. Wesseloo (Ed.), *Deep Mining 2017*:

Proceedings of the Eighth International Conference on Deep and High Stress Mining (pp. 157–172). Australian Centre for Geomechanics, Perth, WA

Zhuang, J.; Ogata, Y.; Vere-Jones, D. Stochastic declustering of space-time earthquake occurrences. *J. Am. Stat. Assoc.* **2002**, *97*, 369–380.